U. S. Department
of Transportation
**Federal Railroad
Administration**

Analyses of Track Shift Under High-Speed Vehicle-Track Interaction

Office of Research
and Development
Washington, D.C. 20590

Safety of High-Speed
Ground Transportation Systems

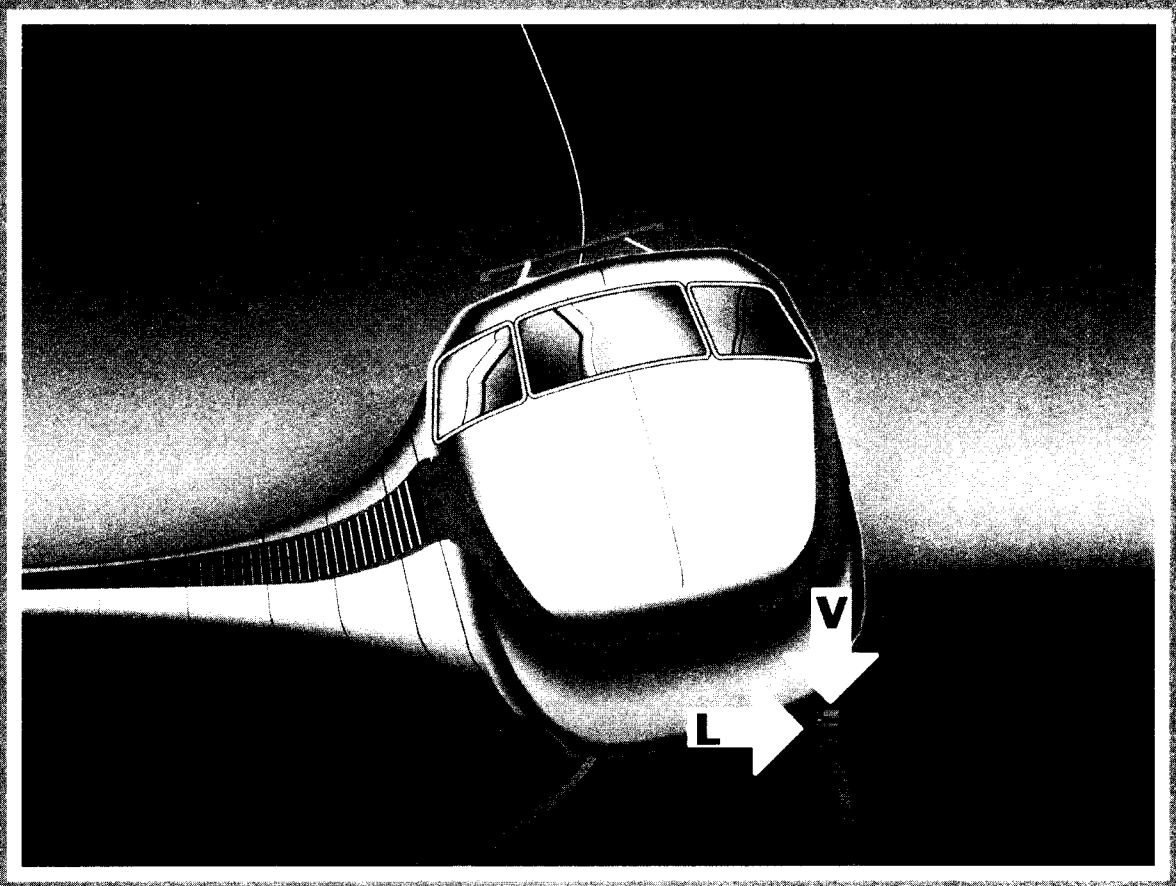

DOT/FRA/ORD-97/02
DOT-VNTSC-FRA-97-3

Final Report
June 1997

REPORT DOCUMENTATION PAGE

Form Approved
OMB No. 0704-0188

1. AGENCY USE ONLY (Leave blank)	2. REPORT DATE	3. REPORT TYPE AND DATES COVERED
	June 1997	Final Report November 1993 - March 1997

4. TITLE AND SUBTITLE
Analyses of Track Shift Under High-Speed Vehicle-Track Interaction - Safety of High-Speed Ground Transportation Systems

5. FUNDING NUMBERS
RR793/R7020
DTRS-57-93-D00028

6. AUTHOR(S)
G. Samavedam, F. Blader, D. Wormley, M. Snyder, J. Gomes, and A. Kish

7. PERFORMING ORGANIZATION NAME(S) AND ADDRESS(ES)
Foster Miller, Inc.
350 Second Avenue
Waltham, MA 02154-1093

8. PERFORMING ORGANIZATION REPORT NUMBER
DOT-VNTSC-FRA-97-3

9. SPONSORING/MONITORING AGENCY NAME(S) AND ADDRESS(ES)
U.S. Department of Transportation
Federal Railroad Administration
Office of Research and Development
400 7th Street, SW
Washington, DC 20590

10. SPONSORING/MONITORING AGENCY REPORT NUMBER
DOT/FRA/ORD-97/02

11. SUPPLEMENTARY NOTES
under contract to: U.S. Department of Transportation
Research and Special Programs Administration
John. A. Volpe National Transportation Systems Center
Cambridge, MA 02142-1093

12a. DISTRIBUTION/AVAILABILITY STATEMENT
This document is available to the public through the National Technical Information Service, Springfield, VA 22161

12b. DISTRIBUTION CODE

13. ABSTRACT (Maximum 200 words)
This report describes analysis tools to predict shift under high-speed vehicle-track interaction. The analysis approach is based on two fundamental models developed (as part of this research); the first model computes the track lateral residual deflections under vehicle passage, whereas the second determines the lateral dynamic loads generated as the vehicle negotiates misaligned tangent or curved tracks. The track residual deflection model takes the loads from the vehicle dynamic model as inputs and is based on a quasi-static beam theory and an appropriate trilinear constitutive representation for the tie-ballast lateral resistance under the wheel vertical loads. The vehicle dynamic model is based on a multibody simulation which maintains a wheel-rail rolling contact connection with a complaint track representation. Computer codes (OMNISIM) for track residual deflection and for vehicle multibody simulation with complaint track element have been developed to facilitate parametric study. OMNISIM, which has been developed through extensive modifications of previous programs (which do not permit a complaint track element) is shown to have several advantages including accuracy in the evaluation of loads and wheel climb predictions.

The track shift computer code can be used to identify the stable and unstable regimes of track shift, and is partially validated by test data on panels under stationary load cycles, and SNCF data on TGV track under moving loads. It is shown that moving load simulation is required for an assessment of track shift. Preliminary results are presented for a representative articulated train with high-speed track traversing track with selected alignment irregularities at selected wavelengths. The results are sensitive to flange clearance and wheel profile. For "AAR wheel profile," the net axle force ratio can reach a high value (~0.49) for a misalignment of 8 mm amplitude and 10 m wavelength, at speeds on the order of 93 mph. However, this force is spread over a finite length of the track and its effect on track shift needs to be investigated.

14. SUBJECT TERMS
track lateral shift, net axle force ratio, vehicle-track interaction, track residual deflection, OMNISIM

15. NUMBER OF PAGES
130

16. PRICE CODE

17. SECURITY CLASSIFICATION OF REPORT	18. SECURITY CLASSIFICATION OF THIS PAGE	19. SECURITY CLASSIFICATION OF ABSTRACT	20. LIMITATION OF ABSTRACT
Unclassified	Unclassified	Unclassified	

PREFACE

This report presents an analysis of track shift for safety evaluation of high-speed trains generating track shift forces. Computational tools for the evaluation of vehicle dynamic loads and the resulting track residual deflections after the vehicle passage have been developed in this report. The tools will be employed in the assessment of lateral shift potential for tracks of different strengths typically seen in revenue service for both conventional and high-speed rail operations. An extensive parametric study is being planned to identify significant parameters of track and vehicles, based on which track shift safety limits will be developed in an upcoming report under this contract.

This work has been performed under the OMNI contract DTRS-57-93-D00028 awarded by the U.S. Department of Transportation's Volpe National Transportation Systems Center (VNTSC) at Cambridge, MA. The work was performed by Foster-Miller, Inc. under the technical direction of Dr. Andrew Kish, the Technical Task Initiator of VNTSC. The work was sponsored by the Federal Railroad Administration's Office of Research and Development, U.S. Department of Transportation at Washington, D.C. The authors are grateful to Dr. Herbert Weinstock of VNTSC for his valuable technical comments on the draft versions of the report, based on which significant revisions have been made.

METRIC/ENGLISH CONVERSION FACTORS

ENGLISH TO METRIC

LENGTH (APPROXIMATE)

1 inch (in) = 2.5 centimeters (cm)
1 foot (ft) = 30 centimeters (cm)
1 yard (yd) = 0.9 meter (m)
1 mile (mi) = 1.6 kilometers (km)

AREA (APPROXIMATE)

1 square inch (sq in, in^2) = 6.5 square centimeters (cm^2)
1 square foot (sq ft, ft^2) = 0.09 square meter (m^2)
1 square yard (sq yd, yd^2) = 0.8 square meter (m^2)
1 square mile (sq mi, mi^2) = 2.6 square kilometers (km^2)
1 acre = 0.4 hectare (ha) = 4,000 square meters (m^2)

MASS - WEIGHT (APPROXIMATE)

1 ounce (oz) = 28 grams (gm)
1 pound (lb) = .45 kilogram (kg)
1 short ton = 2,000 pounds (lb) = 0.9 tonne (t)

VOLUME (APPROXIMATE)

1 teaspoon (tsp) = 5 milliliters (ml)
1 tablespoon (tbsp) = 15 milliliters (ml)
1 fluid ounce (fl oz) = 30 milliliters (ml)
1 cup (c) = 0.24 liter (l)
1 pint (pt) = 0.47 liter (l)
1 quart (qt) = 0.96 liter (l)
1 gallon (gal) = 3.8 liters (l)
1 cubic foot (cu ft, ft^3) = 0.03 cubic meter (m^3)
1 cubic yard (cu yd, yd^3) = 0.76 cubic meter (m^3)

TEMPERATURE (EXACT)

°C=5/9(°F - 32)

METRIC TO ENGLISH

LENGTH (APPROXIMATE)

1 millimeter (mm) = 0.04 inch (in)
1 centimeter (cm) = 0.4 inch (in)
1 meter (m) = 3.3 feet (ft)
1 meter (m) = 1.1 yards (yd)
1 kilometer (km) = 0.6 mile (mi)

AREA (APPROXIMATE)

1 square centimeter (cm^2) = 0.16 square inch (sq in, in^2)
1 square meter (m^2) = 1.2 square yards (sq yd, yd^2)
1 square kilometer (km^2) = 0.4 square mile (sq mi, mi^2)
10,000 square meters (m^2) = 1 hectare (ha) = 2.5 acres

MASS - WEIGHT (APPROXIMATE)

1 gram (gm) = 0.036 ounce (oz)
1 kilogram (kg) = 2.2 pounds (lb)
1 tonne (t) = 1,000 kilograms (kg) = 1.1 short tons

VOLUME (APPROXIMATE)

1 milliliter (ml) = 0.03 fluid ounce (fl oz)
1 liter (l) = 2.1 pints (pt)
1 liter (l) = 1.06 quarts (qt)
1 liter (l) = 0.26 gallon (gal)
1 cubic meter (m^3) = 36 cubic feet (cu ft, ft^3)
1 cubic meter (m^3) = 1.3 cubic yards (cu yd, yd^3)

TEMPERATURE (EXACT)

°F=9/5(°C) + 32

QUICK INCH-CENTIMETER LENGTH CONVERSION

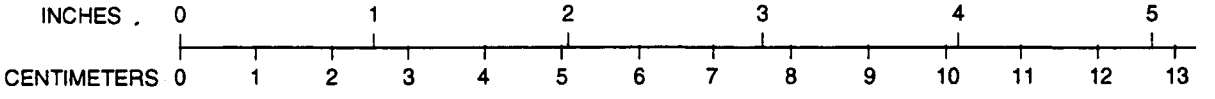

QUICK FAHRENHEIT-CELSIUS TEMPERATURE CONVERSION

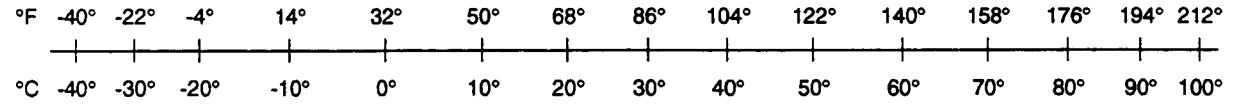

For more exact and or other conversion factors, see NIST Miscellaneous Publication 286, Units of Weights and Measures. Price $2.50. SD Catalog No. C13 10286.

Updated 8/1/96

TABLE OF CONTENTS

TABLE OF CONTENTS (continued)

LIST OF FIGURES

LIST OF FIGURES (continued)

Figure **Page**

LIST OF TABLES

LIST OF SYMBOLS

A	Cross-sectional area for two rails
E	Young's modulus for rail steel
F_e	Elastic limit of tie-ballast resistance
F_p	Tie-ballast peak lateral resistance
H_p	Prud'homme limit for lateral force
I	Moment of inertia for bending in the lateral plane (2 rails)
I_v	Moment of inertia for bending in the vertical plane (2 rails)
k_1, k_2, k_3	Stiffnesses in the trilinear idealization of tie-ballast resistance
k_v	Track foundation vertical stiffness
NAL	Net axle lateral load
NAL/V	Ratio of lateral to vertical forces
N	Number of vehicle passes
P	Track thermal force
R	Track radius of curvature
R_v	Track foundation vertical reaction
S	Ballast reaction in the lateral plane
SE	Superelevation
S_l	Track lateral limiting strength
T	Rail temperature increase above neutral
V	Vehicle vertical axle load
w	Track lateral deflection
w_e	Tie deflection at the elastic limit
δ	Track residual deflection
μ_f	Tie-ballast coefficient of friction

EXECUTIVE SUMMARY

Track lateral shift under vehicle-track interaction loads is an important consideration for safe and economic operations of high-speed rail. This report presents analyses of the problem on the basis of two models, a quasi-static track model and a vehicle dynamic model. The quasi-static model determines the cumulative track residual deflection under known vehicle loads and passes. The dynamic model gives the loads generated on the track as the vehicle negotiates misalignments or curves, and thus provides required inputs to the track model. The vehicle dynamic model assesses also the ride quality and potential for wheel climb. Both models are required and coupled for a complete analysis of track shift.

The quasi-static track residual deflection model is based on the beam theory and utilizes an appropriately idealized trilinear characteristic for the tie-ballast lateral resistance.

Based on the quasi-static beam theory and the constitutive representation, a computer code has been developed and exercised for a preliminary parametric study. The cumulative residual deflections are evaluated for a range of net axle lateral to vertical force ratios, and a range of tie-ballast peak resistances and friction coefficients. The results identify the stable and progressive behavior of track shift that can occur under a range of steadily applied net axle force ratios (0.4 to 0.6) on tracks for a range of track parameters. The results from the theory are compared with French National Railways (SNCF) data from moving load tests on TGV track. Using this code, it is shown that moving loads must be considered for a proper evaluation of track residual deflections and the stationary load idealization underestimates the results. The code is exercised for both single axle and truck load cases. It is found that the single axle load idealization predicts the residual deflection conservatively within about 15 percent larger values compared to those obtained from the truck load considerations.

A computer code (OMNISIM) has also been developed for prediction of loads as the vehicle negotiates misaligned tangent and curved track. The code includes a compliant track element and models the rolling contact at the wheel/rail interface and also dynamics of car body elements. The code was developed through significant modifications on existing vehicle-

interaction codes and permits a "compliant track" representation. The latter is considered to be essential for the study conducted here.

The new code, OMNISIM, is exercised over a range of vehicle and track parameters to study their influence on net axle lateral loads generated. The lateral loads generated by vehicle negotiation are influenced by the severity of misalignments (larger amplitude and smaller wavelength), and the tie-ballast lateral resistance in addition to speed and other parameters. The lateral loads generated are quite sensitive to vehicle speed, as the speed approaches that associated with hunting.

Vehicles negotiating curves with inadequate spiral lengths at speeds significantly higher than balance speeds also generate significant net axle loads. Numerical results for 2 deg and 4 deg curves at 9 in. cant deficiency and with different spiral lengths are presented to show the sensitivity of the lateral loads to this parameter.

1. INTRODUCTION

In this section, a brief description of the track shift problem and objectives of the work performed are presented.

1.1 TRACK SHIFT FUNDAMENTALS

Track shift has been recognized as an important safety and operational issue in European and Japanese high-speed rail service. When a lateral load is exerted on the track by vehicle axles, the track will tend to experience lateral displacements, it being a compliant structure. Due to the "elastoplastic" nature of ballast, or more precisely due to frictional interlocking nature of ballast, the track may generate some permanent residual deflections after the vehicle passage when the vehicle lateral load exceeds a critical value. The residual deflection may grow under each axle passage and may reach a limit after many passes, beyond which no increase in the residual deflection occurs for subsequent passes. In this situation, the track is considered as having "stabilized" track shift. If, however, the deflection never levels off at a finite limit and continuously increases with every pass, the track shift is considered "progressive." Progressive track shift is clearly not acceptable in revenue service as it leads to unsafe operations. Illustrative characteristic responses of track under stable and progressive shift are shown in Figure 1-1, in which the cumulative residual deflection is plotted as a function of the number of axle passes for assumed constant lateral load. For given track and vehicle parameters, analytic determination of the response curves is a primary issue in track shift analysis.

Key track and vehicle parameters governing the track shift are discussed in the next section. One of the important parameters is the net axle lateral load (NAL). This is determined from a vehicle dynamic analysis. Thus, track shift analysis requires both track response and vehicle dynamic modelling. The lateral displacement can be "global" over a long section of the track, such as a curved segment, or it can be local in the form of lateral misalignments with amplitudes of a few millimeters over several meters of wavelength. The rate at which the local misalignments grow with the number of wheel passes is important from the track maintenance point of view. Sufficient growth of the misalignments and sudden "global" track movement can lead to unsafe conditions which could result in wheel climb, gauge widening, ride quality

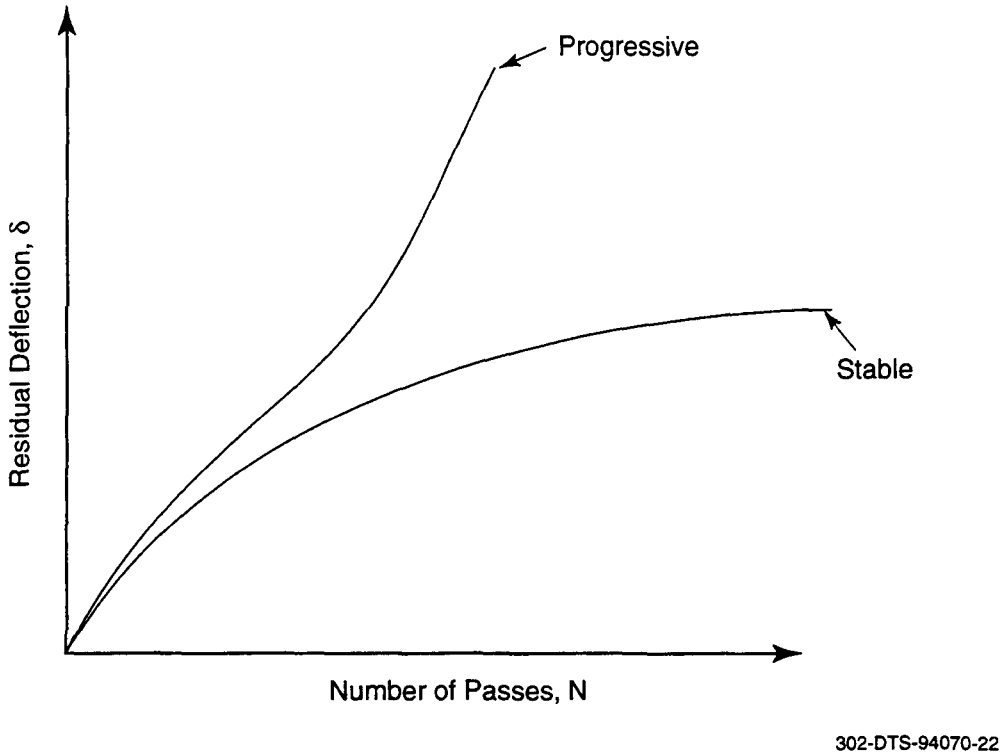

Figure 1-1. Stable and unstable behavior of track shift

deterioration and/or track buckling. For safe revenue operations and economic track maintenance, the track shift must be controlled within the permissible limits. For example, the French National Railway (SNCF) stipulates a limit of about 4 mm for the misalignment amplitude in their high-speed TGV track operations. Clearly, the allowable track shift limit depends on the vehicle and track characteristics including the maximum vehicle speed. Such a limit for the future high-speed operations in the U.S. needs to be established.

1.2 PREVIOUS WORK

A review of literature on track shift is presented in Reference (1). As stated in this reference, studies on track shift have been conducted in England, France, Germany, Sweden and Japan. There is no general agreement on the analytic and test methodology for track shift evaluations. Through an extensive test program, the SNCF determined certain permissible limits on net axle lateral to vertical force ratio (NAL/V) for their vehicle qualification. The Prud'homme limit of

$$\frac{H_p}{V} = 0.33 + \frac{10}{V}$$

H_p = net axle lateral load in kN

V = axle vertical load in kN

is recommended for vehicle operations on tangent tracks, with 85 percent of the limit for vehicles on curves (2). At this limit, the track lateral residual displacements are expected to accumulate very slowly, which will allow a large number of vehicle passes in-between track maintenance intervals.

For modern high-speed track, the Prud'homme formula *appears to be restrictive* due to the speed limitation required to contain net axle load within the limit. In order to achieve higher speeds, particularly on curves (using the tilt technology to assure passenger ride comfort), the Prud'homme limit was exceeded in some recent high-speed operations. It is also considered that modern track can be designed and maintained at higher lateral strength levels than the tracks originally tested by the SNCF in the development of the Prud'homme limit.

Speeds in excess of the balance speed were employed in recent high-speed experiments with foreign vehicles on U.S. curves with 10 to 12 in. cant deficiency. These tests, though limited in their scope, gave a maximum net axle force ratio of slightly under 0.5, which is considered as a vehicle acceptance limit in the U.S. (3). It is important to develop a rational basis for allowable net axle force ratio during revenue operations of the vehicles on U.S. tracks and evaluate the requirements of track strength and alignment.

The required track strength, permissible lateral misalignment and the vehicle qualification limit are related within the context of track shift. The track strength considerations are important to control the growth of lateral misalignments due to the lateral loads exerted by each axle pass. The rate at which the misalignments grow is an important consideration for economic maintenance operations.

The misalignments must stabilize at a finite number of vehicle passes to a limit to assure permissible ride quality and safety against wheel climb, gauge widening and potential track buckling in the presence of thermal and vehicle induced loads. At the stable misalignment, the maximum net axle force ratio for the vehicle should not exceed its permissible limit. Thus, it is important to ensure that all of the permissible limits are consistently established between the track and the vehicle for safe and economic high-speed rail operations.

1.3 OBJECTIVES

The purpose of this report is to provide a rational analytic tool for the evaluation of track shift and its influence on potential failure modes of the vehicle-track system. Specific objectives of the study include the following tasks:

Overall Modelling Approach

- Develop an overall approach to the problem of track shift.

- Identify significant vehicle and track parameters and mechanistic models involved in the overall approach.

- Identify specific issues and limitations of the models.

Track Residual Deflection Analysis

- Develop a track lateral response model that can predict the lateral response and cumulative lateral residual deflections at given lateral loads, under wheel passes.

- Provide a computer code implementing the model theory for numerical evaluations. Validate the model with existing test data in the U.S. and abroad.

- Perform parametric studies evaluating the influence of L/V and tie-ballast resistance and number of passes on the cumulative deflection and identify stable and unstable regimes of track shift.

Vehicle-Track Interaction Loads

- Develop an appropriate vehicle-track interaction model that can determine 1) the lateral loads accounting for track lateral and vertical stiffness, and 2) the failure modes due to hunting, wheel climb and ride quality deterioration.

- Develop a generalized computer code for the vehicle-track interaction model. Compare the differences between this code and existing models without track flexibility.

- Perform parametric studies for high-speed vehicle operations with different track misalignments.

2. THE OVERALL MODELLING APPROACH

The overall approach to the track shift problem is based on two fundamental models, namely:

- The Track Residual Deflection Model.
- The Vehicle Dynamic Model.

The purpose of the first model is to determine the cumulative residual lateral deflections after the passage of each axle in the vehicle consist. The time history of net axle lateral and vertical loads are assumed to be known in this model. The model should also account for the rail thermal load and track curvature influences on the track movement. The model should predict the onset of sudden or excessive track shift.

The purpose of the vehicle dynamic model is to compute the axle loads which will be the inputs in the track residual deflection model. The model should also predict potential failure modes that can occur prior to the onset of track lateral shift. It should account for preexisting track misalignments, curvature and the wheel-rail rolling contact mechanism. The track misalignments may be upgraded on the basis of the results from the track residual deflection model.

2.1 COUPLING OF MODELS

As discussed later, the vehicle model should also include a proper representation of track compliance for an accurate assessment of loads generated and potential failure modes such as wheel climb. A question arises whether the two component models can be combined into a single comprehensive model. Such a comprehensive model will be called Fully Coupled Approach as opposed to a Partially Coupled Approach in which the two models may be exercised under separate computer codes, but the input parameters (lateral loads to the track residual deflection model and misalignments to the vehicle dynamic model) are properly connected and updated.

A discussion of the Fully Coupled Approach and the tradeoffs between the two approaches are presented in Appendix A. Based on these tradeoffs, it is concluded that the Partially Coupled Approach may be adequate initially as it provides a practical and economic tool for track shift analysis. This approach is also the first logical step in the analysis and is the focus of this report. Figure 2-1 illustrates schematically the proposed approach involving the two component models. The fundamental parameter inputs, the models, the output from the models and the failure modes which can be assessed from the results are shown in this figure. These will be discussed in the following paragraphs.

2.2 BASIS OF TRACK RESIDUAL DEFLECTION MODEL

The model is based on the assumption that the moving lateral loads exerted by vehicles can be characterized as quasi-static in the track lateral response evaluations. The track is considered as a beam on springs with nonlinear elastoplastic "hardening and softening" characteristics. The beam bending inertias in the two planes are the sum of individual rail inertias in the respective lateral and vertical planes.

Load characterization issues which are considered and resolved in this report are 1) moving versus stationary loads and 2) single axle versus truck loads. It is shown through numerical work that a moving lateral load predicts the correct behavior of track shift and that the stationary load idealization grossly underestimates the resulting track residual deflection.

Generally, the two adjacent trucks of a car are too far apart to have any influence on one another in regard to the track lateral response. However, the two axles of a truck are sufficiently close so that it is necessary to consider their potential interference. For modern high-speed trucks, the axles are far apart and the axle vertical loads are relatively small compared to that of freight trucks. Preliminary calculations on the maximum deflections under the load which are presented in Appendix B show that the results are not significantly different for the axle and the truck load idealization for the modern high-speed track. Rigorous residual deflection calculations which are presented in Section 3 also confirm this trend.

In the development of empirical criteria for track shift, it has been a concern whether it should be based on the single axle net load or the truck load. The SNCF determined that a single axle load basis is adequate. Although the development of a track shift criterion is an ultimate objective of the study conducted in this report, the main focus of the work is to develop a rational analysis approach, valid for both single axle and truck load cases. Truck load idealization here

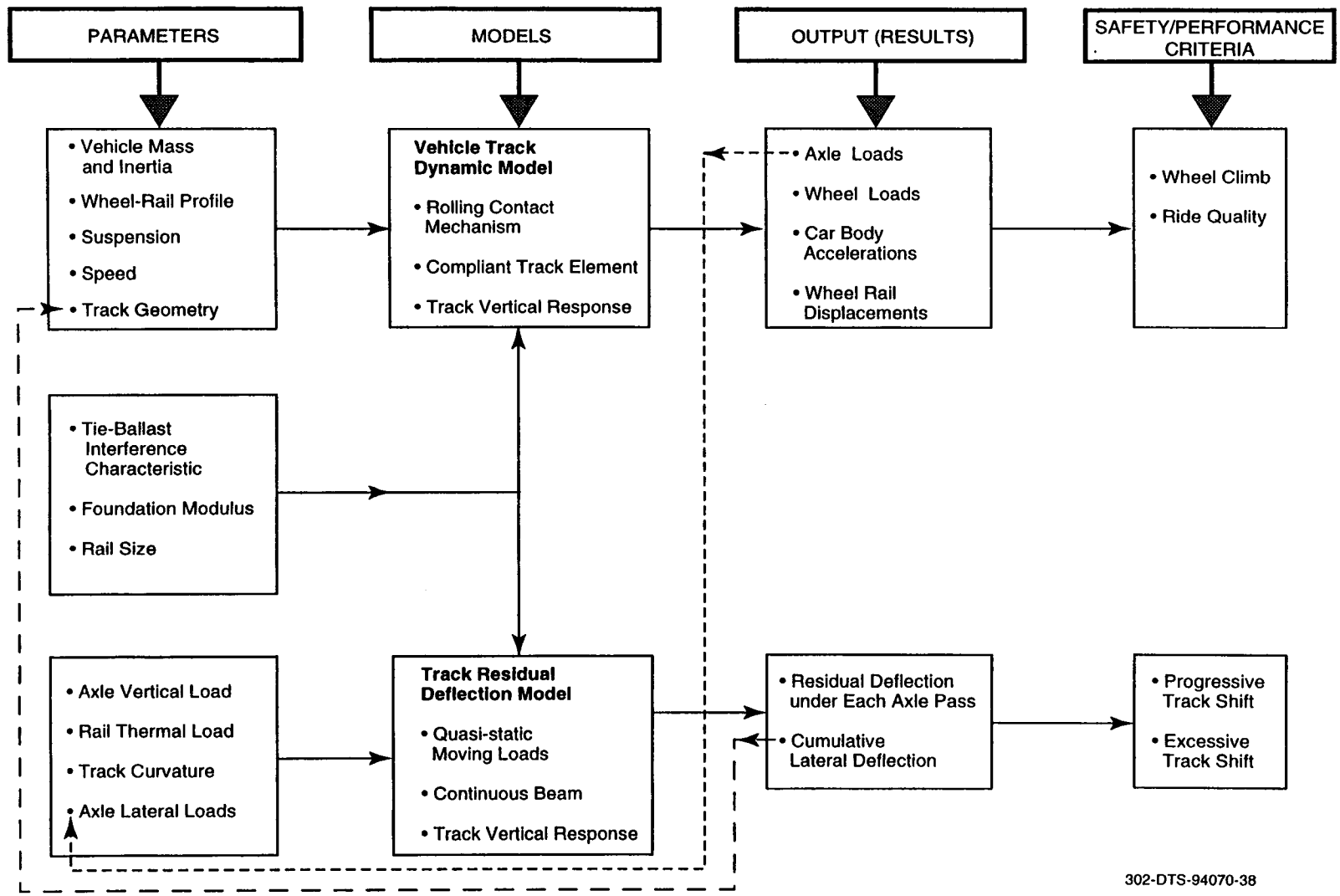

Figure 2-1. Partially coupled modelling approach

means that both axle loads are simulated in the model *simultaneously* to account for any interference between the loads. In contrast, a single axle load idealization implies consideration of each axle load independently, i.e., each axle pass represents a load cycle that may leave some residual deflection. The trailing axle represents a second load cycle (with different load magnitude in the general case) whose contribution to the residual deflection is computed in an appropriate manner taking into consideration the lateral displacement of ties which are already disturbed by the preceding cycle.

In Figure 2-1, key parameters of the track residual deflection model are presented. The ballast vertical foundation modulus is required to determine the track vertical response and hence, the tie load reaction distribution. The latter information is used to determine the net lateral resistance offered by loaded ties, which requires the tie-ballast friction coefficient. Using this lateral resistance, the track response under known lateral loads and the residual deflections after the load passage are computed. An appropriate trilinear stiffness characteristic for the tie ballast lateral resistance is developed for use in the track lateral residual deflection model. The track vertical response is considered to be purely elastic. Track profile degradation in the vertical plane due to vehicle passage is not considered in the analysis.

Track curvature and thermal load effects will also be accounted for in the residual deflection model.

2.3 BASIS OF VEHICLE DYNAMIC MODEL

It is considered essential to simulate the rolling contact mechanism at the wheel/rail interface for the evaluation of vehicle track interaction loads and predictions of potential failure modes including wheel climb. A review of the literature revealed that several codes such as the SYSSIM and NUCARS do satisfy this requirement. However, the existing codes are limited in the sense that they do not have an adequate representation of track, the rails in these codes being grounded through a spring and considered massless. For high-speed vehicle-track interaction, track compliance is considered to be important, as they are expected to influence the load levels generated and the vehicle hunting phenomenon. Furthermore, with laterally moving track a more accurate assessment of wheel climb can be made. Hence, it is considered desirable to include a compliant track element in the vehicle-track interaction study. Such an element, which accounts for rail flexure in the vertical and lateral planes and tie movement in the ballast, has been developed and is presented in Section 4. On this basis, a new advanced vehicle interaction

code, called OMNISIM, has been developed through extensive modifications of the existing codes.

It is considered that the current forms of existing codes (SYSSIM and NUCARS) might be adequate for low speed vehicle-track interaction. For high-speeds, OMNISIM with the compliant track element is essential for the type of study considered in this report.

Because of the track element in OMNISIM, the code can compute the normal pressure between tie-ballast interface and hence the resulting nonlinear lateral resistance. OMNISIM computes the lateral track deflections and tie movements as well as the lateral loads generated, for each vehicle pass. In its present form, it cannot compute the accumulating lateral deflection under several passes. Consequently, the track lateral residual deflection model (track shift model) is also required and provides the key to the track shift studies. As stated, OMNISIM provides inputs on axle loads to the track shift model. Likewise, the track shift model provides the updated misalignment shape after vehicle pass, as an input to OMNISIM. Coupling the inputs of the two codes in this manner, an accurate analysis of track shift under high-speed vehicle-track interaction can be carried out.

Details of the OMNISIM code are given in Appendix E. Parametric studies on a tangent track and curves subjected to high-speed vehicle operations are presented in Section 4.

3. THE TRACK RESIDUAL DEFLECTION MODEL

This section presents a new approach for the determination of the track lateral residual deflections under laterally loaded axles. The phenomenon of stable and unstable track lateral shift, experimentally observed by the SNCF, can now be explained and quantified using the model developed here. Important track parameters in the design and maintenance of track to control the growth of lateral misalignments are identified. The proposed track shift model can be used to aid planning and analysis of track experiments as well as the development of an appropriate track shift safety criterion.

3.1 CONSTITUTIVE MODEL

As stated in the previous report (1), the fundamental parameter required for understanding and analyzing track shift is the loaded and unloaded characteristic of the tie-ballast resistance. The Single Tie Push Test (STPT) fixture is used to determine this characteristic (4). Figure 3-1

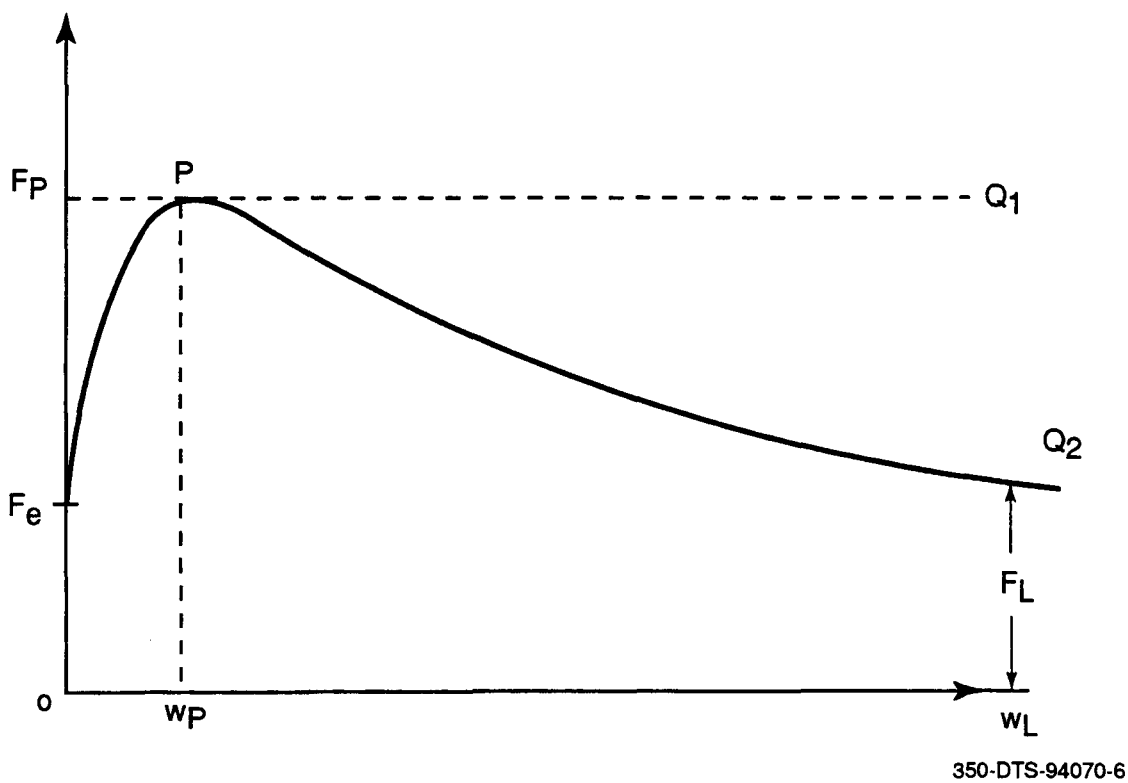

Figure 3-1. Typical tie-ballast resistance characteristic

shows the features of a typical characteristic. The point, F_e, represents the "breakoff" resistance, above which the tie begins to show some movement. This value can be considered as the "elastic resistance," since beyond this resistance, the tie will have residual displacement when the applied load is removed.

The point P represents the peak lateral resistance value, beyond which the resistance may remain constant (PQ_1) for a freshly tamped track, or soften as shown by PQ_2 for consolidated tracks, up to the point Q_2. Beyond Q_2 the resistance remains constant at this limiting value. For track buckling evaluations Q_2 is also an important consideration. For track shift analysis, only a small portion of the curve beyond P needs to be considered.

Clearly, for the purpose of residual deflection analysis, we need to define the path of tie deflection when it is laterally unloaded. This can be done as in Figure 3-2 in which the unloaded path is parallel to the resistance axis. This idealization considers zero elastic displacement limit, but may be involved from a computational point of view. A simpler trilinear idealization will introduce a "fictitious" elastic displacement limit as in Figure 3-3 in which w_e will be defined. The finite w_e will facilitate numerical work, and it does not introduce significant errors in the results for ultimate track shift strength providing w_e is chosen to be reasonably small (<1 mm).

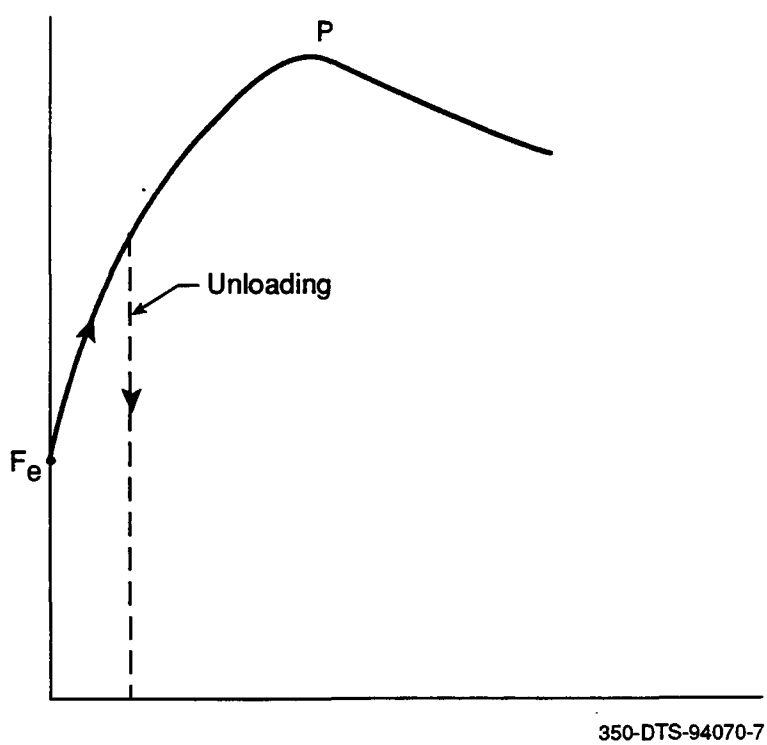

Figure 3-2. Definition of unloading path

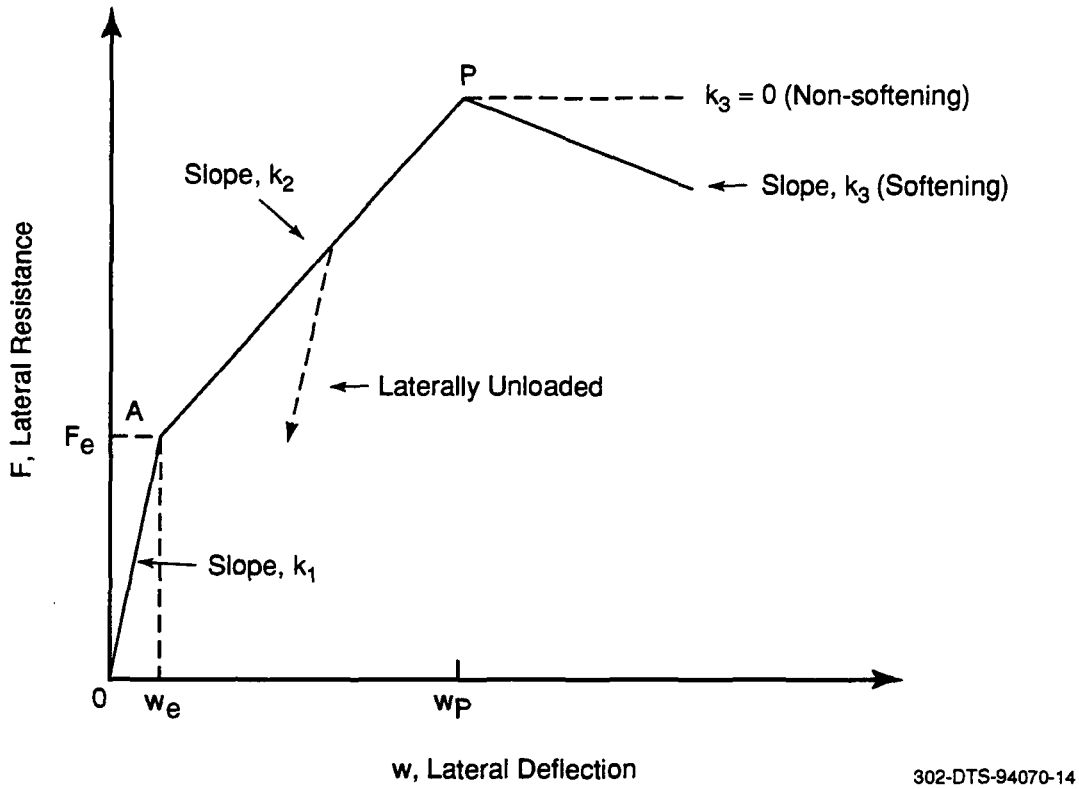

Figure 3-3. Trilinear idealized lateral resistance characteristic

It should be noted that the lateral resistance is a function of the vertical load. The elastic resistance value, F_e, and the peak resistance value, F_p, of each lateral spring are increased by the additional friction resistance due to the vertical reaction force, R_v, caused by the vertical wheel load. Figure 3-4 shows the loaded tie resistance curve, in which w_e and w_p, are assumed to remain at the same values as in the unloaded tie. The tie-ballast friction coefficient is represented by μ_f.

3.2 QUASI-STATIC BEAM THEORY

On the basis of the foregoing idealization, the track shift under lateral loads will be determined using a beam model. The model can be used for both stationary and moving loads. The model is partially validated by the following means:

1. The model results for the stationary load case are compared with those from the Finite Element code (NIKE3D).

2. The stationary load case is correlated with the available data from the previous U.S. tests.

3. The moving load case results are compared with those published by the SNCF.

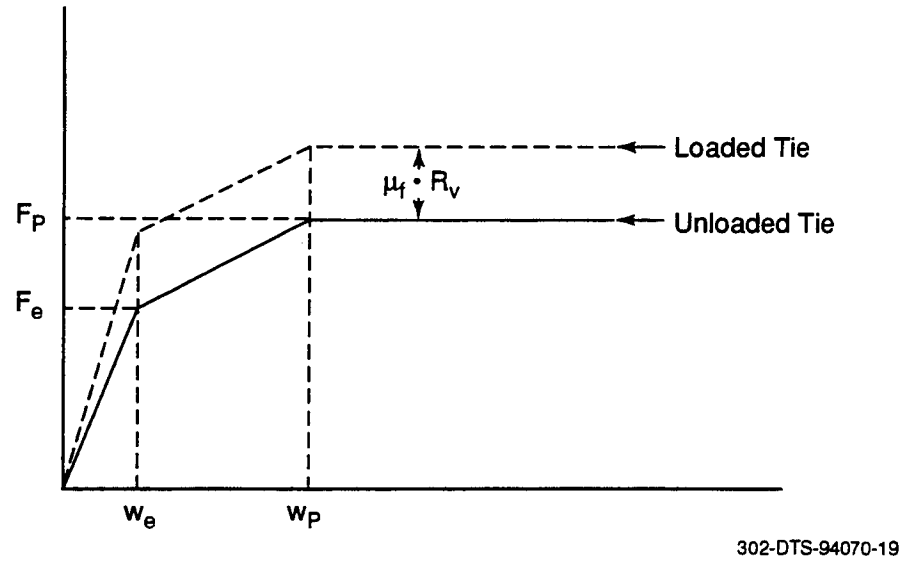

Figure 3-4. Lateral resistance of tie with vertical load

A schematic representation of the track model is shown in Figure 3-5. The model includes a track section of N ties with the tie spacing Δ and an overall length of (N+1) Δ. The rails of the track are represented by an equivalent beam with clamped ends. Provided that the length of the modeled track section is sufficiently large, i.e., greater than the deflected wavelength of the track, the clamped boundary conditions should not adversely affect the track response. This provides the desired "regularity" conditions of zero deflection and slope at positions far from the zone of interest. The lateral resistance of the track is represented by a series of nonlinear springs, as shown on the figure. The relevant equations for the track lateral response are given in Appendix C.

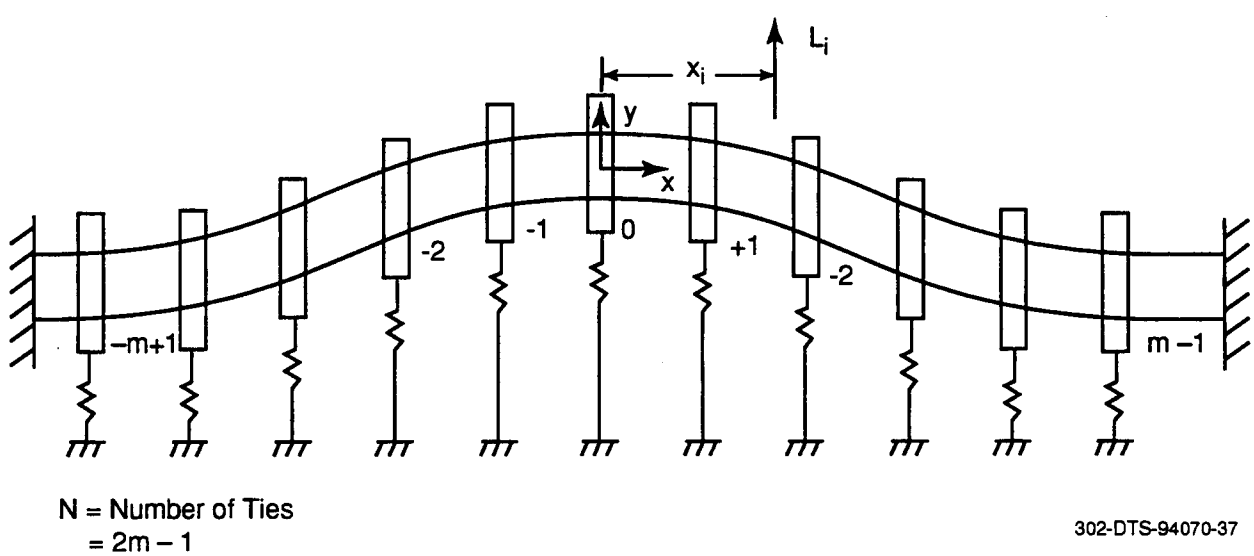

Figure 3-5. Track model schematic

A computer model has been developed to solve the equations presented in Appendix C to determine the track lateral response to applied lateral loads. To verify the model, several special cases are considered. The results of this model are compared with analytical solutions for simple cases, and to the results of finite element models. These are described below.

3.3 STATIONARY LOAD CASE

3.3.1 Linear Resistance Case

By using perfectly elastic springs in the model, the lateral response of the track can be compared to the analytic solution for a beam on an elastic "foundation." Table 3-1 compares results of the track model to the analytic solution and results obtained from the finite element model developed for the following input case.

- Lateral load (L): 20 kips (89 kN).
- Rail: AREA 136.
- Lateral stiffness: 400 lb/in./in. (no peak limit) (2760 kN/m/m).

As shown in Table 3-1, the results of the track model are in excellent agreement with the analytic solution and the results of the finite element model.

As a further comparison, the complete waveforms calculated by the model and the FE model were evaluated for one case which considered the following input.

- Rail: AREA 136.
- Vertical axle load: 37,400 lb (166 kN).
- Lateral axle load: 10,000 lb (45 kN).
- Lateral stiffness: 400 psi (2400 lb/tie, 10.7 kN/tie) at 24 in. (0.6m) spacing with $w_p = 0.25$ in. (6.4 mm)).
- Vertical modulus: 6000 psi (41,000 kN/m^2).

Table 3-1. Comparison of results for track with linear-elastic foundation and no vertical load

	Maximum Deflection in. (mm)	
Model	Positive	Negative
Analytic solution	0.45358 (11.521)	0.01955 (-0.4966)
Stationary model	0.45350 (11.519)	0.01939 (-0.4925)
FE model (NIKE3D)	0.44370 (11.270)	0.01967 (-0.4996)

- Friction coefficient: 0.5.

The two calculated waveforms are shown at peak load in Figure 3-6. For convenience, the NIKE3D results are indicated by the solid line and the stationary load beam analytical model results are indicated by the points. The agreement between the two models is excellent at all points along the waveform with the slight difference at the center. With a finer mesh, the finite element model result could be expected to converge to the analytical solution.

3.3.2 Nonlinear Resistance

The results produced for the stationary load case were then compared with the NIKE3D finite element model to validate the predicted track response for the nonlinear foundation case. For this evaluation, the following track parameters were used. The assumed lateral resistance characteristic is shown in Figure 3-7. The parameters are:

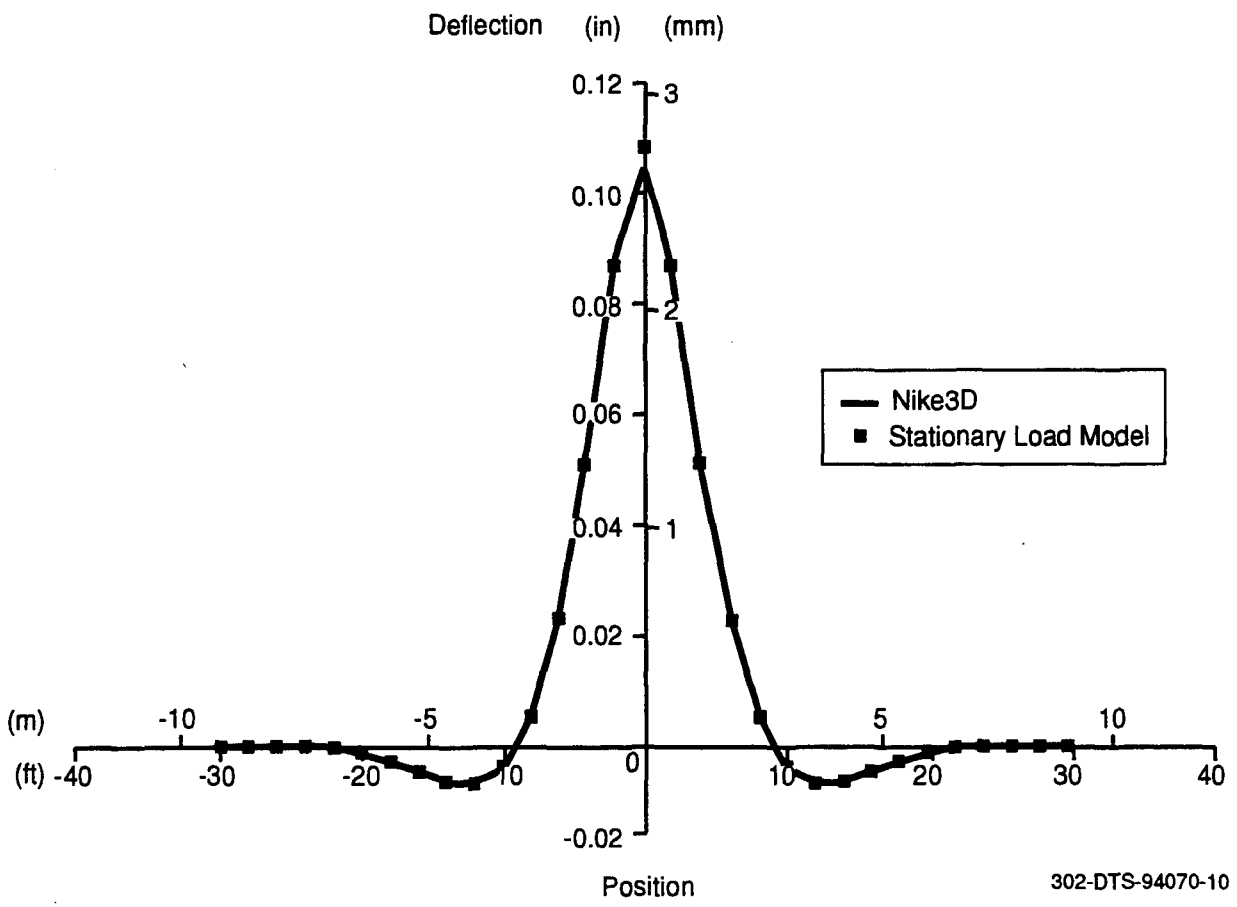

Figure 3-6. Comparison of NIKE3D and stationary load model

- Rail: 136 lb/yd (0.66 kN/m).
- Peak lateral resistance: 1000 lb/tie (4.5 kN/tie).
- Deflection at peak resistance: 0.20 in. (5 mm).
- Tie spacing: 24 in. (0.6m).
- Vertical modulus: 6000 psi (41,000 kN/m^2).
- Friction coefficient: 0.5.
- Vertical axle load: 37,400 lb (166 kN).

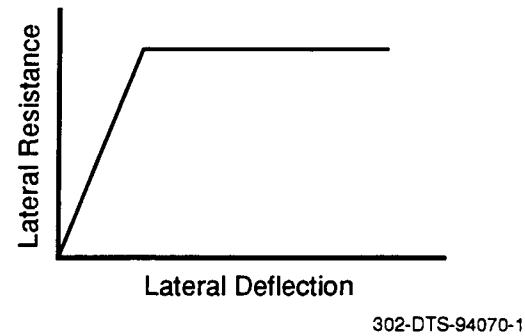

Figure 3-7. Assumed lateral load characteristics

The input parameters selected for this evaluation are representative of an extremely weak track using typical European tie spacing. This low resistance example was selected to ensure that the lateral load resulted in plastic deformation of the track structure and thereby fully exercised the nonlinear track model. In practice, the track can be expected to have a single tie lateral resistance peak of at least 1500 lb (6.7 kN). Thus, the loaded and residual deflections calculated below are substantially greater than would result on a typical tamped track.

The track response was calculated using both models at two lateral load levels (24 kips (107 kN) and 28 kips (125 kN)). Figure 3-8 provides the loaded and unloaded track waveforms for both of the lateral load cases as calculated by the stationary load continuum beam model. The peak and residual deflections for each case, as calculated by the finite element model, are shown by the points in the figure. In both cases the agreement between the two models is excellent.

3.3.3 Numerical Result for Special Case: $V_0 = 0$

This baseline case was experimentally studied in the track lateral pull test (TLPT), (Figure 3-9). No vertical load was applied during these tests. Thus, the peak lateral resistance of the ties is unchanged along the length of the track.

The test case used in this validation was measured on a tangent track which had 0.1 MGT traffic after tamping. In this test section, the following parameters were also measured.

- F_p = 1000 lb/tie (4.5 kN/tie) (tamped ballast, wood tie track).
- w_p = 0.25 in. (6.4 mm).

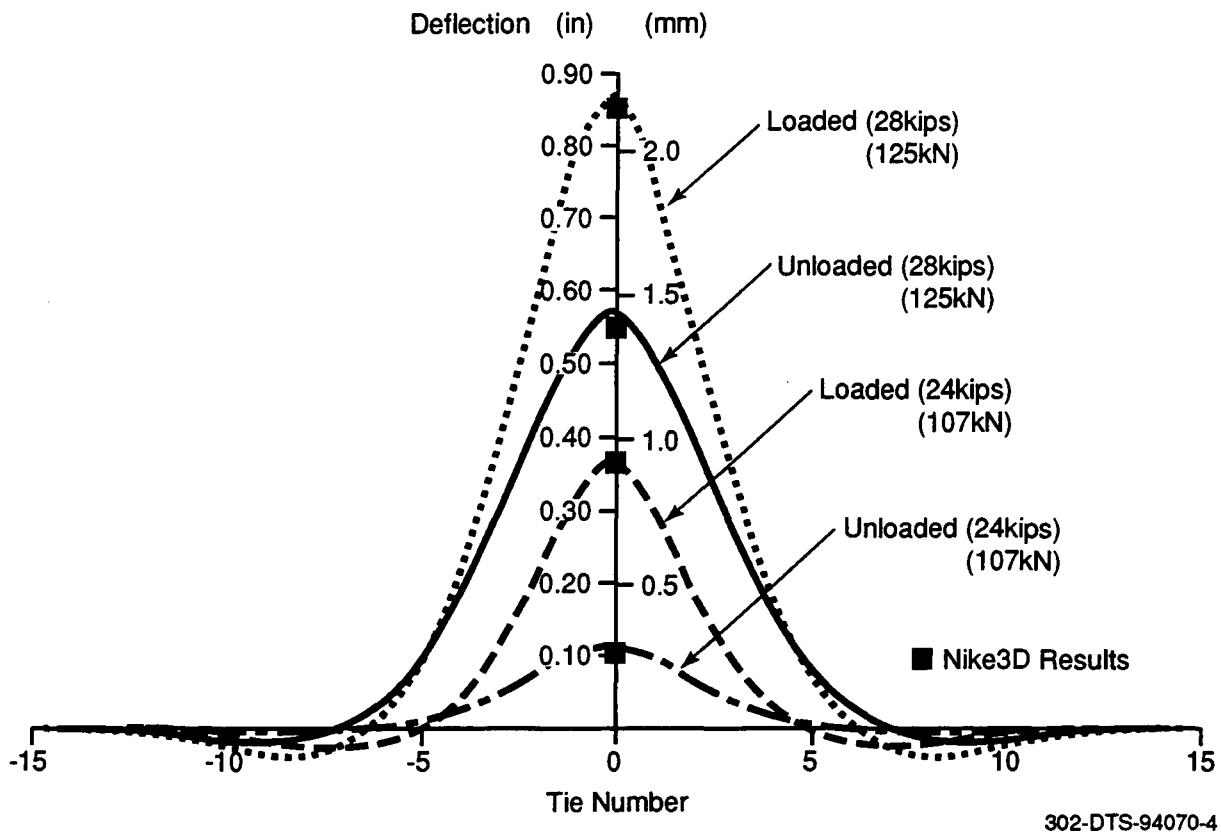

Figure 3-8. Loaded and unloaded track lateral deflection profiles (stationary load case)

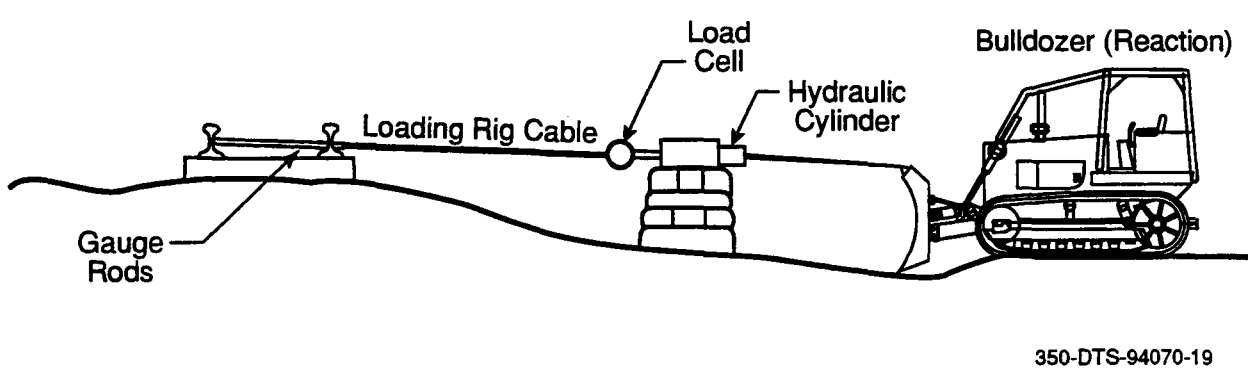

Figure 3-9. Track lateral pull test (TLPT)

- Rail = 136 lb AREA (0.66 kN/m).
- Tie spacing = 20 in. (0.5m).

The model was run with this input to calculate the track lateral response. The dashed line in Figure 3-10 shows the calculated relationship between applied lateral load and track deflection. The measured data is indicated by the solid line. The model response agrees with the data during both loading and unloading of the track, giving an indication that the "elastic-plastic" model provides a reasonable representation of the tie-ballast interface, though in the unloading portion of the curve, the agreement between theory and test is not good, which is attributed to sudden release of the pressure in the hydraulic cylinder.

The stationary load model is studied here as it provides a building block for the complete analysis of the lateral track shift under moving loads. Comparison with results from the moving load case (presented later in this section) reveal that the stationary load underestimates the deflection. Also, the model does not allow the track to accumulate residual deflections under constant amplitude cyclic stationary loads, which is an important feature of track shift. Hence, it is concluded that the stationary load idealization is of limited value and the moving load simulation is an important part of the track shift study.

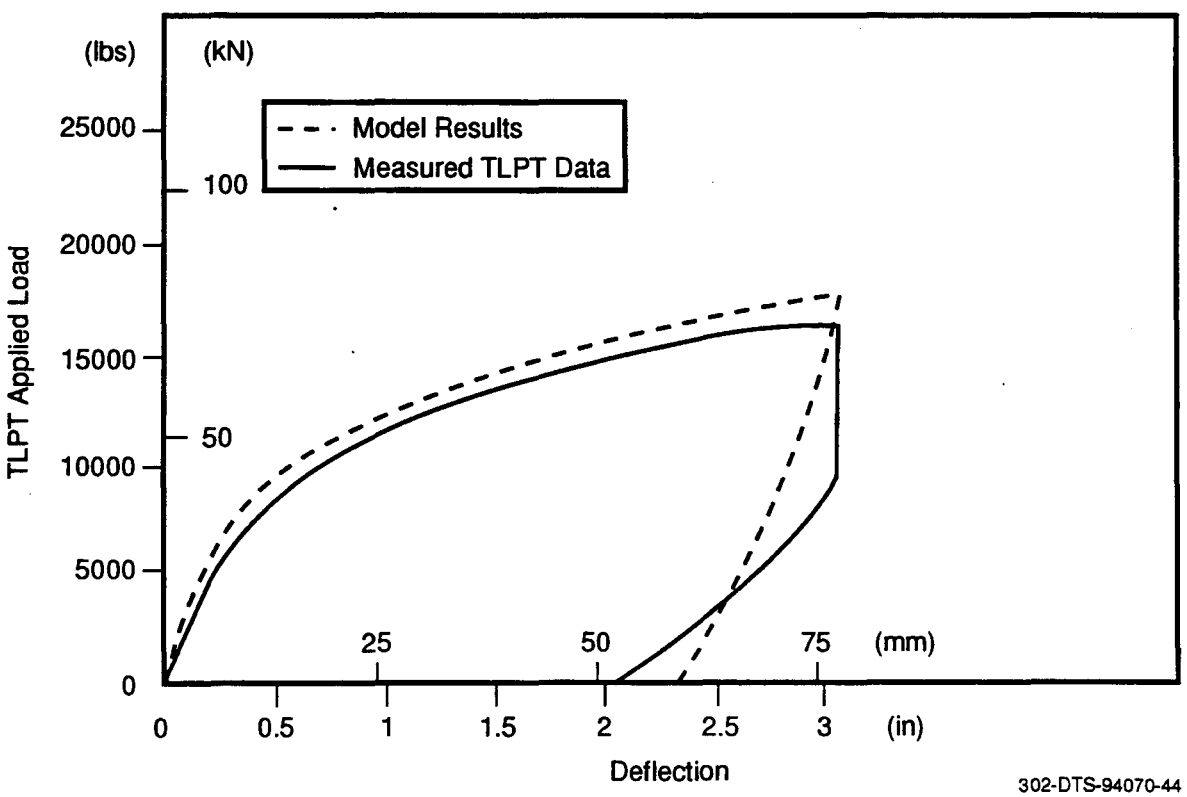

Figure 3-10. Comparison of theoretical and measured data for $V_0 = 0$

3.4 MOVING LOADS

To simulate the moving load, a lateral force is applied to the beam, starting at one end, and is incrementally moved to the other end. The resulting equation for the incremental lateral deflection based on an incremental location of the load is given in Equation (C-10).

3.4.1 Comparison of Track Response Under Stationary and Moving Loads

Figure 3-11 compares the deflected shape of the beam for stationary and moving load cases. The stationary load is applied at x = 0. Figure 3-12 shows the deflection profile of the moving load when the load is at L/4, L/2, 3L/4, and after one pass. Note the negative deflection wave produced ahead of the moving load, which was also recorded in the SNCF tests (1).

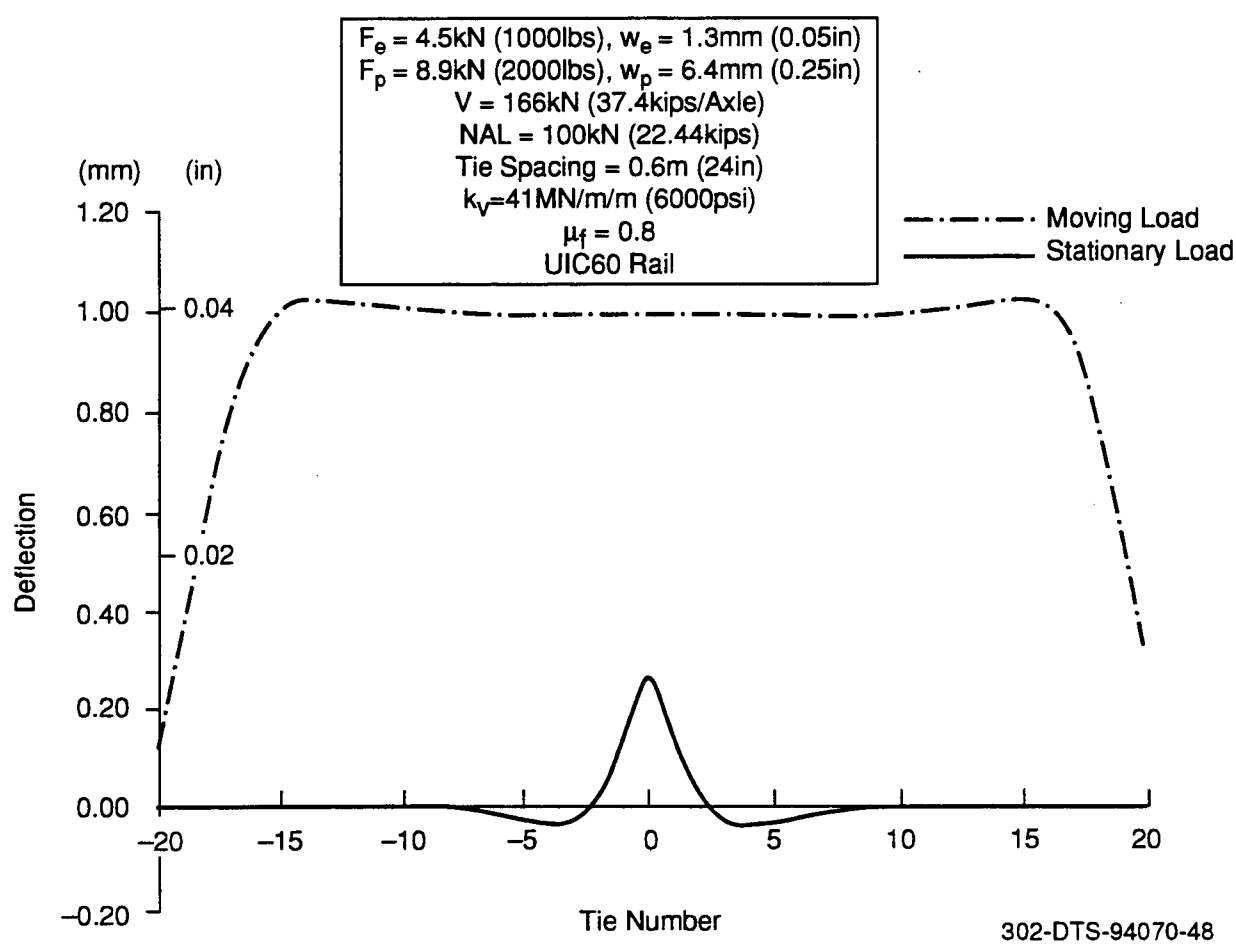

Figure 3-11. Residual deflection

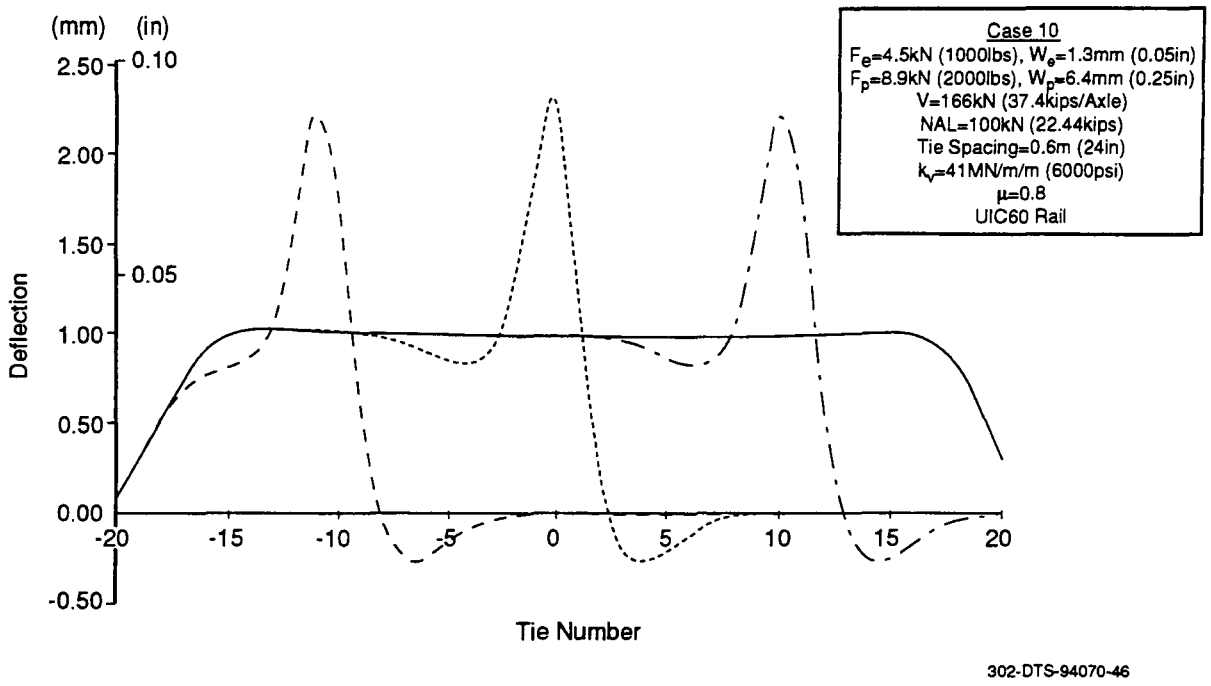

Figure 3-12. Deflection as a function of moving load location

Because of the significant differences in the deflection magnitudes and profiles between the stationary and moving load models, the stationary load cannot be considered appropriate to model the lateral track shift. It should be stated that inertial effects of the track and the speed of the moving load are not considered in the track shift analysis. The significant factor causing the difference in track responses under stationary and moving loads is the nonlinear "elasto-plastic" behavior of the lateral resistance.

3.5 COMPARISON OF THE MOVING LOAD RESULTS WITH SNCF DATA

The moving load model with the idealized tie-ballast resistance relation (Figure 3-3) will now be compared with the SNCF data (1). Table 3-2 shows the SNCF test conditions which were modeled.

With the trilinear tie-ballast lateral resistance, the values for F_e, w_e, F_p, w_p, and k_3 (Table 3-3) are assumed, which are expected to be within the range for the TGV track, although the track parameters were not explicitly stated

Table 3-2. SNCF load spectrum

Vertical Load (per axle) kips (kN)	Lateral Load kips (kN)	No. Passes per Load
18.5 (82.3)	14.68 (65.3)	3
18.5 (82.3)	15.4 (68.5)	3
18.5 (82.3)	16.1 (71.6)	3
18.5 (82.3)	16.8 (74.8)	3
18.5 (82.3)	18.2 (81.1)	3
18.5 (82.3)	19.6 (87.4)	3
18.5 (82.3)	21.1 (93.8)	3

Table 3-3. Tie-ballast lateral resistance parameters

	Case I	Case II	Case III	Case IV
w_e (in.) (mm)	0.1 (2.5)	0.1 (2.5)	0.1 (2.5)	0.1 (2.5)
F_e (lb) (kN)	2000 (8.9)	2500 (11.1)	2500 (11.1)	2500 (11.1)
w_p (in.) (mm)	0.2 (5.1)	0.2 (5.1)	0.3 (7.6)	0.3 (7.6)
F_p (lb) (kN)	3500 (15.6)	3500 (15.6)	3900 (17.4)	3900 (17.9)
k_1 (lb/in.) (kN/mm)	20000 (3.5)	25000 (4.4)	25000 (4.4)	25000 (4.4)
k_2 (lb/in.) (kN/mm)	15000 (2.6)	10000 (1.8)	7000 (1.2)	7000 (1.2)
k_3 (lb/in.) kN/mm)	0	0	0	-300 (-0.05)

by the SNCF researchers. The parameters for the tie-ballast lateral resistance were intentionally set with only small differences to ensure that the model is sensitive to these differences. Cases I, II and III represent the nonsoftening characteristic (constant resistance beyond w_p), and Case IV represents a softening characteristic (beyond w_p).

In addition, the following values were used in the parametric study:

- Tie spacing: 24 in. (0.6m).
- Vertical modulus: 6000 psi (41,000 kN/m/m).
- Friction coefficient: 0.5.
- Vertical axle load: 18.5 kips (82.3 kN).
- Number of ties: 31.

Figure 3-13 shows the results for a cumulative deflection for each pass and load level for the cases described in Table 3-3 and also for the SNCF test data. Lower values of load Cases I and II have lower residual deflections than Cases III and IV, primarily due to their higher k_2 values. At higher lateral loads, this trend is reversed due to lower F_p values for Cases I and II. The residual deflections for Cases I and II begin to increase rapidly, when the deflection reaches their approximate w_p values ($\approx$0.3 in. or 7.5 mm). Likewise Cases III and IV show rapid growth in residual deflections at their w_p ($\approx$0.2 in. or 5 mm).

The difference between III and IV is in the stiffness parameter k_3 beyond their w_p. The softening k_3 for Case IV tends to increase the residual deflection even more rapidly after w_p is reached.

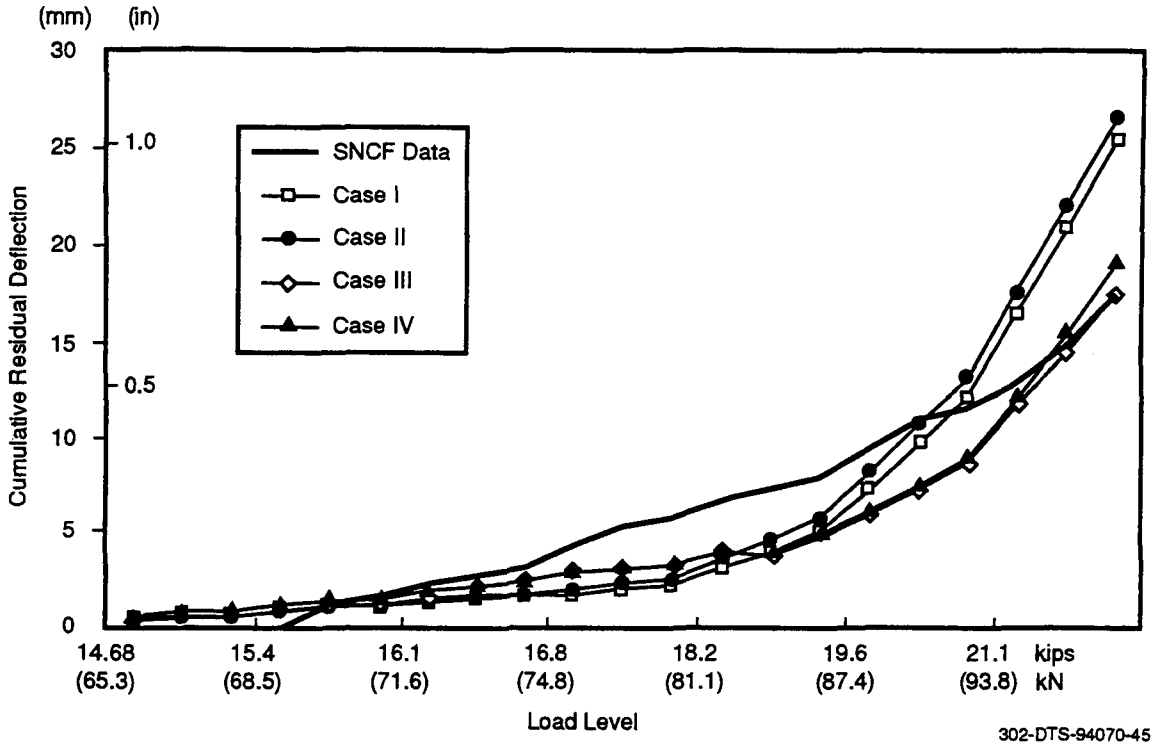

Figure 3-13. Residual deflection under SNCF load spectrum

The reasonable agreement between the theoretical results and the SNCF data gives confidence in the computer model that can account for the most significant parameters of the track lateral resistance.

Of the four test cases, Cases III and IV have been chosen for closer examination. Table 3-4 shows a comparison of the change in residual deflection for each pass and load level of Cases III and IV (Table 3-3). Figure 3-14 gives the change in deflection with each pass for the nonsoftening (Case III) tie characteristic whereas Figure 3-15 gives the results for the softening (Case IV) characteristic. The SNCF data is also in the figures. The moving load cases clearly show the accumulation of deflection with number of passes. Furthermore, the SNCF and the present theoretical data show that for small loads, the change in deflection decreases with each additional cycle at that load level, and hence the track will stabilize. However, at larger load levels, the track deflection does not decrease with passes, and hence stabilization will not occur even for the nonsoftening characteristic. For the softening characteristic in which $k_3 < 0$, this accumulation occurs more rapidly.

Table 3-4. Change in residual deflection with pass number

Load (kips) (kN)	SNCF Data		Case III		Case IV	
	(mm)	(in.)	(mm)	(in.)	(mm)	(in.)
14.68 (653)	0	0.0000	0	0.0000	0	0.0000
14.68	0	0.0000	0.23	0.0091	0.23	0.0091
14.68	0	0.0000	0.15	0.0059	0.15	0.0059
15.4 (68.5)	0.09	0.0035	0.39	0.0154	0.39	0.0154
15.4	1.16	0.0457	0.26	0.0102	0.26	0.0102
15.4	0.27	0.0106	0.18	0.0071	0.18	0.0071
16.1 (71.6)	0.7	0.0276	0.4	0.0157	0.4	0.0157
16.1	0.43	0.0169	0.27	0.0106	0.27	0.0106
16.1	0.35	0.0138	0.18	0.0071	0.18	0.0071
16.8 (74.8)	1.25	0.0492	0.4	0.0157	0.4	0.0157
16.8	0.95	0.0374	0.27	0.0106	0.27	0.0106
16.8	0.5	0.0197	0.18	0.0071	0.18	0.0071
18.2 (81.1)	0.87	0.0343	0.68	0.0268	0.68	0.0268
18.2	0.63	0.0248	0.47	0.0185	0.47	0.0185
18.2	0.6	0.0236	0.44	0.0173	0.45	0.0177
19.6 (87.4)	1.6	0.0630	1.28	0.0504	1.31	0.0516
19.6	1.45	0.0571	1.31	0.0516	1.36	0.0535
19.6	0.65	0.0256	1.31	0.0516	1.39	0.0547
21.1 (93.8)	1.45	0.0571	2.94	0.1157	3.24	0.1276
21.1	1.93	0.0760	2.99	0.1177	3.46	0.1362
21.1	2.92	0.1150	3.01	0.1185	3.63	0.1429

3.6 PARAMETRIC STUDY

To further understand the track resistance parameters and lateral load levels under which the track shift deflection will stabilize, a parametric study has been conducted using the moving load model. The parameters are shown in Table 3-5. The calculations are performed for 136 lb (0.66 kN/m) rail, with tie spacing of 24 in. (0.6m).

For several combinations of μ_f, NAL/V and F_p, numerical results for cumulative residual deflections under several wheel passes are evaluated and presented in Figures 3-16 to 3-18 for NAL/V of 0.4, 0.5, and 0.6, respectively. The resulting track shift for each of the cases studied is classified as stabilized (S) or progressive (P) track conditions. There are also a combination of parameters for which the residual deflections are negligible, which are represented by (E) in the figures.

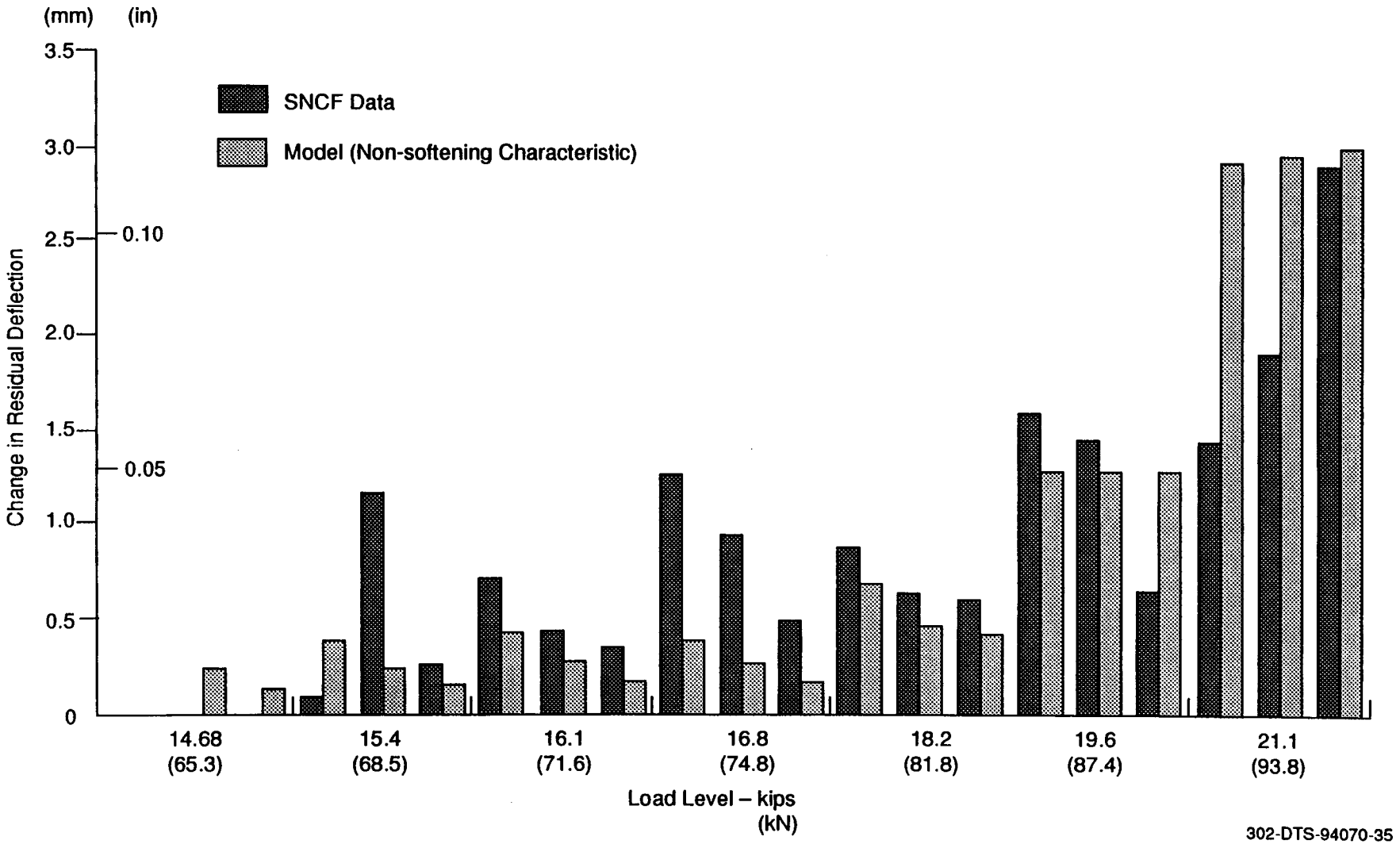

Figure 3-14. Change in deflection, nonsoftening characteristic (Case III)

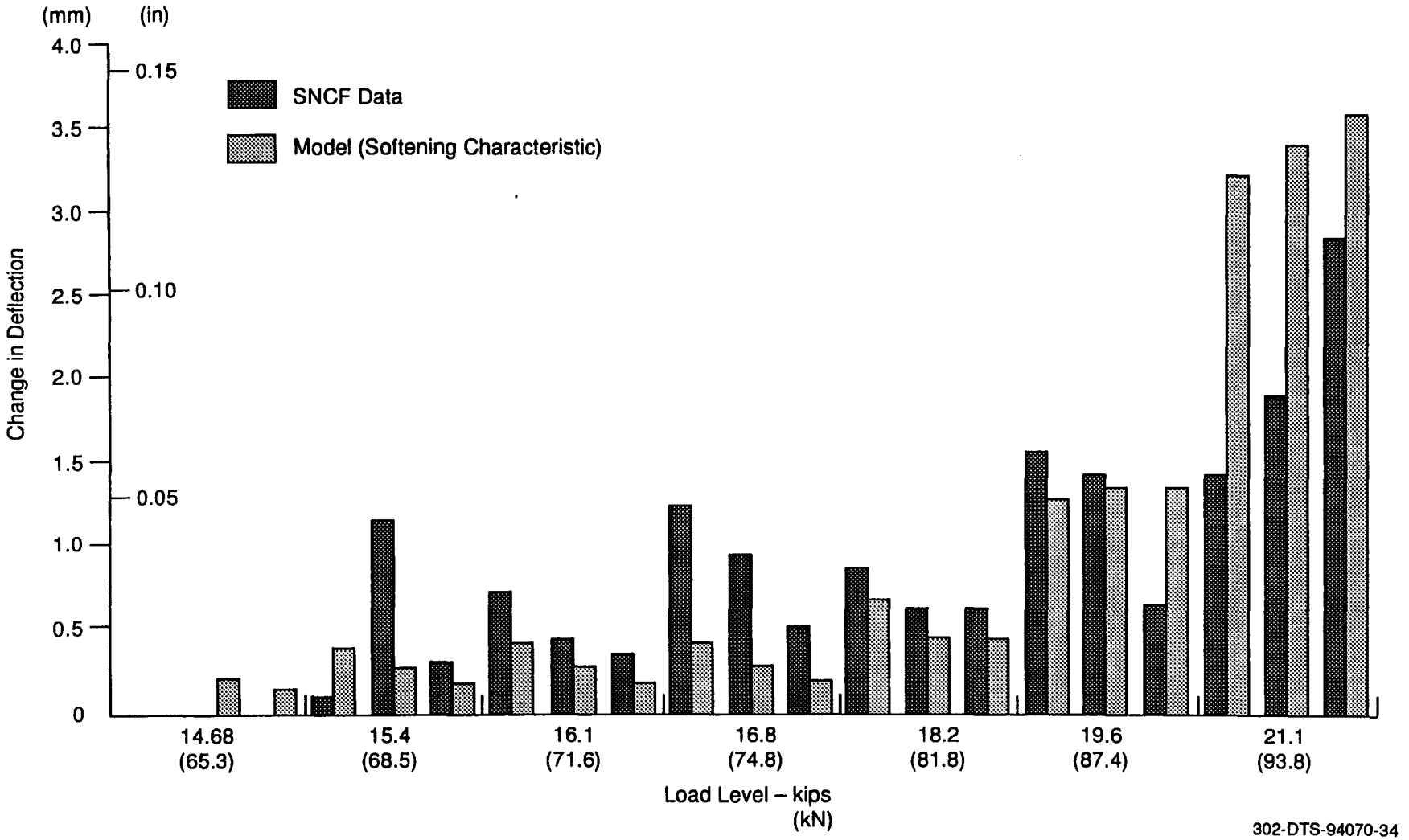

Figure 3-15. Change in deflection, softening characteristic (Case IV)

Inspection of the theoretical data shows that both μ_f and F_p play important roles in controlling the track shift behavior for a given NAL/V. Case I in Figure 3-16 can represent a freshly tamped condition with low μ_f (0.4) and F_p (2000 lb). Even for NAL/V = 0.4, the deflections are not stable. Likewise even for consolidated conditions, such as in Figure 3-18 Cases I and II, NAL/V = 0.6 is not acceptable, as it leads excessive unstable growth of deflection with number of passes. In these cases μ_f is taken as 0.4, which may result if the concrete tie bottom becomes smooth in revenue service due to grinding action between the tie surface and the ballast beneath it.

Table 3-5. Assumed parameters

Symbol	Parameter	Range/Value
V	Vertical axle load	37.4 kips (166 kN)
F_e	Elastic resistance	1000 lb (4.5 kN)
w_e	Elastic displacement	0.05 in. (1.3 mm)
F_p	Peak resistance	2000, 3000, 4000 lb (8.9, 13.4, 17.8 kN)
w_p	Displacement at peak	0.25 in. (6.4 mm)
k_3	Softening stiffness	0
μ_f	Tie-ballast friction coefficient	0.4, 0.8
NAL/V	Net axle force ratio	0.4, 0.5, 0.6

In the above analysis, thermal loads are not included, which may further reduce the net axle loads for the same levels of track shift.

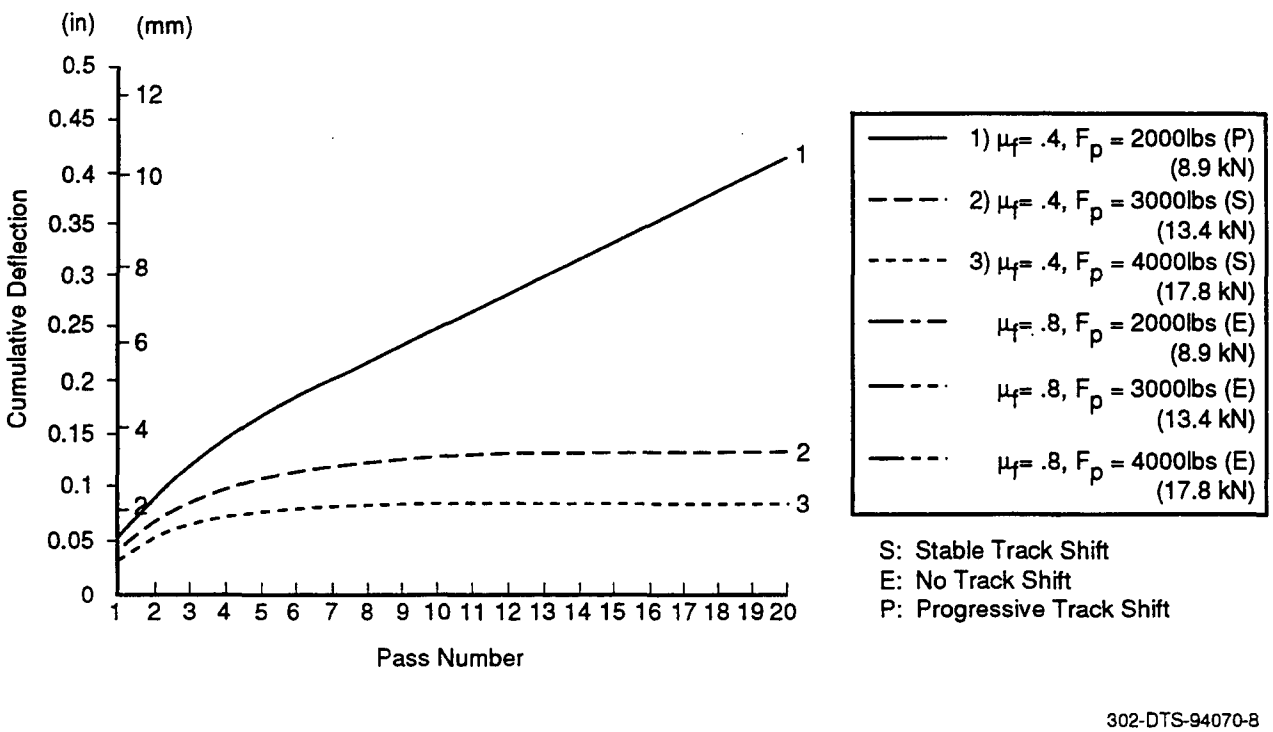

Figure 3-16. Cumulative deflection versus number of passes for NAL/V = 0.4

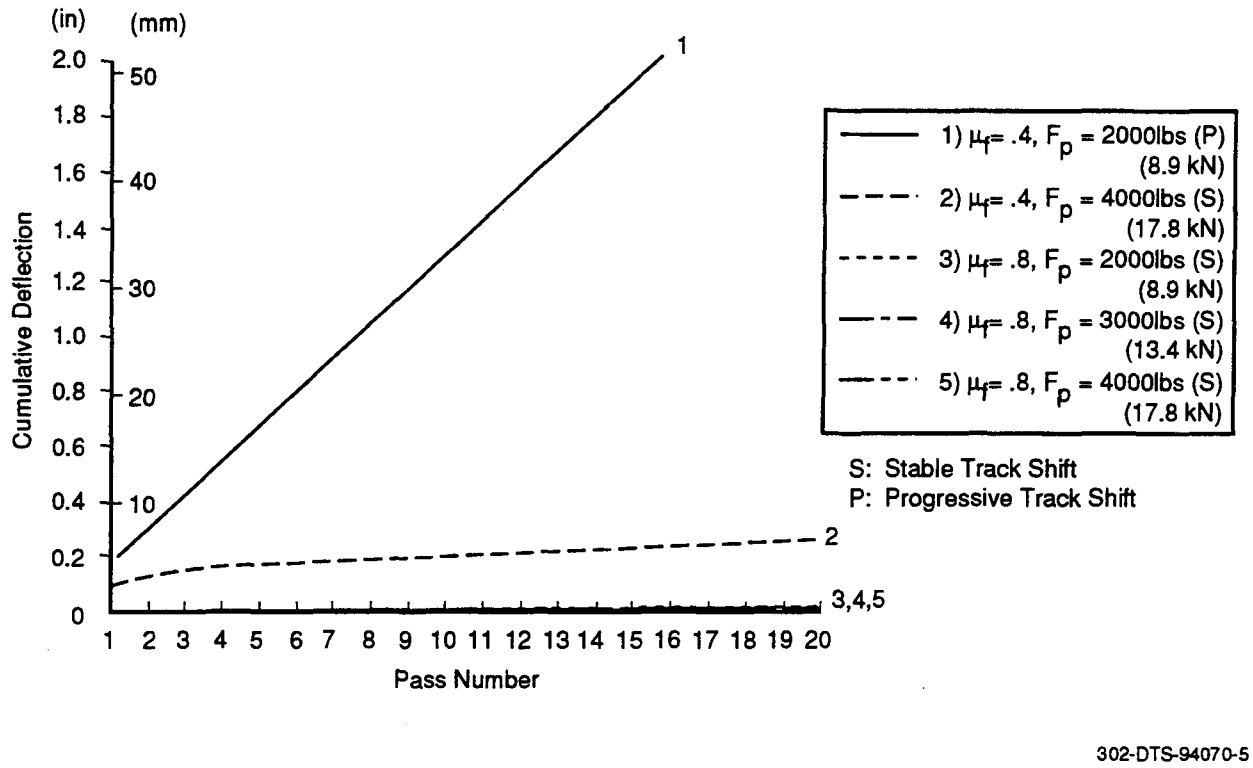

Figure 3-17. Cumulative deflection versus number of passes for NAL/V = 0.5

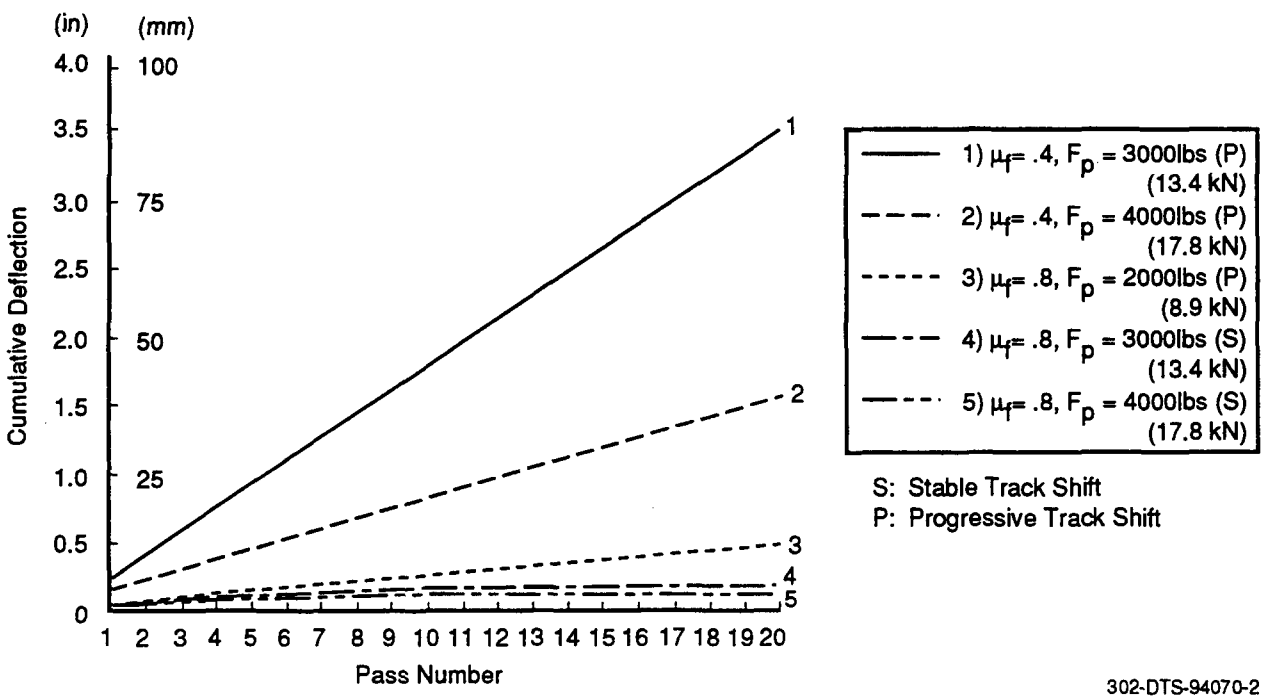

Figure 3-18. Cumulative deflection versus number of passes for NAL/V = 0.6

In Figure 3-18 Case (4) represents a consolidated track condition which stabilizes at a lateral deflection (≈ 5 mm), (for NAL/V = 0.6). According to the existing SNCF practice, this is not allowable from ride comfort and other safety considerations. Hence, another constraint on net axle loads for the stabilized track deflection situation is the maximum deflection permissible from track maintenance point of view.

3.7 TRUCK LOAD EFFECTS

In the previous subsections, each axle load influence on track lateral deflection is evaluated separately from that of its adjacent axle. In this subsection, both axles of a truck are simultaneously treated. For simplicity, both axles are considered to exert equal lateral loads on the track. Thus, a single truck pass represents two equivalent axle passes on the track. However, the finite number of passes is not important in this study, which is intended to evaluate the residual deflections after a sufficiently large number of passes.

The computer code for the single axle case has been modified for the truck load case. Figure 3-19 shows a comparison of residual deflection results for the single axle and the truck load cases. It is seen that the results are close, and the stable characteristic response is predicted in both cases for the assumed net axle force ratio of 0.5.

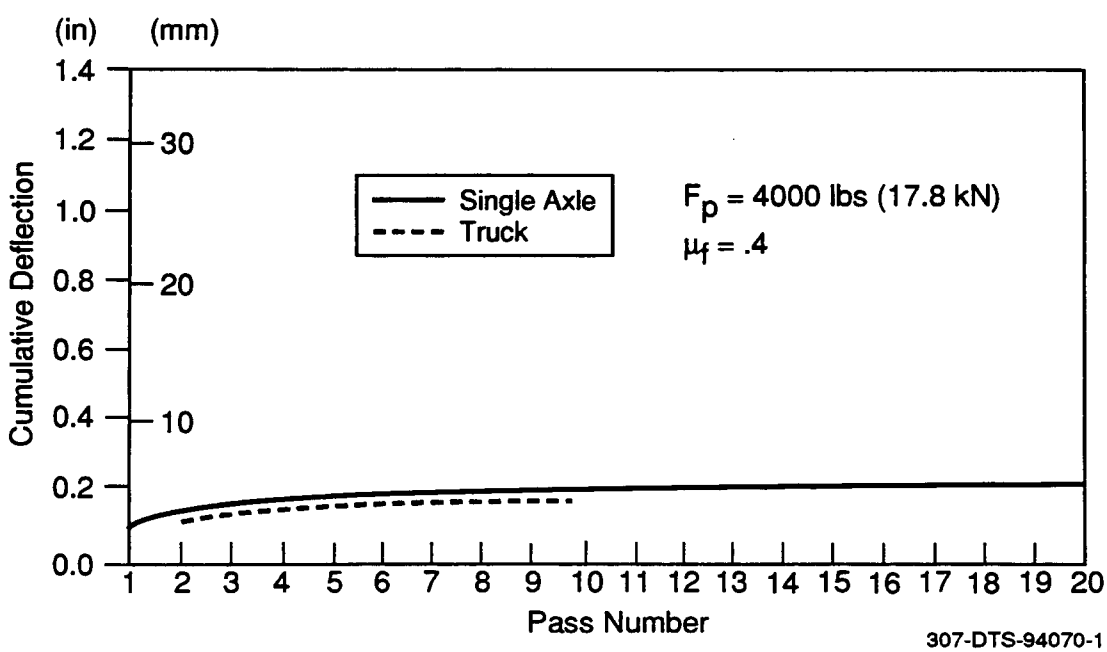

Figure 3-19. Comparison of single axle versus truck load simulation (NAL/V = 0.5)

Figure 3-20 provides another comparison between the single axle and truck load cases for a larger net axle force ratio (0.6). Progressive track shift characteristic is predicted in both cases.

The truck load simulation gives slightly lower residual deflections as one would expect due to the stabilizing influence of one adjacent axle on the other (see Appendix B). The single axle simulation overestimates the deflection by about 15 percent and is considered to be on the conservative side. The single axle simulation for track shift was considered to be adequate in previous SNCF studies (5).

3.8 SUMMARY

1. A moving load model is required to understand and quantify the lateral track shift observed in the tests with moving lateral loads.

2. A key to understanding the track shift phenomenon is a proper representation of the tie ballast lateral resistance. The proposed trilinear idealization with an elastic stiffness k_1

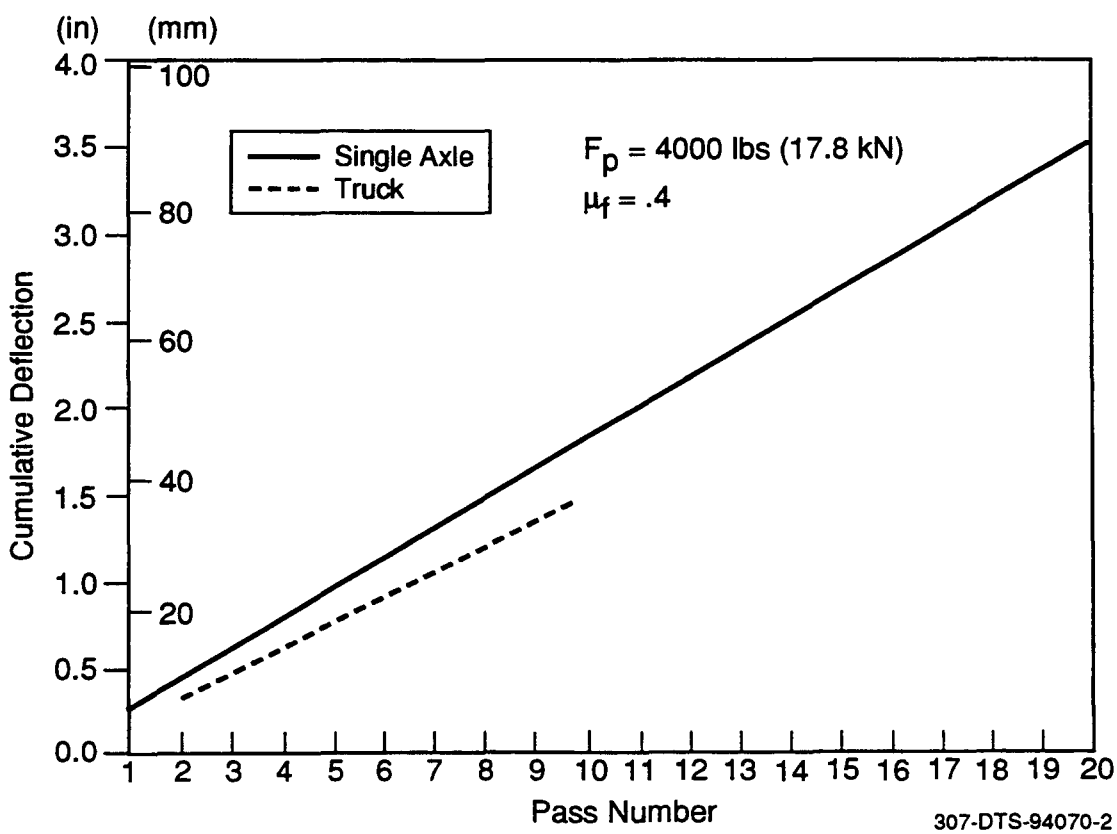

Figure 3-20. Comparison of single axle versus truck load simulation (NAL/V = 0.6)

(up to w_e displacement), hardening stiffness k_2 (up to w_p displacement) and thereafter a zero or softening stiffness k_3 seems to be adequate for modelling the track shift behavior under moving lateral loads. The elastic displacement is typically under 2 mm and is a convenience to facilitate numerical work using the algorithm developed in this work. The exact value of the elastic point is not important to determine whether or not the track shift stabilizes, provided that the limit is not chosen to be unduly large. The peak value of the resistance F_p and the displacement w_p at this point are critical for the track shift analysis. Another important parameter for the analysis is the tie ballast friction coefficient which controls the tie lateral resistance under vertical axle loading.

3. On the basis of net axle force ratio and track parameters, the track shift can be quantified as a function of number of vehicle passes. Unstable growth of track deflections under vehicle passes must be avoided by proper design, maintenance of the track and controlling net axle force. Even stabilized track shift may have to be limited at a preassigned limit as determined from ride comfort, wheel climb or gauge widening considerations.

4. Moving single axle load simulations seem to be adequate and conservative for track shift predictions. Moving truck load simulations give smaller residual deflections, but do not change the characteristic response of track shift.

5. The methodology developed in this report for moving loads is also applicable for evaluation of track degradation in the vertical plane, under repeated axle passes. Likewise the gage widening phenomenon involves moving loads and elastoplastic restraints, causing permanent rail deformations. Stationary load idealizations for this class of problems may not be adequate, as found in the track shift analysis presented here. Residual vertical track deflections and residual changes in the gage should be studied as functions of the number of wheel passes and limiting safe conditions identified.

4. THE VEHICLE-TRACK DYNAMIC MODEL

The purpose of the vehicle-track dynamic model is to characterize and quantify the lateral loads generated by the vehicle on the track, and to predict potential failure modes such as wheel climb, ride quality deterioration and gauge widening. The lateral loads may be generated from curving action and/or in the negotiation of existing lateral misalignment in the track. These loads provide the inputs to the track model described in the previous section, which determines the cumulative growth of misalignments and potential unstable track shift conditions.

In a previous report (1), the vehicle dynamic code SYSSIM was employed in a preliminary evaluation of vehicle lateral loads and conditions at which failure modes can occur. A complete vehicle model was initially developed to include the full set of parameters for all three types of vehicle in the TGV: locomotive, lead car, and intermediate car. It was later demonstrated (Appendix D) that a vehicle with a single truck representation was adequate for the track shift studies reported herein. The complete vehicle model was accordingly reduced to the form presented in Figures 4-1 through 4-4 in which the trailing truck is replaced by a guided mass that is connected to the car body via a secondary suspension system. This elimination of the trailing truck and its degrees of freedom was done to substantially reduce the level of computational effort so that the requisite vehicle-track dynamic simulations could be effectively performed on a personal computer.

The degrees of freedom for all bodies in the reduced vehicle model are shown in Figures 4-1 and 4-2. These are lateral and vertical translations as well as roll and yaw rotations. In addition, there are pitch rotations for the truck frame and the car body. Connections between these bodies are shown in Figures 4-3 and 4-4. The connections between the axles and the truck frame and between the truck frame and the car body represent the primary and secondary suspension systems, respectively. Both suspensions have parallel stiffness and damping elements that are oriented to control motions in the vertical, lateral, and yaw directions. In Figures 4-3 and 4-4, the various suspension elements are identified. Note that "k" denotes a stiffness element and "c" indicates a damping element. The subscripts "1" and "2" refer to the primary and secondary suspensions, whereas "V", "L", and "Y" refer to the vertical, lateral, and yaw degrees of freedom, respectively.

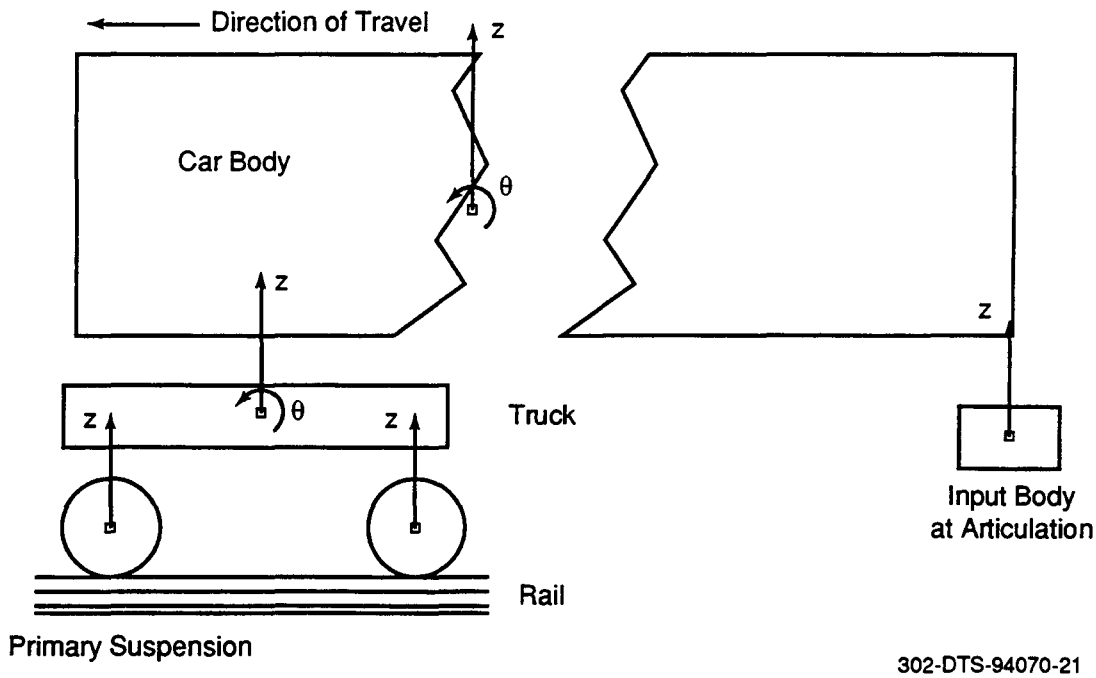

Figure 4-1. Vehicle longitudinal view showing vertical translation and pitch degrees of freedom

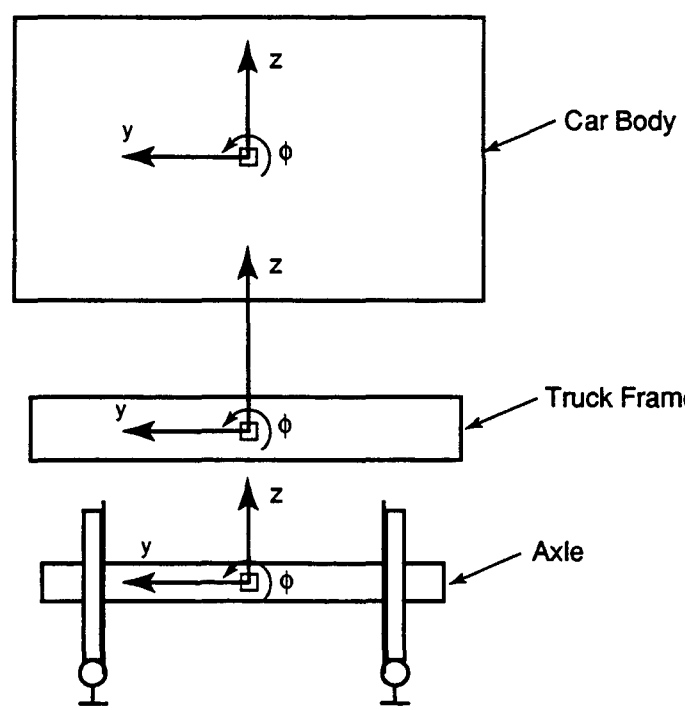

Figure 4-2. Vehicle lateral view showing vertical translation, lateral translation and roll degrees of freedom

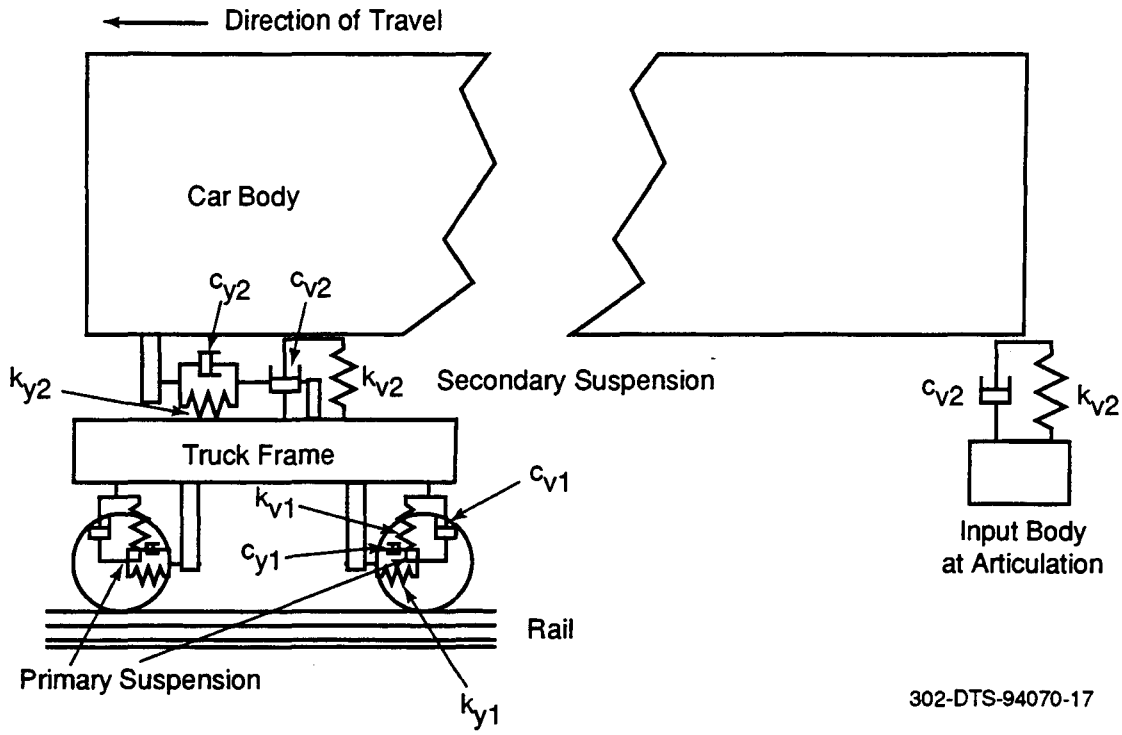

Figure 4-3. Vehicle longitudinal view showing primary and secondary suspension elements

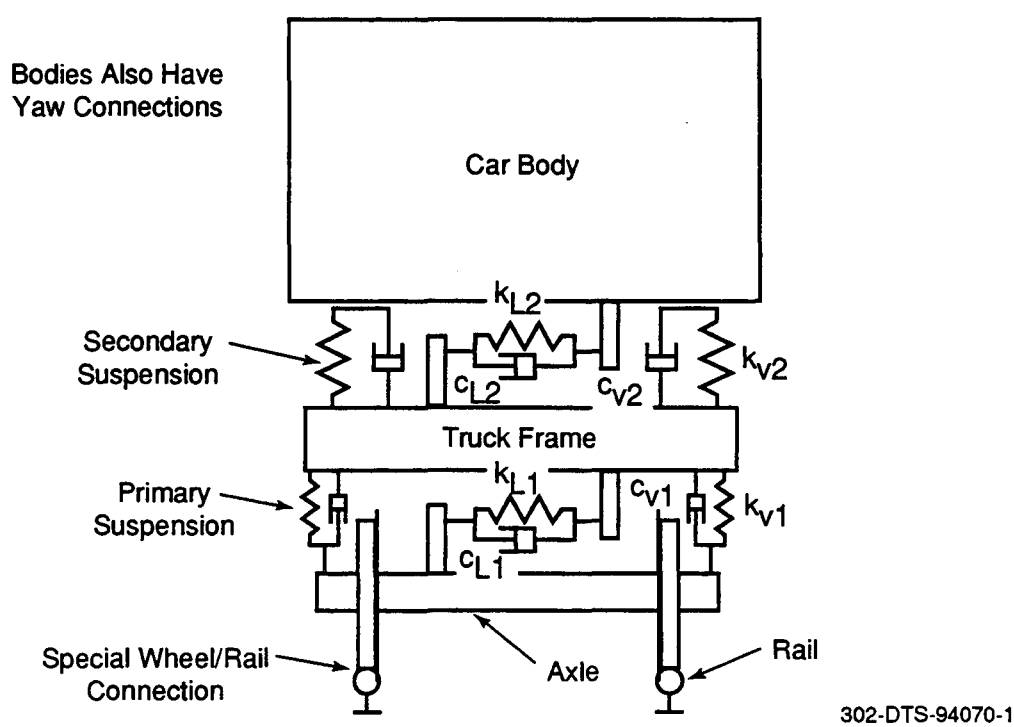

Figure 4-4. Vehicle lateral view showing primary and secondary suspension elements

Figure 4-5 shows the "track model" previously used with the SYSSIM code. While SYSSIM does include the rolling contact connection between the wheel and rail, it does not allow for a proper representation of the actual track structure. Specifically, *rail inertia is neglected* and there are only parallel springs and dampers in both lateral and vertical directions between *the wheel and ground. This means that the model does not properly represent the effects of rail mass, ties and ballast with lateral resistance.* Track compliance is important in the evaluation of loads and for an accurate assessment of wheel climb. The SYSSIM track model is therefore inadequate for the present study of track shift.

A more general vehicle dynamic code called OMNISIM has been developed to facilitate improved modelling of the track in vehicle-track interaction studies. A comprehensive description of OMNISIM is presented in Appendix E. While the previously-discussed reduced vehicle model was employed for the work reported here, future studies can be performed on consists with two-truck vehicle representations. For this purpose, OMNISIM has also been installed on a UNIX workstation at Foster-Miller.

Figures 4-6 and 4-7 show the basic OMNISIM "track module" which represents two short lengths of rail and a single tie. All three bodies have lateral and vertical degrees of freedom. The rails also have pitch and yaw (i.e., bending) degrees of freedom. The track module is presently assumed to move with the vehicle, and therefore any longitudinal degrees of freedom are neglected. Fifteen interconnected modules are currently used in OMNISIM to represent the complete track structure.

As shown in Figure 4-8, the individual track modules are coupled to each other by enforcing continuity of the translational, pitch, and yaw degrees of freedom. Since the short rail sections are considered to be rigid bodies, these connections require the specification of translational and

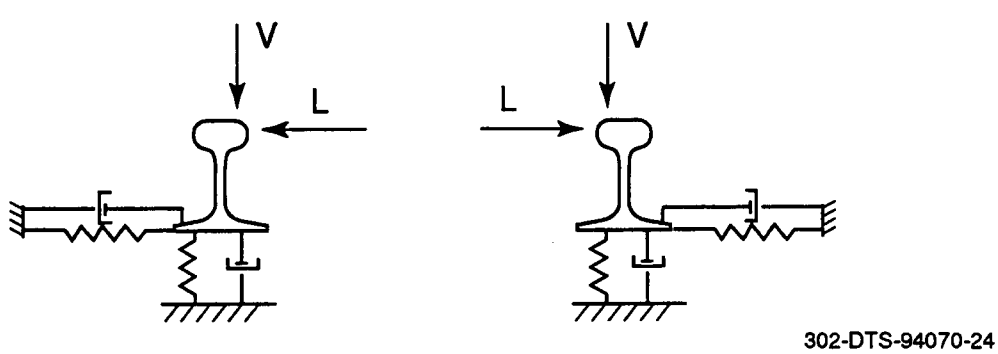

Figure 4-5. SYSSIM track model showing rails independently connected to ground

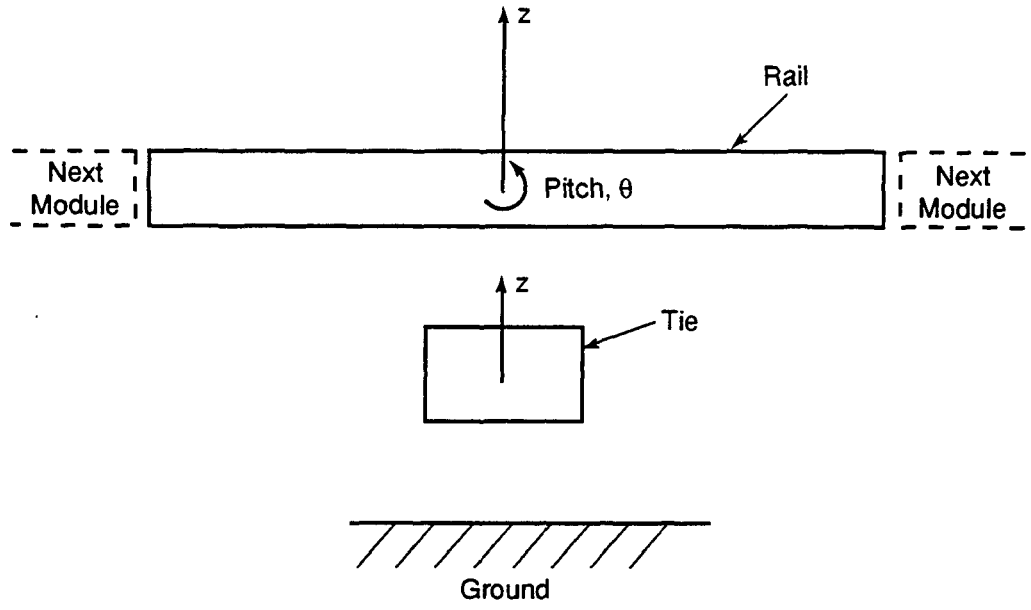

Note: Rails also have a yaw degree of freedom

302-DTS-94070-28

Figure 4-6. Track module longitudinal view showing vertical translation and pitch degrees of freedom

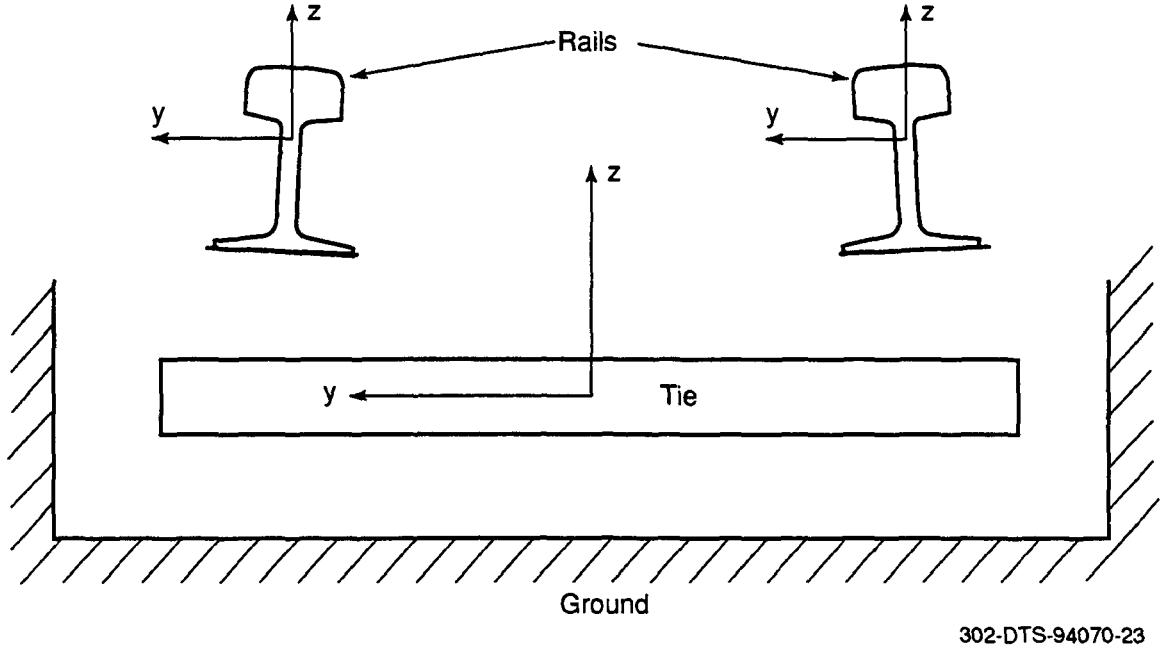

302-DTS-94070-23

Figure 4-7. Track module lateral view showing vertical and lateral translation degrees of freedom

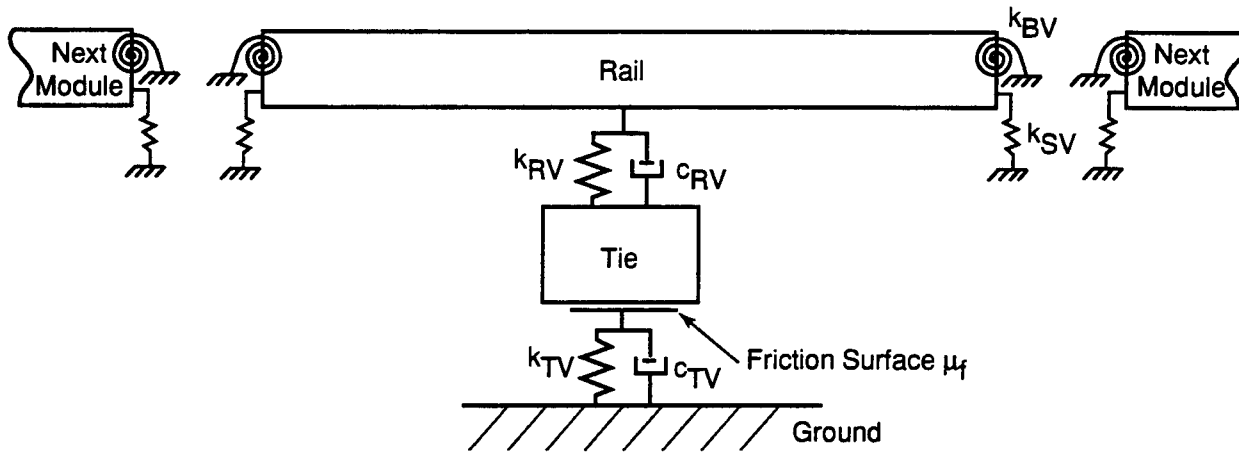

Note: Similar connections exist in the lateral plane with rail stiffnesses k_{BL} and k_{SL}

302-DTS-94070-25

Figure 4-8. Track module longitudinal view showing connection elements

rotational springs that represent the shear and bending stiffnesses of the rail in the lateral and vertical planes. The required intermodule stiffnesses are computed from the given sectional properties of rail using a lumped parameter approach. These stiffnesses are shown in Table 4-1 for the 136 pound rail that is studied here.

Referring to Figure 4-9, lateral and vertical connections between each rail segment and a tie are made using parallel springs and damping elements. The vertical spring and damper are denoted by k_{RV} and c_{RV}, while the lateral spring and damper are k_{RL} and c_{RL}. These elements allow for the motion of the rails relative to the tie that results from the deformation of fastening components such as rail pads. In turn, each tie is connected to ground through a vertical spring k_{TV} ,which is derived from the track foundation modulus k_V , and a damper c_{TV}. There is also a lateral friction element μ_f with a limiting force that is a function of the vertical load. With no vertical load on the tie, it is equal to the tie peak resistance F_p. These elements allow for the motion of the tie relative to the ballast.

Thus, the OMNISIM track model is consistent with the requirements of the track residual deflection model discussed in Section 3.

Table 4-1. Assumed model parameters

I. Vehicle Parameters -

Body	Weight	Mass
Car Body	95,000 lb (422 kN)	43.183 (Mega Grams)
Bogie Frame	9,900 lb (44 kN)	4.5 (Mega Grams)
Axle	4,620 lb (20.6 kN)	2.1 (Mega Grams)

Suspension/Connection Parameters -

Suspension	Degree of Freedom	Stiffness (MN/m or MN/rad)	Damping (MN-s/m or MN-s/rad)
Primary Suspension (Axle to Bogie)	Lateral	3.00E+01 (k_{L1})	3.00E-01 (c_{L1})
	Vertical	1.67E+00 (k_{V1})	5.00E-03 (c_{V1})
	Yaw	6.20E+01 (k_{Y1})	6.20E-01 (c_{Y1})
Secondary Suspension (Bogie to Car)	Lateral	6.10E-01 (k_{L2})	1.00E-03 (c_{L2})
	Vertical	2.50E+00 (k_{V2})	5.00E-02 (c_{V2})
	Yaw	6.40E-01 (k_{Y2})	2.50E-02 (c_{Y2})
Wheel Profile	AAR1B, TGV		

II. Track Parameters -

Parameter	Assumed Values
Rail	AREA 136, UIC 60
Tie	275 lb (1.2 kN), 800 lb (3.6 kN)
Tie Spacing (Δ)	24 in. (0.6m)
Tie Peak Resistance (F_p)	2000 lb (8.9 kN) - 4000 lb (17.8 kN)
Tie Deflection at Peak Resistance (w_p)	0.10 in. (2.5 mm) - 0.30 in. (7.6 mm)
Tie to Ballast Friction Coefficient (μ_f)	0.5
Track Foundation Modulus (k_v)	6000 psi (41 MN/m/m, 10,000 psi (69 MN/m/m)
Track Curvature	0 deg, 2 deg
Track Superelevation	0, 5.75 in. (146 mm)

III. Track Connections -

Connection	Degree of Freedom	Stiffness (MN/m)	Damping (MN-s/m)
Rail to Tie	Lateral	1.75E+02 (k_{RL})	1.75E-01 (c_{RL})
	Vertical	1.75E+02 (k_{RV})	1.75E-01 (c_{RV})
Tie to Ballast	Lateral	F_p/w_p (k_{TL})	1.0E-02 (c_{TL})
	Vertical	$k_v \bullet \Delta$ (k_{TV})	2.0E-02 (c_{TV})
Rail Module to Module	Lateral Shear	56.0 (k_{SL})	-
	Lateral Bending*	1.74 (k_{BL})	-
	Vertical Shear	335.0 (k_{SV})	-
	Vertical Bending*	10.4 (k_{BV})	-

*Units are MN-m/rad

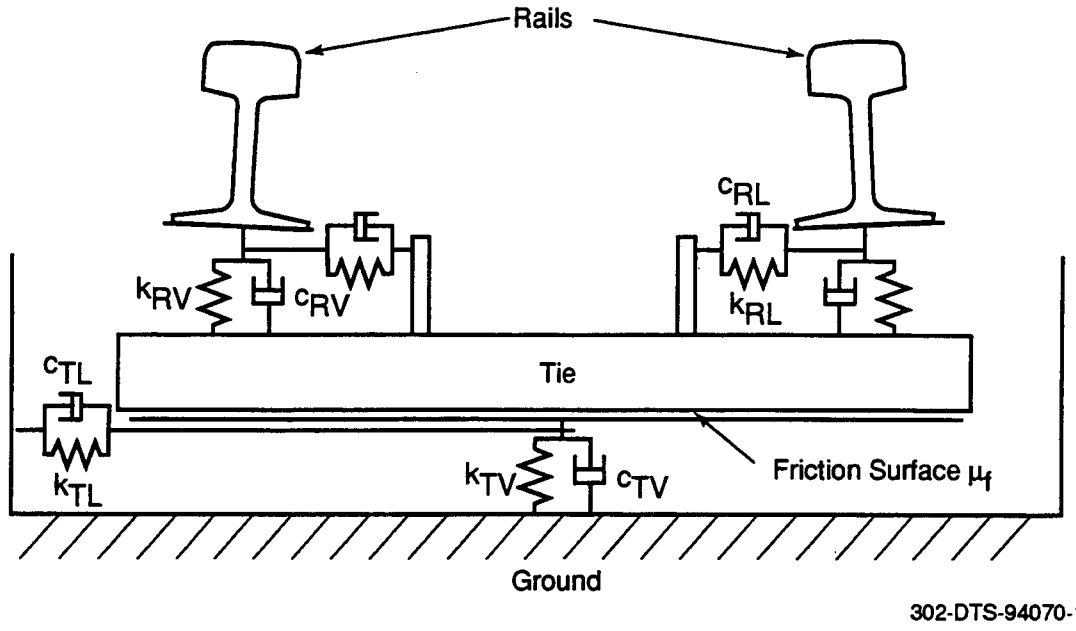

Figure 4-9. Track module lateral view showing connection elements

In summary, the OMNISIM track representation employed in the present study has the following features:

- The model directly incorporates the track structure compliance using the known ballast stiffness parameters in the vertical and the lateral planes. The model results will show the influence of ballast tamping and consolidation on the vehicle performance.

- An improved wheel climb assessment can be made with the model, since it can predict the track lateral movement under the wheel passage.

- The model accounts for rail and tie inertia as well as damping in the ballast. It can, therefore, represent the influence of concrete and wood tie track on the vehicle performance.

Although the OMNISIM track model gives the instantaneous lateral deflections under the loaded wheels, in its present form, it cannot compute the accumulated residual deflections due to the passage of each wheel. Therefore, the track residual deflection model presented in Section 3 is required and forms a key to the track shift study. The load inputs to the residual deflection

model are derived using the proposed OMNISIM code. The lateral misalignment input required in the OMNISIM code can also be updated for subsequent vehicle passes using the output of the track residual deflection model. In this manner, the two models are partially coupled to provide an adequate analysis of the track shift problem.

4.1 MODEL PARAMETERS

Table 4-1 presents the vehicle and track stiffness and damping parameters for the OMNISIM model which are employed in the following study. A high-speed vehicle was assumed. The data was primarily obtained from available vehicle specifications and experimental data.

Whereas the stiffness and damping parameters in the vehicle primary and secondary suspensions are fairly well defined, only limited data exists for damping in the track components. A high damping coefficient is assumed between the rail and the tie to represent a "rigid" connection between the two in the fasteners. A low damping coefficient is assumed between the tie and the ballast so that the tie response is essentially controlled by its resistance as defined in the previous section. It is believed that the trends in the track response will not be different if measured values of damping were to be used in the numerical study.

The model based on the OMNISIM code has been partially verified through several special numerical examples which degenerate to the SYSSIM code. The model results for the tie reaction distribution, the loaded track lateral stiffness and the track deflections under the loads are also compared with known analytic solutions. For example, Figure 4-10 presents a comparison of the tie reactions with the known analytic solution for a beam on the Winkler foundation.

4.2 PARAMETRIC STUDY

Preliminary parametric results obtained from the improved track representation using the OMNISIM code are provided for the following cases:

- Vehicles negotiating misaligned tangent tracks.
- Vehicles experiencing hunting instabilities.
- Vehicles negotiating curves at higher than balance speeds.

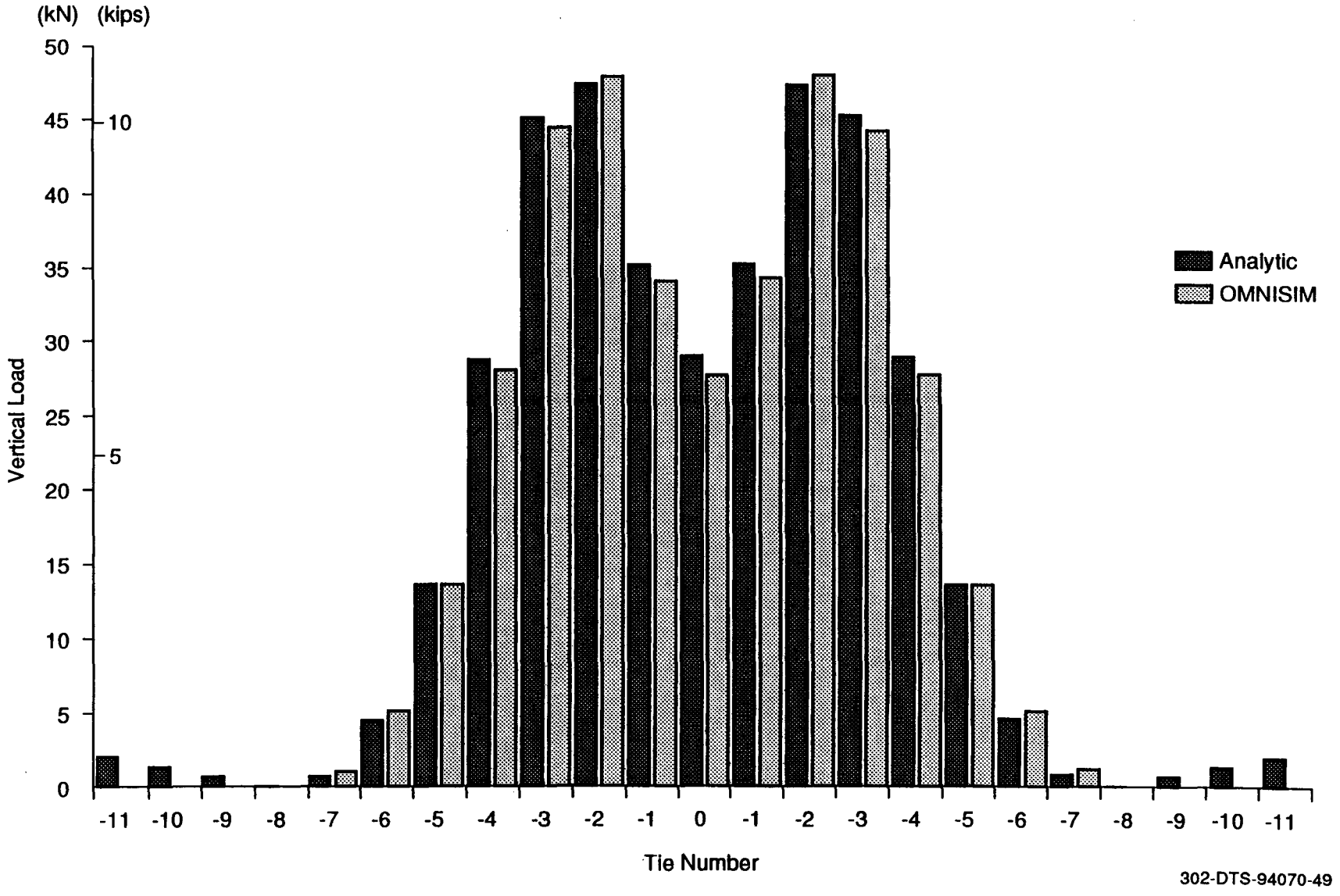

Figure 4-10. Tie loading from a single truck

Net axle lateral loads, ride quality and potential for wheel climb failure are also assessed in the parametric study.

The range of parameters is shown in Table 4-1. A high-speed car body is assumed in the studies. Both TGV and AAR1B wheel profiles are used in the simulation to provide a comparison between a wheel profile specifically designed for high-speed passenger vehicles and a profile designed for lower speed vehicles, which has alterations due to wear.

The TGV wheel profile is used in conjunction with UIC 60 rail. The AAR1B profile is used on 136 lb rail. The flange clearances for these two cases are 0.39 and 0.37 in., respectively. Although the flange clearance is an important parameter, it is not explicitly included in the parametric study presented here.

4.2.1 Loads on Misaligned Tangent Tracks

Ranges of lateral misalignment lengths (8 to 20m) and amplitudes (4 to 20 mm) are considered. The results on net axle loads and acceleration levels are shown in Tables 4-2 and 4-3 for AAR1B and TGV wheel profiles.

Net Axle Force Loads

1. Influence of Wheel Profile - As seen from Table 4-3, the net axle forces generated from TGV wheels are significantly less than those from AAR1B wheels (Table 4-2) at misalignments of 12 mm or greater amplitude. Except for severe misalignment cases (20 mm over 8 and 10m length), the net axle loads are small even with the AAR1B wheels. For Class 5 tracks which permit speeds up to 90 mph, the permissible misalignment amplitude is about 20 mm (0.75 in.), which if spread over a short wavelength, will generate a large net axle load force ratio, as shown in Figure 4-11. Because of the short wavelength over which the peak force occurs, the potential for track shift is not as severe, as it would be for the constant force situation studied in Section 3. The potential for track shift will be investigated in a forthcoming report.

   The results from the improved track model show that no wheel climb occurs even for the 20 mm misalignment amplitude case. Previous results from the SYSSIM code with simple track representation showed wheel climb derailment at this amplitude for the same

Table 4-2. Summary of model results for 150 km/hr (94 mph) on tangent track (AAR1B wheel profile)

Misalignment Amplitude (mm)	Misalignment Length (m)	Maximum Net Axle Lateral Force (kN)	Jolt Peak-to-Peak Lateral Acceleration (g)	Maximum Truckside Force Ratio	Maximum Net Axle Force Ratio
4	8	1	0.02	0.01	0.01
8	8	4	0.05	0.04	0.02
12	8	27	0.09	0.23	0.16
20	8	82	0.14	0.52	0.49*
4	10	2	0.02	0.01	0.01
8	10	5	0.06	0.06	0.03
12	10	30	0.12	0.28	0.18
20	10	68	0.19	0.47	0.41*
4	15	3	0.03	0.02	0.02
8	15	9	0.08	0.12	0.05
12	15	23	0.15	0.24	0.14
20	15	49	0.23	0.38	0.30*
4	20	3	0.03	0.02	0.02
8	20	7	0.09	0.12	0.04
12	20	16	0.16	0.20	0.10
20	20	32	0.27	0.30	0.20

*The sudden increase in the net axle forces is attributed to the flange contact.

vehicle parameters (1). Thus an improved track model is useful in proper assessments of vehicle-track interactions, even at moderate speeds.

Detailed analysis of car body accelerations is not presented here. It is often considered that the lateral car body acceleration reaches its permissible peak value (≈0.12g) prior to wheel climb and occurrence of excessive wheel loads, hence it can be used as an early warning to the potential derailment due to these causes. For the short wavelength, large wheel-rail forces can be developed and wheel climb can occur without high car body accelerations. Hence there is not always an adequate margin for the acceleration to be a reliable indicator of critical axle forces in all situations.

2. Influence of Track Lateral Resistance - Figures 4-12 and 4-13 give the results on net axle lateral force ratios as influenced by the track lateral resistance. The net axle force increases with track resistance as one would expect. This example shows the importance

Table 4-3. Summary of model results for 150 km/hr (94 mph) on tangent track (TGV wheel profile)

Misalignment (mm)	Wavelength (m)	Maximum Net Axle Lateral Force (kN)	Jolt Peak-to-Peak Lateral Acceleration (g)	Maximum Truckside Force Ratio	Maximum Net Axle Force Ratio
4	8	2	0.03	0.01	0.01
8	8	3	0.04	0.01	0.02
12	8	10	0.12	0.10	0.06
20	8	31	0.13	0.17	0.18
4	10	2	0.03	0.01	0.01
8	10	4	0.06	0.03	0.02
12	10	11	0.12	0.09	0.06
20	10	11	0.23	0.07	0.07
4	15	4	0.05	0.02	0.02
8	15	7	0.11	0.08	0.04
12	15	8	0.12	0.11	0.05
20	15	10	0.18	0.08	0.06
4	20	6	0.09	0.08	0.04
8	20	8	0.12	0.09	0.05
12	20	11	0.11	0.15	0.07
20	20	17	0.25	0.19	0.10

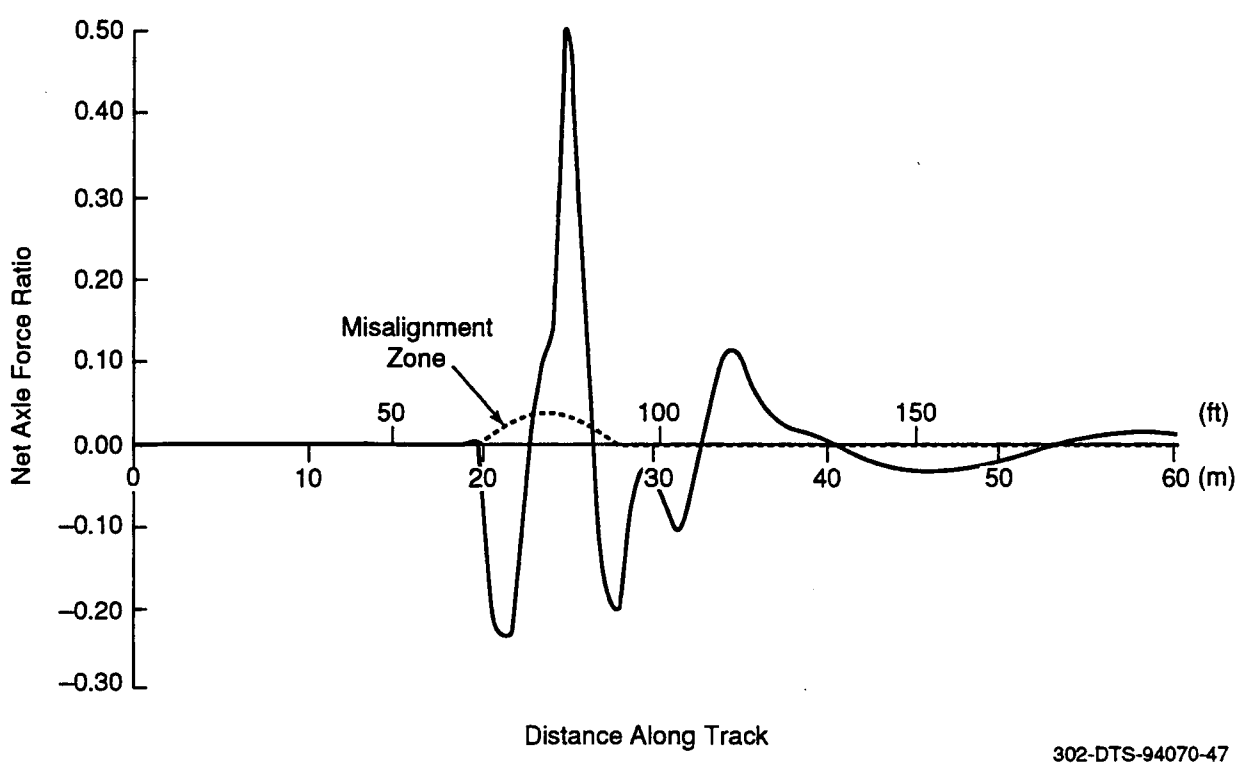

Figure 4-11. NAL for large track imperfection at 150 km/hr (94 mph)

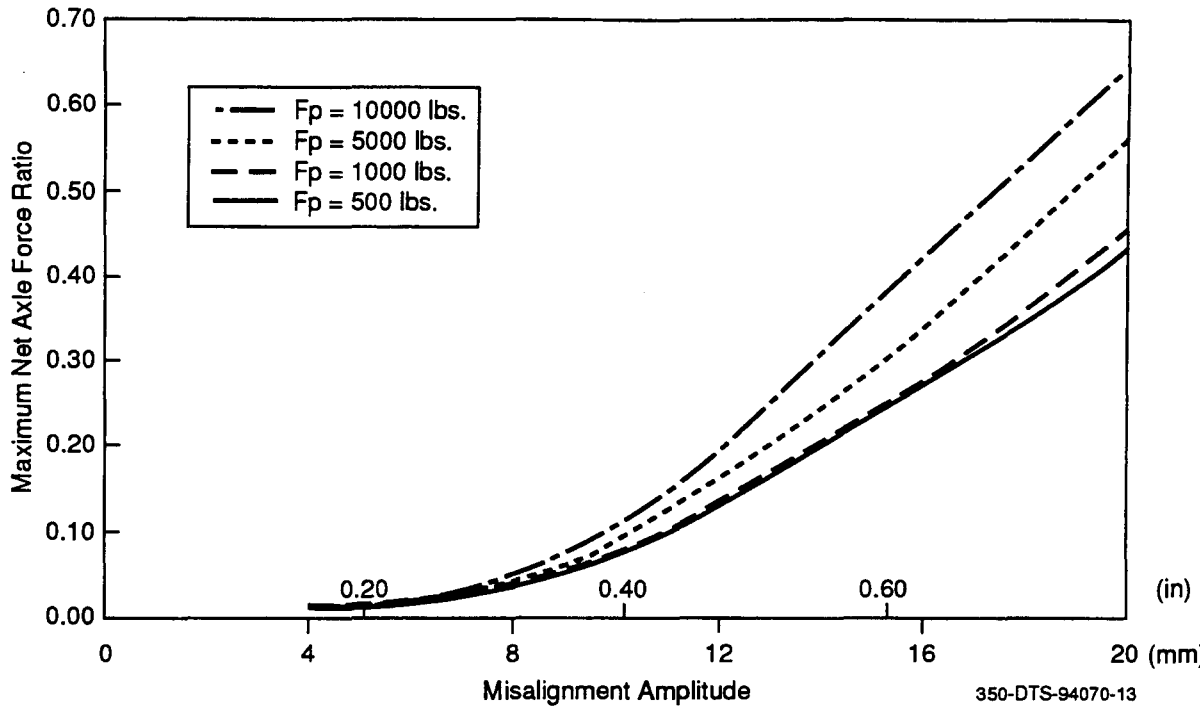

Figure 4-12. Influence of misalignments on net axle force ratio (tangent track)

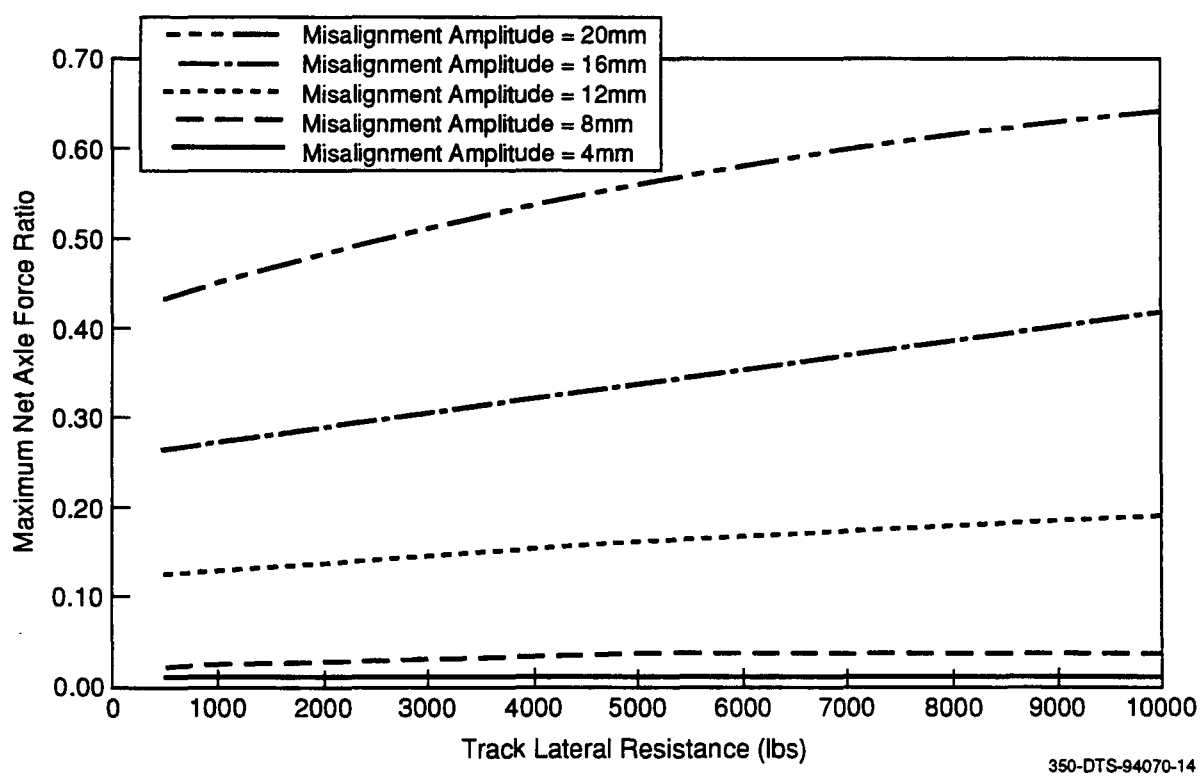

Figure 4-13. Influence of track lateral resistance on net axle force ratio (tangent track)

of tie-ballast lateral resistance parameter on lateral loads generated, particularly under severe misalignments with large amplitudes over small wavelengths. Although the net axle force increases with increased track resistance, the tie lateral movement reduces with resistance as one would expect. This is shown in Figure 4-14 for two different values of lateral resistance. The tie movement contributes to the track residual deflections, which can be reduced with higher lateral resistance.

3. Influence of Speed - The influence of vehicle speed on NAL for tangent track with initial misalignment is shown in Figure 4-15. As one would expect, the net axle force ratio increases with increase in speed. The speed in this example is limited to 140 mph, which is close but smaller than the hunting speed for the assumed vehicle parameters with the AAR1B wheel profile. It must be stated that the AAR1B profile at this high-speed is used here for illustration of worn wheel profile effects. Clearly, such profiles are not in use for high-speed rail.

4. Influence of Trailing Axle - It must be noted that all the foregoing results are for the leading axle of the leading truck. The trailing axle of the leading truck will also generate lateral loads, although these are small in comparison to those of the leading axle, as seen from the example presented in Figure 4-16 for the tangent track.

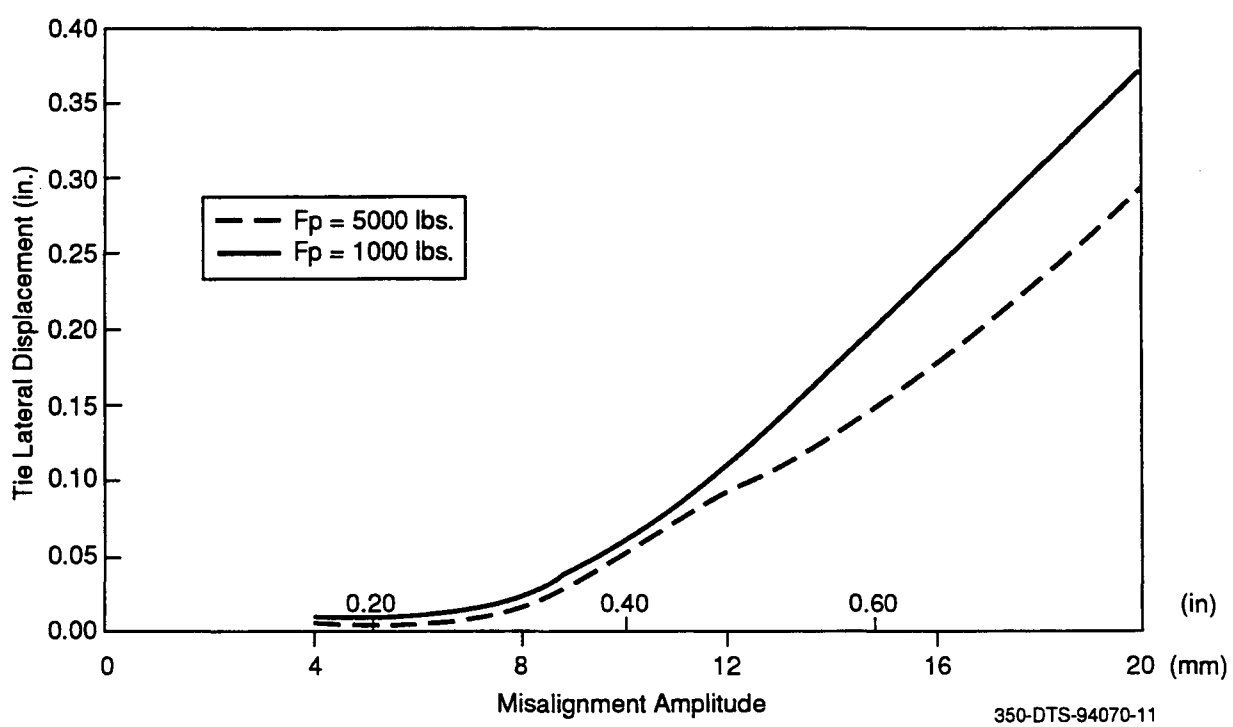

Figure 4-14. Influence of track lateral resistance on tie lateral displacement (tangent track)

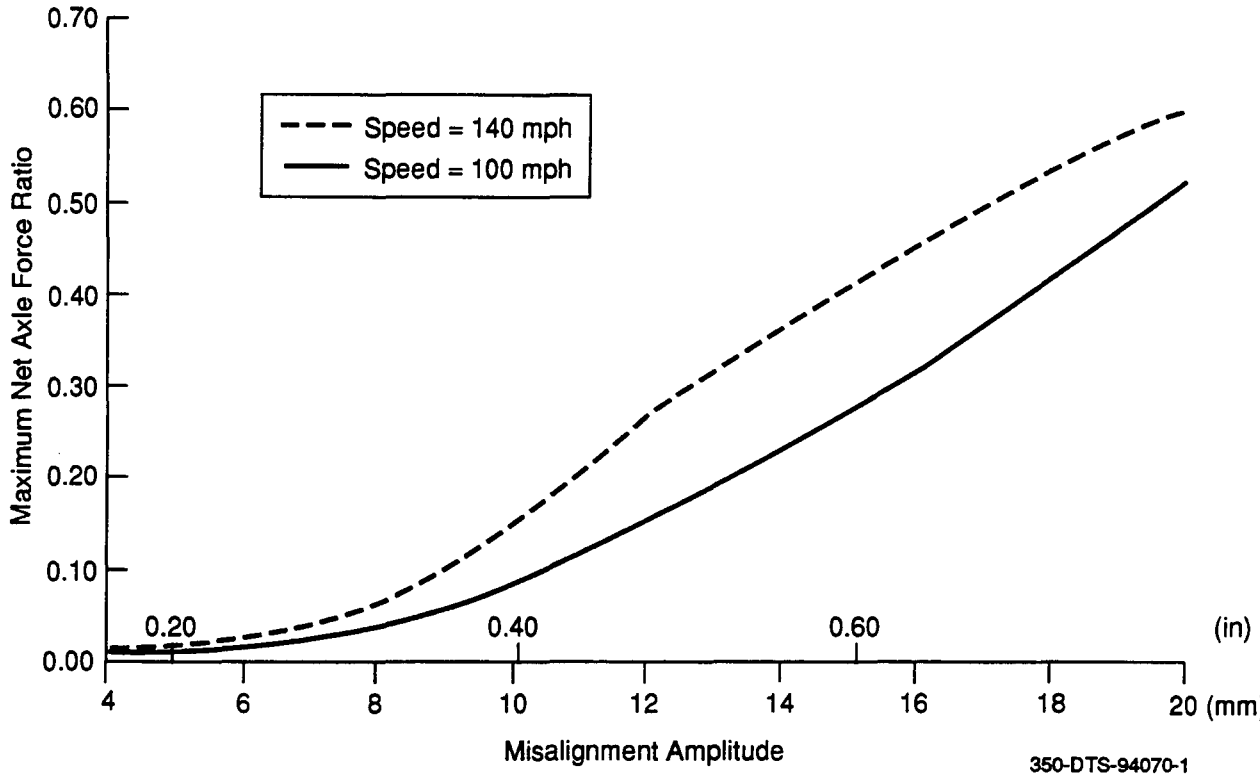

Figure 4-15. Influence of speed on NAL for tangent track with misalignment

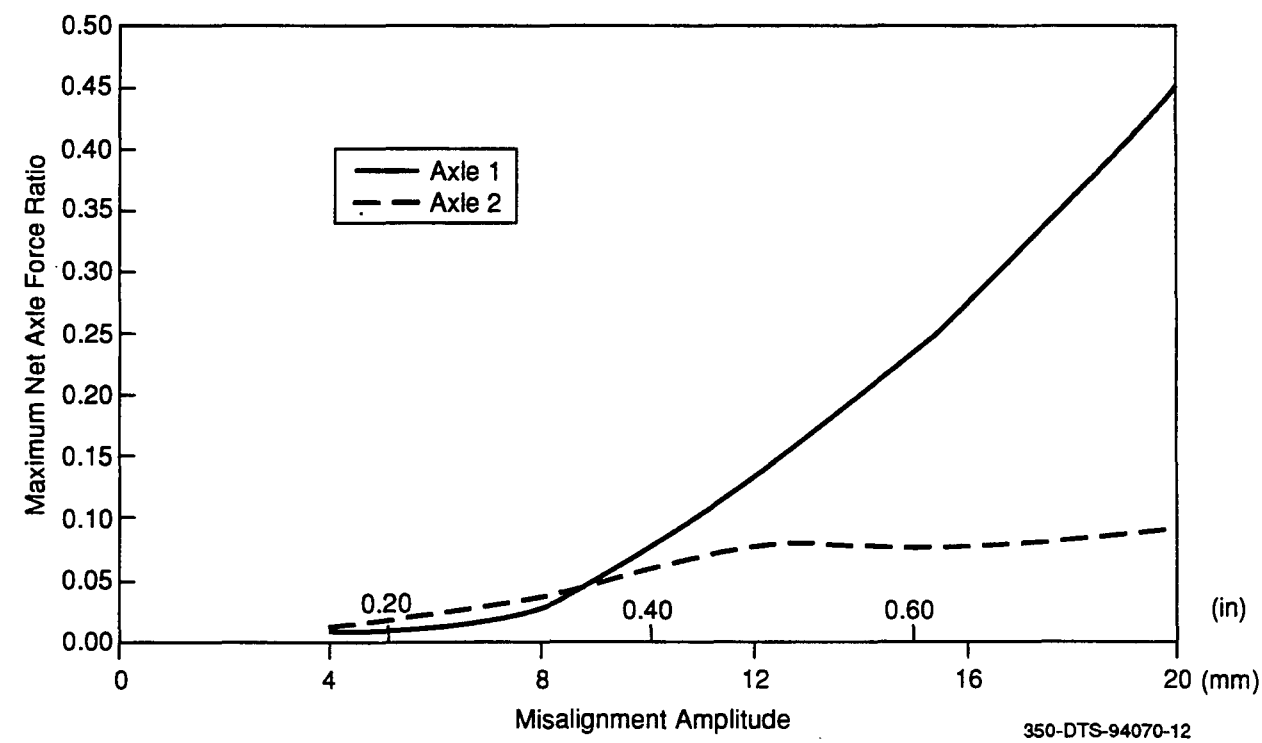

Figure 4-16. Comparison of net axle force ratios generated by leading and trailing axles (tangent track)

4.2.2 Loads from Truck Hunting

Vehicle hunting oscillations can generate large lateral loads which should not be permitted on revenue lines. The hunting phenomenon can be predicted using the OMNISIM code. As shown in the following numerical studies, the track parameters can have significant influence on the vehicle hunting behavior.

In the OMNISIM code, the hunting speed is determined by studying the truck lateral response as a function of vehicle speed, as the vehicle negotiates a lateral perturbation. Below the critical speed, the net axle force ratio and the axle lateral displacement decay with the vehicle passage, whereas above the speed, the amplitudes of the oscillations increase with distance from the perturbation.

Figure 4-17 shows the net axle force oscillations produced when the vehicle with the AAR1B wheel profile negotiates an imperfection of about 0.75 in. (20 mm) over a 8m wavelength. It is seen that the speed at which hunting starts to occur is about 142 mph.

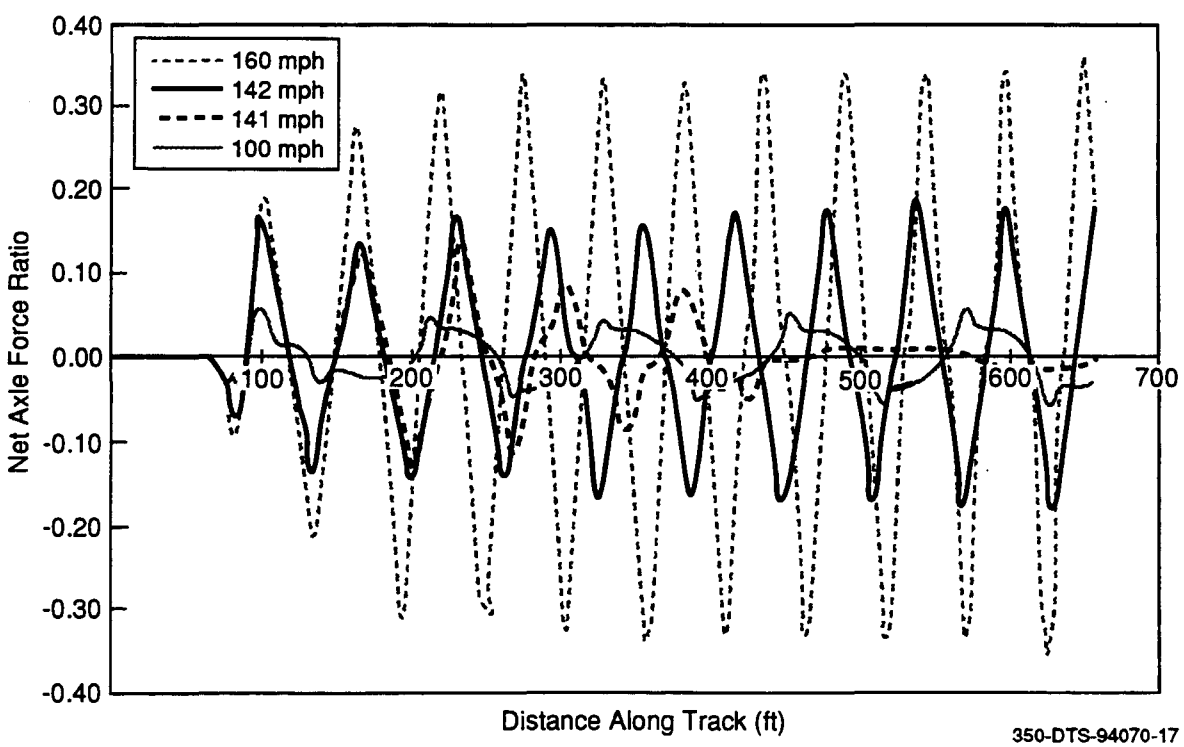

Figure 4-17. Dynamic response of vehicle at and above hunting speeds

The hunting speed is not significantly affected by the tie ballast lateral resistance. However, the net axle lateral force generated when the vehicle negotiates the perturbation increases significantly at speeds equal to that of hunting and above. It is interesting to note that up to the hunting speed, the net axle force increases with tie lateral resistance and thereafter reduces (Figure 4-18). The lateral deflection amplitude, however, always increases with reduced lateral resistance, more significantly beyond hunting speeds (Figure 4-19).

The above example illustrates the use of OMNISIM in evaluating vehicle track dynamic response at high-speeds including hunting speed. Clearly, hunting condition must be avoided by proper design of vehicle parameters including wheel profile.

4.2.3 Loads Generated in Curving

Vehicles negotiating curves with cant deficiency can generate large lateral loads even without pre-existing lateral misalignments in the tracks. The guidance provided by spirals connecting the tangent and the curve with constant radius will also generate lateral loads. The track geometry parameters influencing the vehicle dynamic forces are:

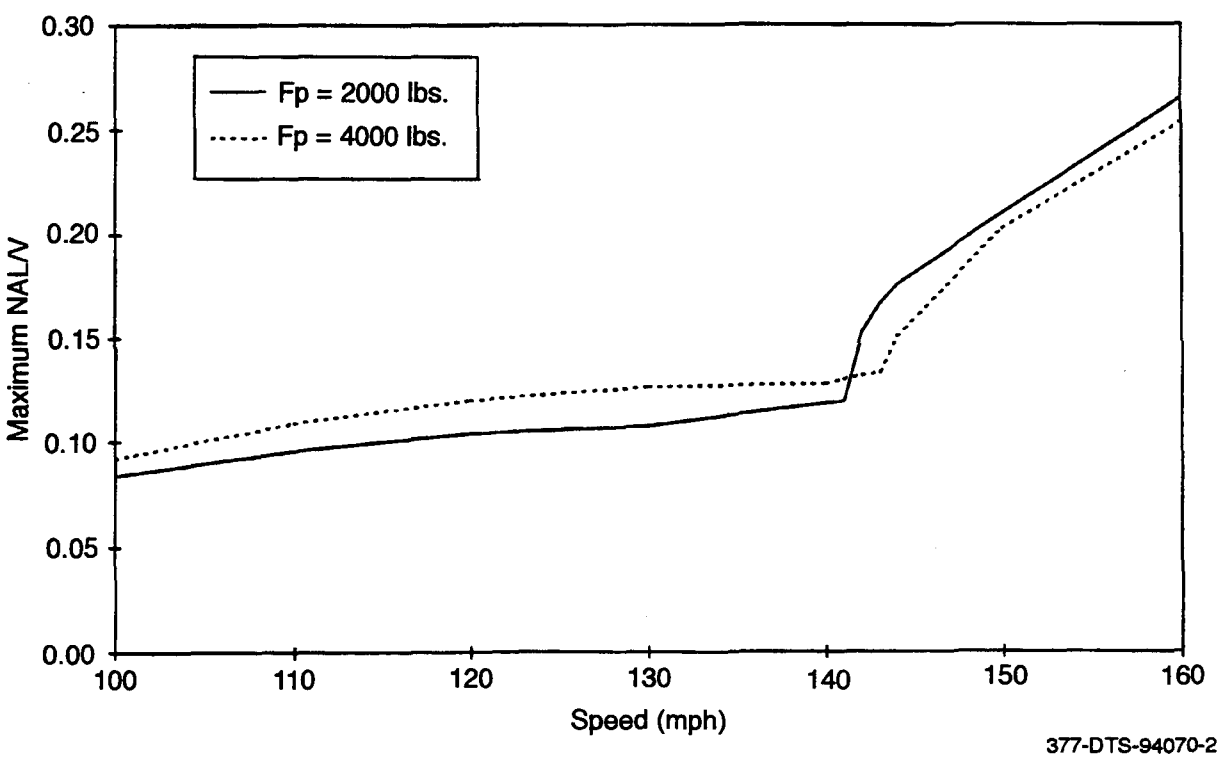

Figure 4-18. Net axle force ratios at and above hunting speeds

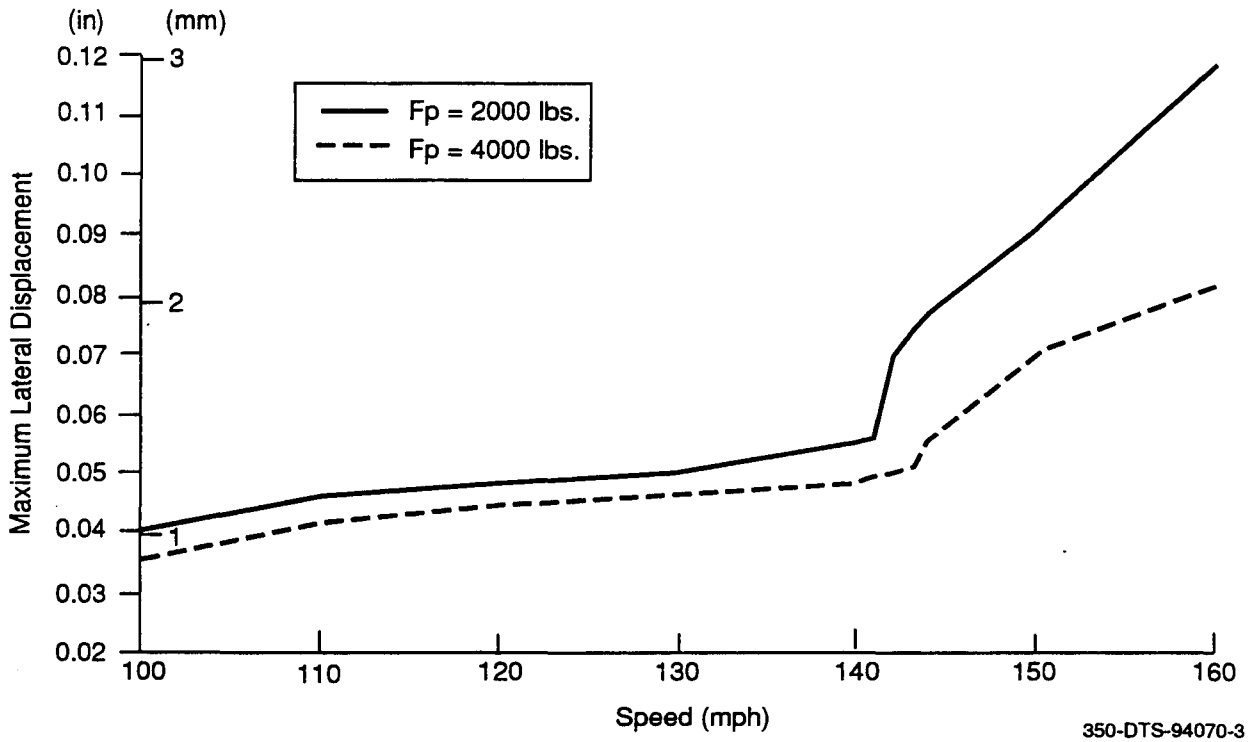

Figure 4-19. Tie lateral movement at and above hunting speeds

- Curvature.
- Super elevation.
- Speed or cant deficiency.
- Spiral length.
- Initial misalignments.

The track geometry is assumed to be as in Figures 4-20 and 4-21. Figures 4-22 and 4-23 show the net axle force ratios for 2 deg and 4 deg curves with 3 in. superelevation, with cant deficiencies up to 9 in. for three different spiral lengths. The largest spiral length quoted in each of the cases represents the AREA recommended value. The other two lengths used are respectively one half and one quarter of the AREA recommended values. Clearly, as seen from the data, the spiral length has a significant influence on the net axle loads. At high cant deficiencies, the force ratio exceeds 0.4 and track shift potential can exist on weak tracks.

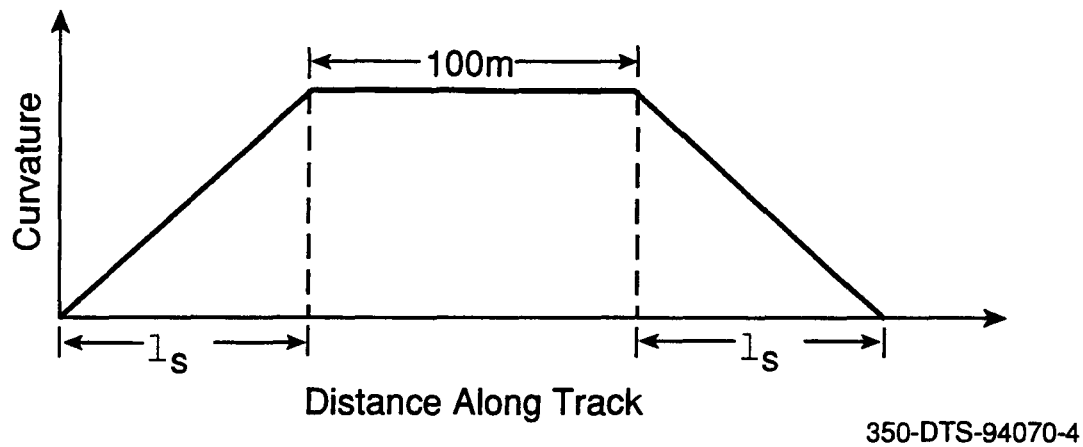

Figure 4- 20. Assumed curvature distribution

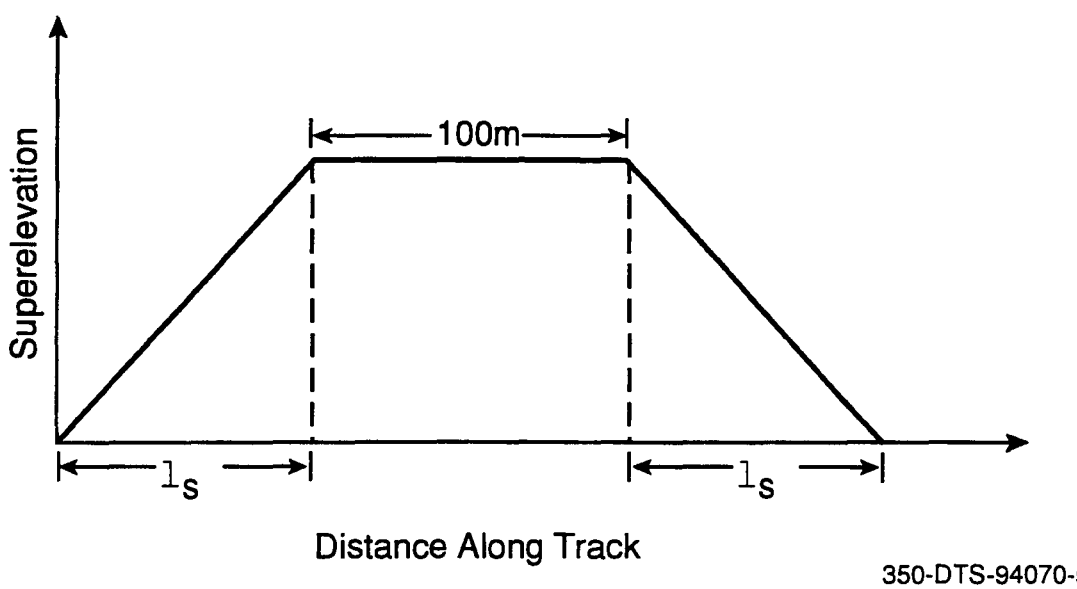

Figure 4-21. Assumed superelevation distribution

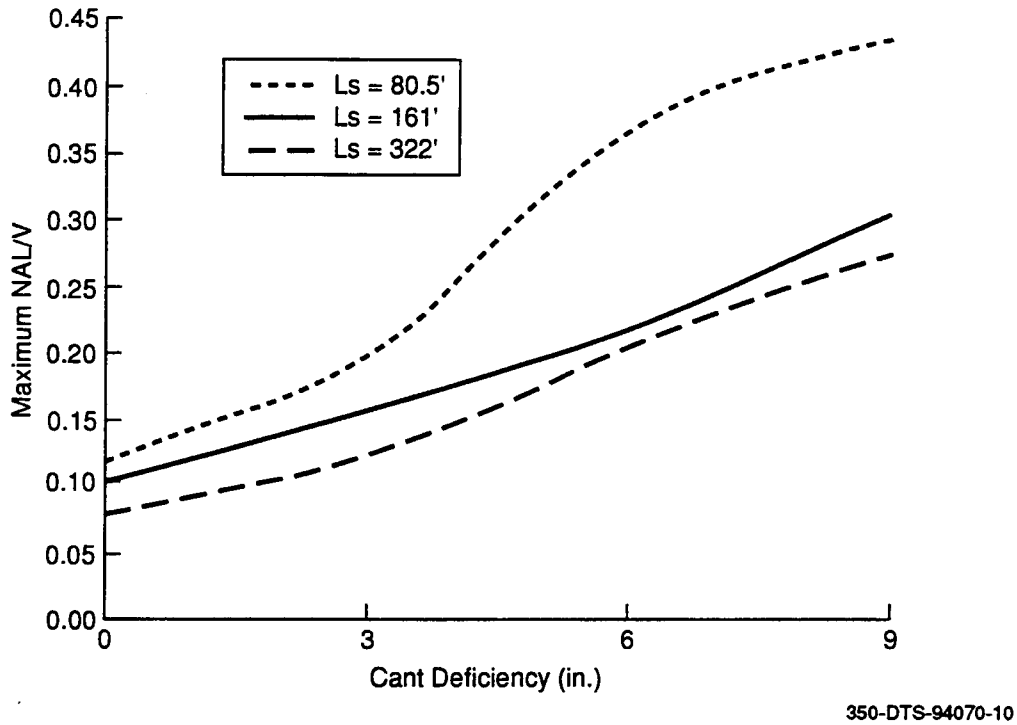

Figure 4-22. Net axle force ratio for 2 deg curve

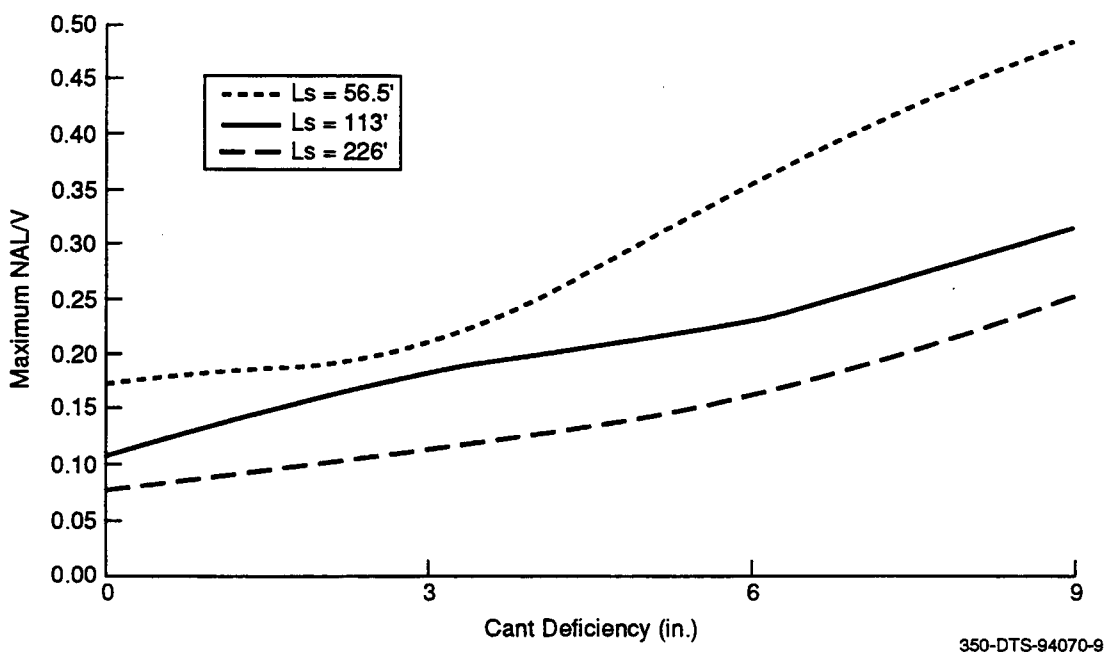

Figure 4-23. Net axle force ratio for 4 deg curve

Figure 4-24 shows an example of a 2 deg curve with 3 in. superelevation. The net axle loads generated on the two axles for the balanced speed are shown. The loads oppose each other, giving a zero net truck load. Figures 4-25 and 4-26 show examples for the 2 deg curve with 9 and 12 in. cant deficiencies. From these figures it is seen that the two axle loads are more or less "in phase" and roughly uniform in the body of the curve. With increase in cant deficiency, the net axle load shared by the trailing axle increases. This is in contrast with the tangent track misalignment case, where the leading axle exerts larger lateral load, compared to that of the trailing axle.

4.3 SUMMARY

1. The OMNISIM code developed under this effort has a compliant track representation to predict vehicle dynamic behavior, loads and track movement. The code can also predict wheel climb and other modes of failures. The introduction of compliance permits a more complete analysis of wheel climb behavior and track deflection.

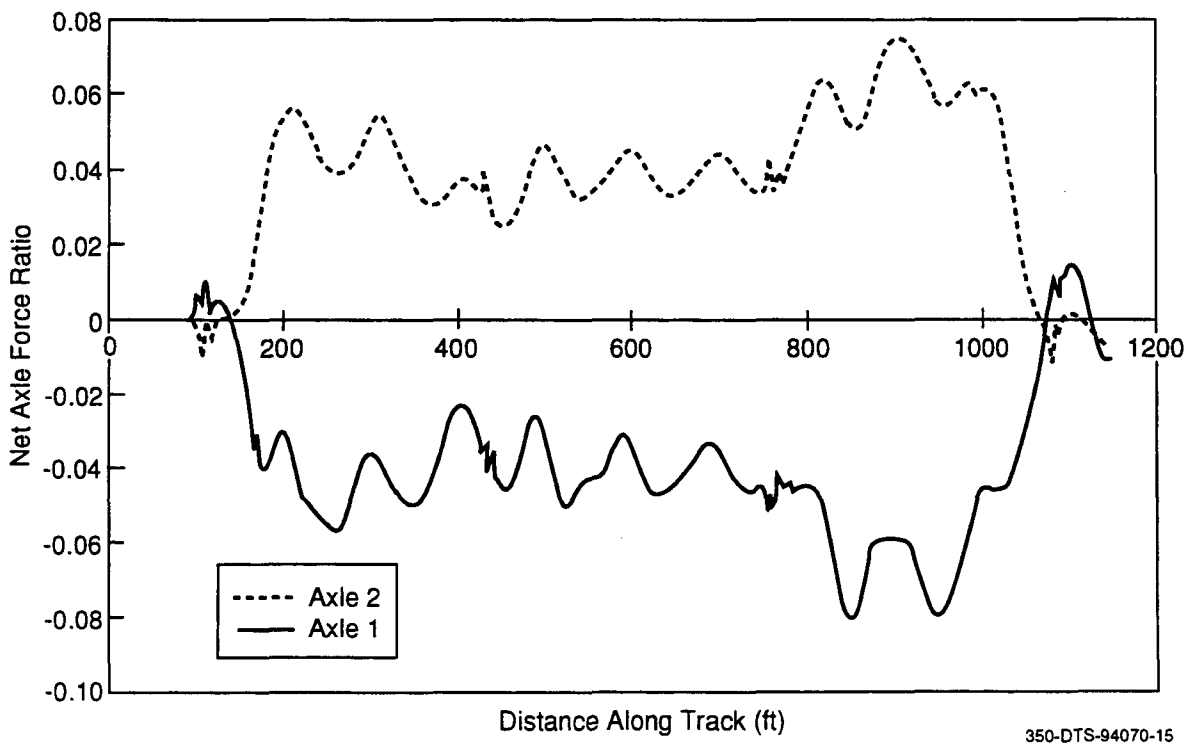

Figure 4-24. Net axle load distribution at balance speed (46 mph)

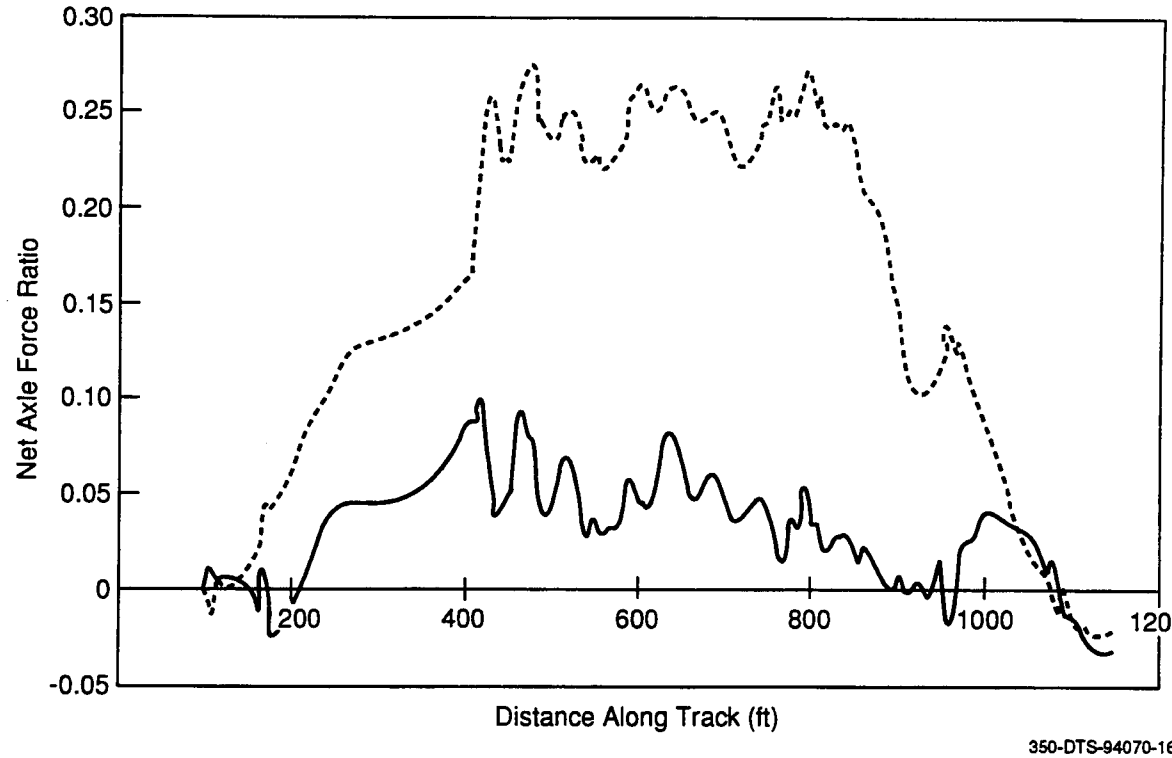

Figure 4-25. Net axle load distribution at 9 in. cant deficiency (93 mph)

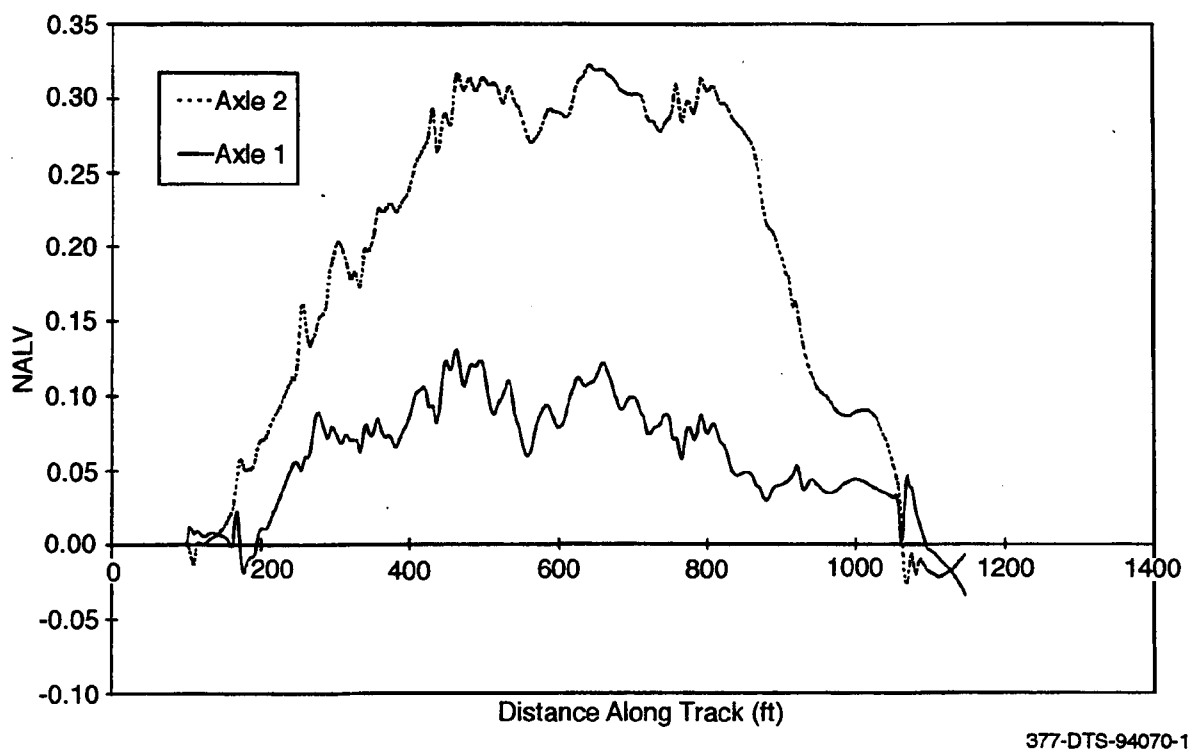

Figure 4-26. Net axle load distribution at 12 in. cant deficiency (104 mph)

2. Tie lateral resistance has a very small influence on the critical hunting speed. However, the lateral loads generated increase significantly with vehicle speed increase over the critical speed.

3. Under the vehicle loads, the lateral movement of tie always increases with reduction in its lateral resistance. Hence, softer tracks would be expected to have larger residual lateral displacements after vehicle passage.

4. As known in previous literature, the lateral loads generated in vehicle negotiation of the tangent track increase with increasing misalignment amplitude and decreasing wavelength. The leading axle of the truck generates larger lateral loads than does the trailing axle.

5. The wheel profile has a significant influence on the lateral loads generated while negotiating a lateral misalignment. The AAR1B wheel on 136 lb rail can generate lateral loads two to three times that generated by the new TGV wheel on UIC 60 rail, due to the larger conicity and smaller flange clearance involved with the former.

6. Lateral loads generated in vehicle curving are significantly influenced by the spiral length and cant deficiency. At balance speed with AREA recommended spiral lengths, the net axle lateral loads are very small. At high cant deficiency ($\geq$12 in.) on a 2 deg curve, the net axle lateral loads increase rapidly.

5. CONCLUSIONS AND RECOMMENDATIONS

5.1 CONCLUSIONS

1. Assessment of track shift can be performed using two partially coupled models as presented in this report, namely the Track Residual Deflection Model and the Vehicle Dynamic Model. The former determines the lateral residual deflections and identifies the stable and progressive regimes of track shift under vehicle passes. The latter model gives the vehicle dynamic loads on the track which are used as input in the first model.

2. The Track Residual Deflection Model is based on a moving loading simulation on a quasi-static beam on a nonlinear lateral foundation with a constitutive representation for the tie ballast resistance. A code has been developed for the tangent track based on this model. The inputs to the code are the axle vertical and lateral loads, parameters in the trilinear idealization for the tie-ballast resistance, track vertical foundation modulus, rail sectional properties and the number of passes.

3. In track shift analysis, the issue of single axle versus truck load simulation is an important consideration. Since the two axles seldom share the lateral load in equal proportion, truck load simulation becomes complicated. The SNCF practice is to treat each axle case independently from the adjacent axle and it is shown here that this single axle simulation conservatively overestimates the cumulative deflection by about 15 percent when compared with the results from the track load simulation with the assumption that the axles share the load equally. The nature of predicted track shift characteristics (progressive or stable) is the same from both simulations. Hence, it is concluded that the single axle simulation is adequate for track shift predictions, at least for the axle spacing considered in this report.

4. The track shift code can be used for both stationary and moving loads. The results from the code show that for quantification of track shift under vehicle passage, the moving load simulation is essential, even though the loads are idealized as quasi-static. The stationary load idealization grossly underestimates the residual deflection and, as such, it is considered to be nonconservative.

5. The SNCF test data on their TGV track is in a reasonable agreement with the track residual deflection model developed in this report. This provides partial validation of the analytic method.

6. Parametric studies using the code show that even for low net axle lateral to vertical force ratio (0.4), weak tangent tracks (low lateral resistance; low tie-ballast friction coefficient) can experience track shift. For a steady net axle force ratio approaching 0.6, even tracks traditionally considered as strong (lateral resistance = 4000 lb) may experience significant track shift. Hence, when the net axle force ratios exceed 0.4, the required track strength must be carefully assessed to assure safety against potential track shift. It must be stated that such large net axle force ratios typically occur over short durations. The finite wavelength over which the force is spread, is also an important factor to be considered, although this has not been included in the present analysis.

7. The Vehicle Dynamic Model which gives the generated lateral loads is based on a new vehicle-track interaction code called OMNISIM. The model has a compliant track element and maintains a rolling contact connection at the wheel rail interface. The compliant track representation accounts for the track inertial effects and lateral and vertical stiffness. Therefore, the results from the vehicle dynamic model are believed to be more appropriate than those from existing codes (such as the SYSSIM) in the track shift studies, which neglect the tie-ballast interaction.

8. The vehicle dynamic model is intended also to assess wheel climb potential and ride quality. Numerical studies using the model have shown that large net axle forces (lateral to vertical force ratio = 0.5) can occur before wheel climb potential exists. Previous results based on simple track representation showed that wheel climb occurs prior to such levels of net axle loads on the track. Hence, simple track models in vehicle dynamic analysis, though appearing as conservative from wheel climb considerations, may underestimate track shift potential.

9. The net axle lateral loads generated on curves depend on curvature, superelevation, vehicle speed or cant deficiency and spiral length, as well as initial misalignments. High cant deficiency and short spiral lengths can generate significant loads to cause track shift.

5.2 RECOMMENDATIONS

1. The proposed constitutive representation of the tie-ballast lateral resistance for loading and unloading should be experimentally validated. Practical range of the parameters should be established.

2. The track residual deflection model should be extended to include "short duration high peak" net axle lateral loads. Sinusoidal type force distributions should be studied, as they occur frequently in misalignment zones. Application of results based on constant force may be overly conservative in such cases.

3. Thermal loads and curvature effects must be included in the track residual deflection model and the track shift code modified accordingly. These effects are considered to be significant and will provide a more realistic assessment of required track lateral strength and allowable track shift.

4. The track residual deflection model should be validated for both cyclic stationary and moving loads by direct experiments on tracks with known or measured parameters. The stationary load test can be conducted using the Track Lateral Pull Test (TLPT) hardware. For moving load, the feasibility of the AAR Track Loading Vehicle (TLV) may be examined.

5. The track residual deflection and the vehicle dynamic models may be combined into a single code that will establish appropriate couplings of the input/output results. A user-friendly interface should also be developed for ease of using the computer program.

6. A combined code should be exercised over the ranges of significant parameters to establish stable and unstable track shift regimes and allowable stabilized track residual deflections as functions of net axle force ratio, vehicle speed, tie ballast friction coefficient and peak tie resistance. Using such a comprehensive database and a prescribed vehicle qualification limit, the required track strength for stabilized track shift should be evaluated. The allowable track shift should also be defined for given allowable ride quality deterioration and potential wheel climb derailment.

7. The methodology developed for the evaluation of track lateral residual deflections under vehicle loads may provide a valuable tool for other track structure problems in this class. For example, a track degradation model involves prediction of track settlement in the vertical plane (due to the elasto-plastic nature of the ballast) under repeated vertical loads. The dynamic wheel loads can be predicted using the vehicle dynamic code, and the track settlement can be evaluated using a moving load simulation on the track structure. Likewise, a gauge widening model can be developed using a moving load simulation on each rail restrained in their fasteners in an elasto-plastic manner. At present, track degradation and gauge widening models use stationary load simulations which may be inadequate.

6. REFERENCES

1. Samavedam, G., F. Blader and D. Thomson, "Track Lateral Shift: Fundamentals and State-of-the-Art Review," Final Report, DOT/FRA/ORD, August 1995.

2. Prud'homme, A., "Resistance of the Track to Lateral Loads Exerted by Rolling Stock," *Revue Générale des Chemins de fer*, January 1967.

3. Whitten, B.T. and B.T. Scales, "X2000 U.S. Demonstration, Vehicle Dynamics Tests, Final Test Report," DOT/FRA/ORD-94/15, November 1993.

4. Samavedam, G., A Kanaan, J. Pietrak, A. Kish, and A. Sluz, "Wood Tie Track Resistance Characterization and Correlations Study," DOT/FRA/ORD-94/07 Final Report, January 1995.

5. Amans, F. and R. Sauvage, "Railway Track Stability in Relation to Transverse Stresses Exerted by Rolling Stock. A Theoretical Study of Track Behavior," Bulletin of the International Railway Congress Association, January 1969.

6. Snyder, Mark D., "An Effective Solution Algorithm for Finite Element Thermo-Elastic-Plastic and Creep Analysis," Ph.D. thesis, Massachusetts Institute of Technology, Department of Mechanical Engineering, 1980.

7. Blader, F.B., et al., "Development and Validation of a General Railroad Vehicle Dynamics Simulation (NUCARS)," Proceedings of the 1989 IEEE/ASME Joint Railroad Conference, April 25-27, 1989, Philadelphia, Pennsylvania, pp. 39-46.

8. Cooperrider, N.K. and Heller, R., *User's Manual for the Asymmetric Wheel/Rail Contact Characterization Program*, Federal Railroad Administration Report FRA/ORD-78/05, December 1977.

9. Kalker, J.J.," The Computation of Three Dimensional Rolling Contact with Dry Friction," *International Journal for Numerical Methods in Engineering*, Vol. 14, pp. 1293,1307, 1979.

APPENDIX A

FULLY COUPLED APPROACH AND TRADEOFFS

In the fully coupled approach, the vehicle-track interaction loads and the track displacements are computed simultaneously. The vehicle dynamic equations and the track deflections will be evaluated in a single formulation, which maintains the displacement compatibility and force continuity conditions at the wheel-rail interface.

In developing the fully coupled method, two modeling approaches have been considered for incorporating a rail model: a continuous rail model; and a lumped parameter rail model.

The continuous rail model approach represents the rails using the differential equations for a beam experiencing bending and thermal loads. This approach is similar to the methods used in the analysis of CWR track buckling. However, this approach is not consistent with the current structure of the SYSSIM program, which uses a lumped parameter approach in the assessment of the vehicle dynamic response. Combining the lumped approach of SYSSIM with the continuous beam model is expected to be a challenging and potentially time consuming task. This level of effort is considered to be prohibitive for the current program.

The lumped parameter approach of track modeling is, as noted above, more consistent with the current structure of SYSSIM, and would be considerably easier to develop and program. In this approach, a long outer module representing the track structure would be defined, as shown in Figure A-1. This long outer module defines a moving window or moving range of influence that travels with the vehicle, and covers a range of perhaps 10 ties on either side of the leading and trailing axles. Beyond this distance of 10 ties from the axle loads, the influence of the vehicle on the track is assumed to be negligibly small. Within the moving window defined by the outer module, the track is modeled using repeating inner modules of lumped parameters which represent a single tie spacing, as shown in Figure A-2. Using a time stepping approach, the effect of the vehicle loads and the track deflections are simultaneously computed over each tie spacing within the outer module. As the vehicle progresses down the track, the vehicle and track modules travel together, incrementing forward with each time step.

As noted, the advantages of the lumped parameter over the continuous rail approach include the relative ease of programming and implementation. However, due to the extent of the outer module, which must extend to a length which is perhaps 20 tie spacings greater than the overall length of the vehicle, the number of degrees of freedom in the model can be quite large. The large size of the model could result in a long computational time. For this reason, this lumped parameter approach should be used with the simplest vehicle model permissible, (such as the single truck model currently under development). The small size of this vehicle model will limit

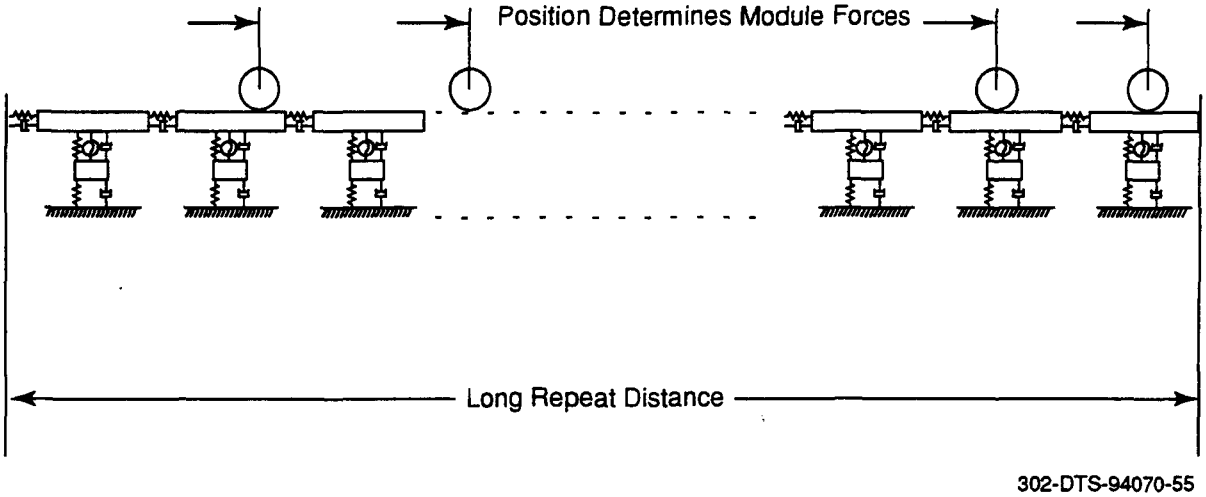

Figure A-1. Long outer module used in SYSSIM coupled lumped parameter model

the extent of track (and degrees of freedom) to be modeled in the moving outer module, and will thereby allow for greater computational speed.

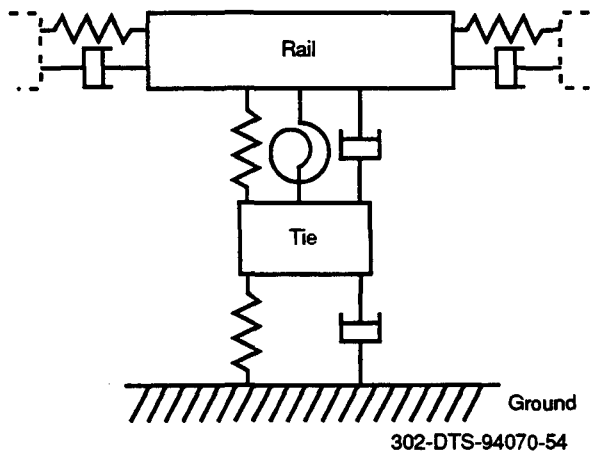

Figure A-2. Short module used in SYSSIM coupled lumped parameter model

Overall, the fully coupled approach (using either continuous or lumped parameter rail models) offers potential advantages and disadvantages over the partially coupled approach. The coupled approach will provide a direct and more accurate assessment of the track and vehicle motions, since the new rail model within OMNISIM connects the left and right rails using ties, include lateral, vertical and torsional resistances for each rail relative to the ties, and include the lateral resistance of the ties relative to ground. These model enhancements will account for the motions of the track, and of each rail, including rail roll and gauge widening. Thus a significant advantage of the fully coupled approach is that it will allow OMNISIM to fundamentally indicate the potential not only for wheel climb derailments (as it does currently) and track shift, but also for rail rollover and gauge widening derailments.

Although significant development effort is required, this coupled approach has good potential, particularly if simple models are used for the resistance of the rails and the lateral resistance of the track. However, the track lateral resistance model is itself complex and highly nonlinear. Thus, the primary disadvantages of the fully coupled approach are that it is more expensive and complex to develop and program, in addition to requiring greater effort and time.

The risks involved in developing a fully coupled method have been reduced by adopting the lumped parameter method using a two stage developmental approach; first by improving the track model representation within SYSSIM, and then incorporating the moving frame of reference for motion of the vehicle relative to the track. The first milestone in this process is to modify and improve the rail models currently used within SYSSIM. As discussed in Section 3, the current SYSSIM rail model lacks a structural connection between the left and right rails, and does not adequately represent the lateral resistance of the track. An improved track model, such used in the short module shown in Figure A-2, has been developed and implemented. The decision whether or not to pursue the second phase of development, which would incorporate the relative motion between vehicle and track, will be made later.

Summary

Table A-1 gives a brief summary of tradeoffs for the two modelling approaches described in this report. Based on the analysis presented here, it is recommended that the partially coupled approach be the first priority of development, as it will provide a useful and practical tool at relatively low risk. Upon completion of this phase of work, the decision can then be made either to further pursue the development and completion of the fully coupled approach, or to abandon its further development in favor of the proposed partially coupled approach.

Table A-1. Tradeoffs between fully coupled and proposed partially coupled track shift modelling approaches

Criterion	Fully Coupled Approach	Partially Coupled Approach
Accuracy	High • Dynamic track loading • Improved representation of rail/track motion	Good • Static track loading • Good representation of rail/track motion
Development effort required	High	Comparatively low
Programming difficulties	Difficulty in coupling vehicle and track models and incorporating relative motion	Relatively straightforward for programming
Execution time required	High due to large number of degrees of freedom	Moderate, more comparable to CWR buckling program

APPENDIX B

TRACK ANALYSIS ISSUES

An important issue in the development of the track lateral shift model is whether a simplified, single axle vehicle model will be sufficient and thereby reduce the complexity and run-time of the overall model. This section presents an initial investigation of track lateral shift due to single and multiple vehicle axle loads. The objectives of this analysis are as follows:

- Investigate and compare the effects of single and multiple axle static loads on track lateral shift.

- Determine which loading case (single or multiple axles) results in a reasonably conservative "worst case" scenario for further implementation in the track lateral shift analysis.

B.1 ANALYSIS OF SINGLE VERSUS MULTIPLE AXLE LOADS

The analyses presented here are carried out using the NIKE3D nonlinear finite element software running on a Silicon Graphics workstation. The cases considered here are shown in Figure B-1. Figure B-1a, b, and c represent a single axle, the two axles of a truck, and the four axles of two adjacent trucks, respectively. Each case assumes a vertical load of 37.4 kips/axle (166.43 kN), similar to the TGV vehicle. The lateral loads are assumed to be equal in each of these three cases. The loading case in Figure B-1d is studied to evaluate the influence of vertical load of an adjacent axle on the deflection under a laterally loaded axle.

In these analyses, analytical and finite element models were constructed for the load cases shown in Figure B-1. The vertical deflections and lateral stiffness distributions were calculated, and the influence of adjacent axles on the lateral response of the track were examined. Results of these analyses are described below.

B.2 VERTICAL DEFLECTION

The vertical deflection is first determined as shown in Figure B-2. The assumed parameters for two rails combined (136# AREA) are as follows:

I_v = 189.8 in.^{4} (7.4 x 10^7 mm^4).
A = 26.7 in.^{2} (16,700 mm^2).
k_v = 6000 psi (41,000 kN/m^2).
V = 37.4 kips/axle (TGV-type axle load) (166.43 kN).
D = axle spacing = 120 in. (3m).

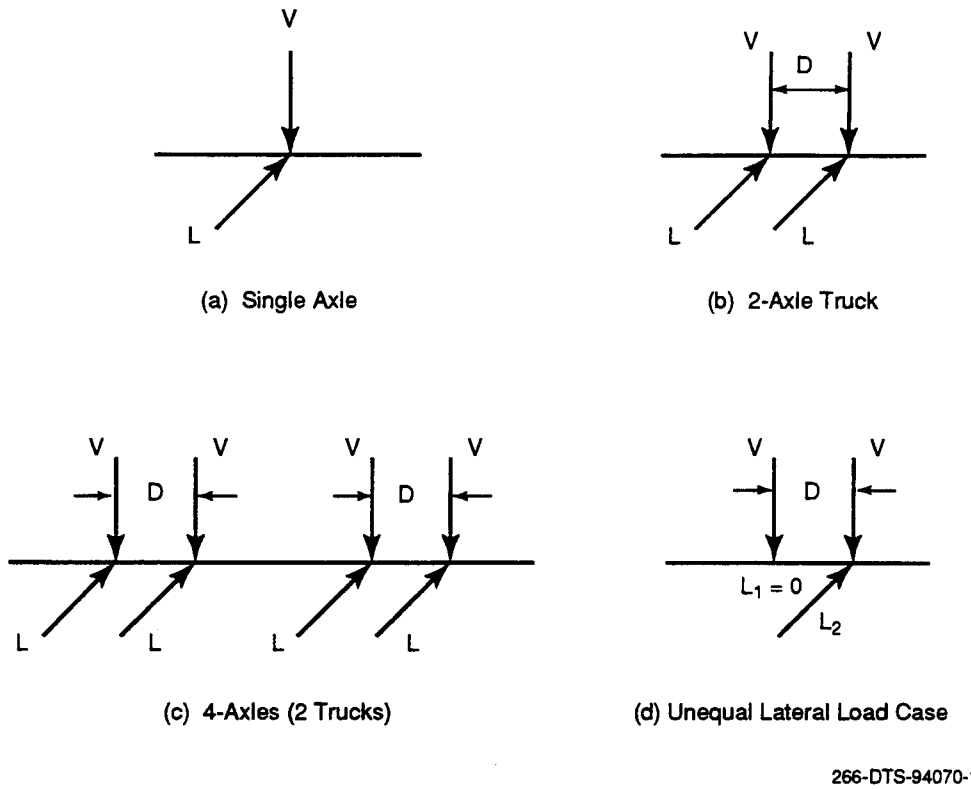

Figure B-1. Vertical and lateral load cases

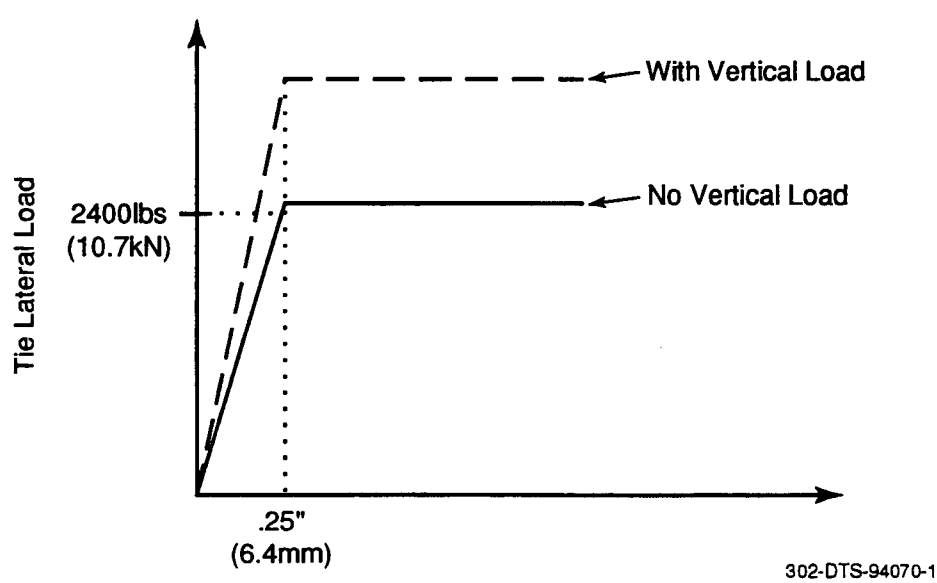

Figure B-2. Assumed STPT characteristic in the numerical work

The peak vertical deflection in all cases is found to be approximately 0.07 in. (1.75 mm), showing that the single axle idealization is adequate for the determination of maximum vertical deflection. It should be noted here that if the track foundation is very soft (small k_v), then the single axle idealization may not be adequate. In such a case, the multiple axle effects will cause a greater maximum deflection than that due to a single axle. However, for high speed track, the 6000 psi (41,000 kN/m^2) value used here for k_v can be considered to be a reasonable minimum value, indicating that the single axle idealization will be adequate for the TGV-type axle loads and spacing used in this analysis.

B.3 LATERAL STIFFNESS

As explained in Reference (1), the lateral stiffness is influenced by the vertical load. The stiffness is computed by assuming a static resistance of 100 lb/in. (17.8 N/m), a tie-ballast friction coefficient of 0.5 (Figure B-2) and using the vertical pressure distribution calculated from the vertical deflection analysis (Figure B-3). These are shown for the single axle and two axle cases in Figure B-4. For an illustrative comparison, the location of one of the two axles of the truck is shown as the same as that of the single axle case. Clearly, under the two axle truck, the lateral stiffness (per axle) increases, though the change in the close vicinity of the load is negligible. Hence, the lateral deflection under the two axle case will be smaller compared to that of the single axle, if the lateral load per axle in both loading cases is considered to be equal.

B.4 RESULTS

Figures B-5 and B-6 show the results of lateral deflection for equal lateral loads on one and two axles. The peak deflections for these two cases are very close, although the wavelengths are different. The deflection profile for the two axle case can be obtained by superimposing the results for each axle.

In the above analysis, the lateral load levels are not large enough to give permanent deflections. At these loads, it is shown that the influence of adjacent axles on one another is negligible. To study the effects of large lateral loads and the potential interference of adjacent axles, the case of a two axle truck as in Figure B-1d is studied. The deflection under load is shown in Figure B-7. The load-deflection relationship becomes nonlinear at about 25 kips (111 kN) for the track parameters assumed here. As L/V approaches 1, large lateral deflections are generated. The data for a single axle case (Figure B-1a) is also shown. Comparison of the

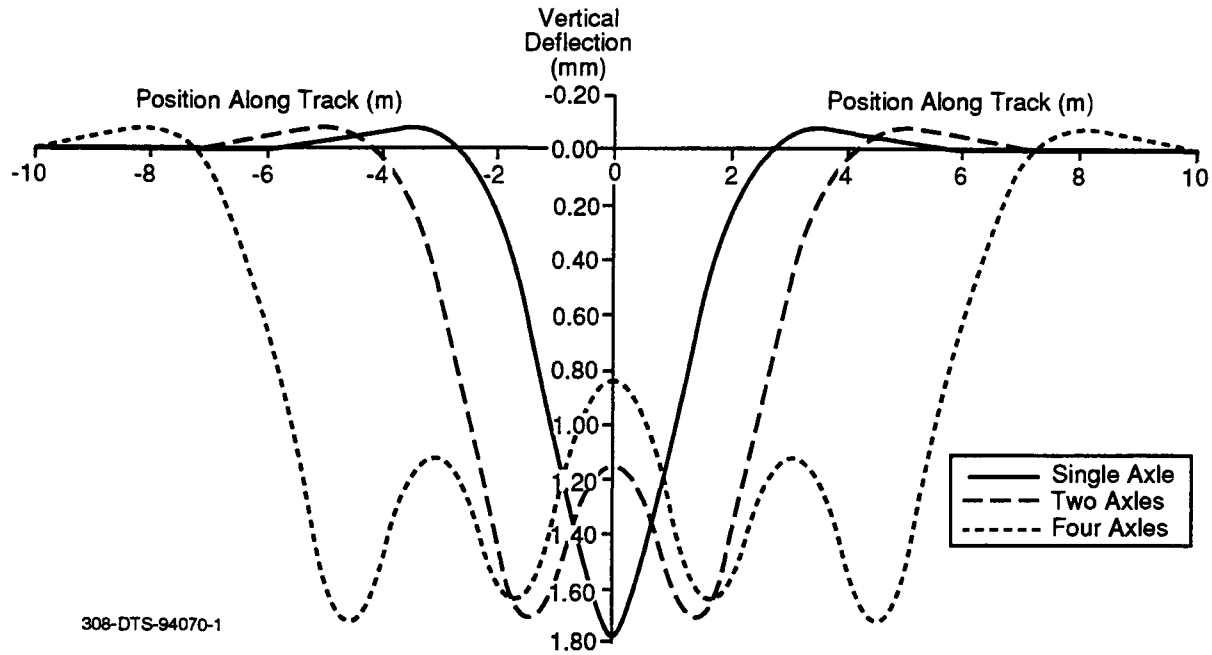

Figure B-3. Vertical deflection due to single and multiple axle loads

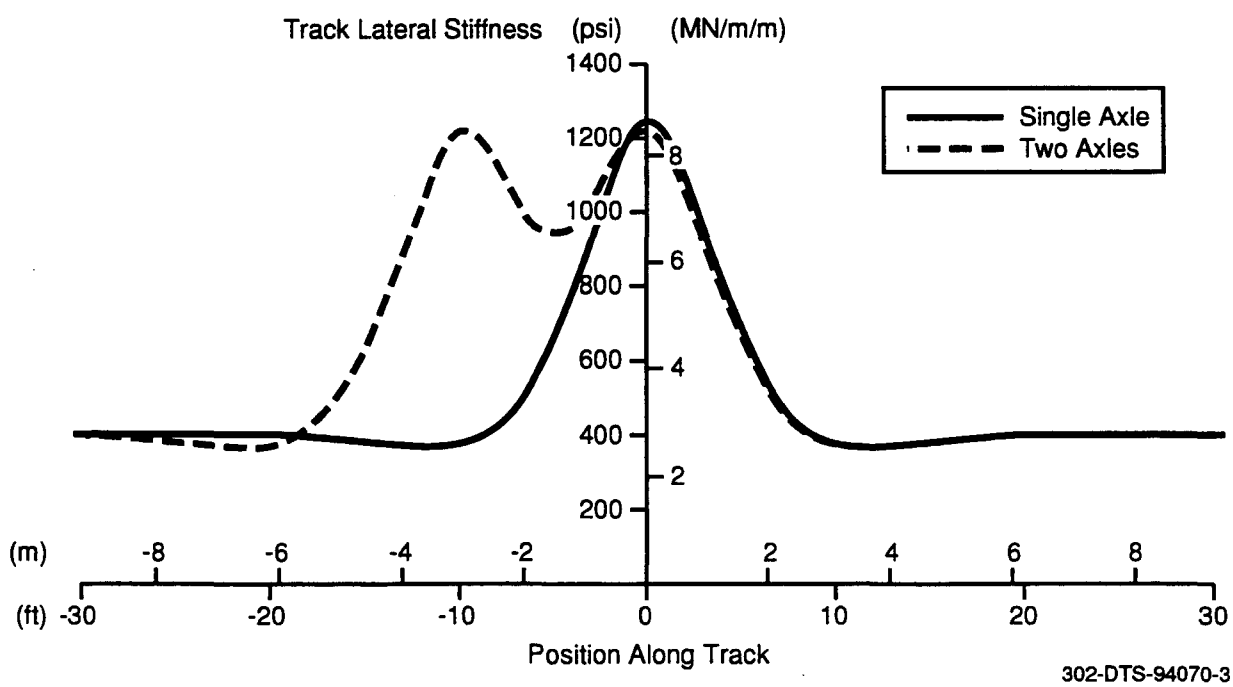

Figure B-4. Track lateral stiffness comparison

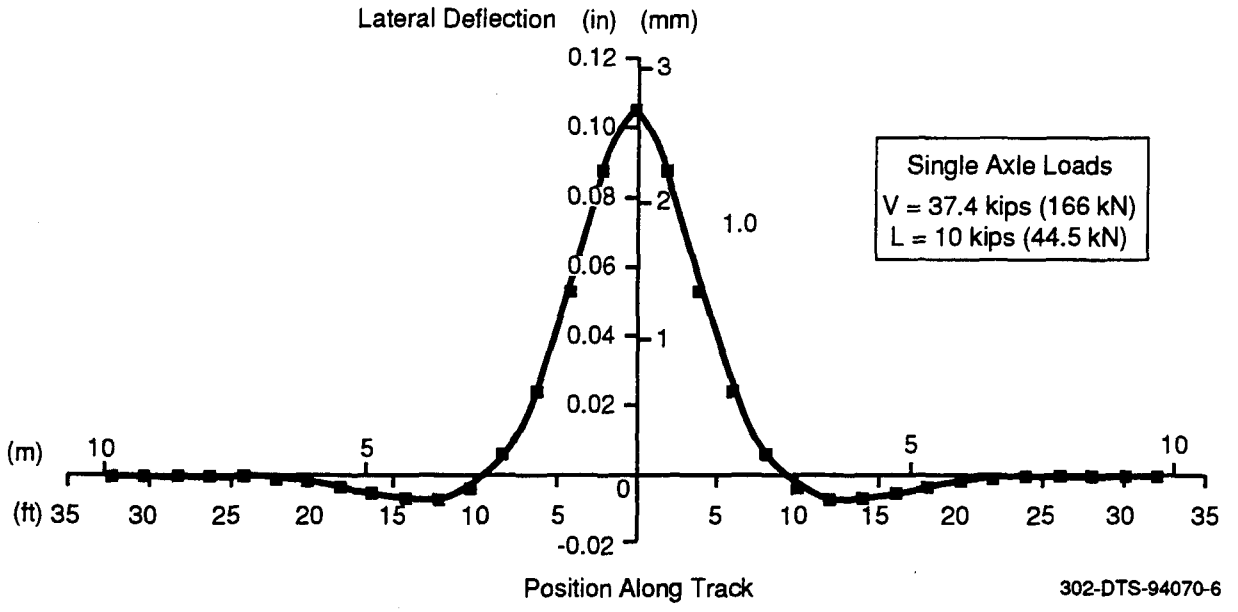

Figure B-5. Track lateral response for a single axle load

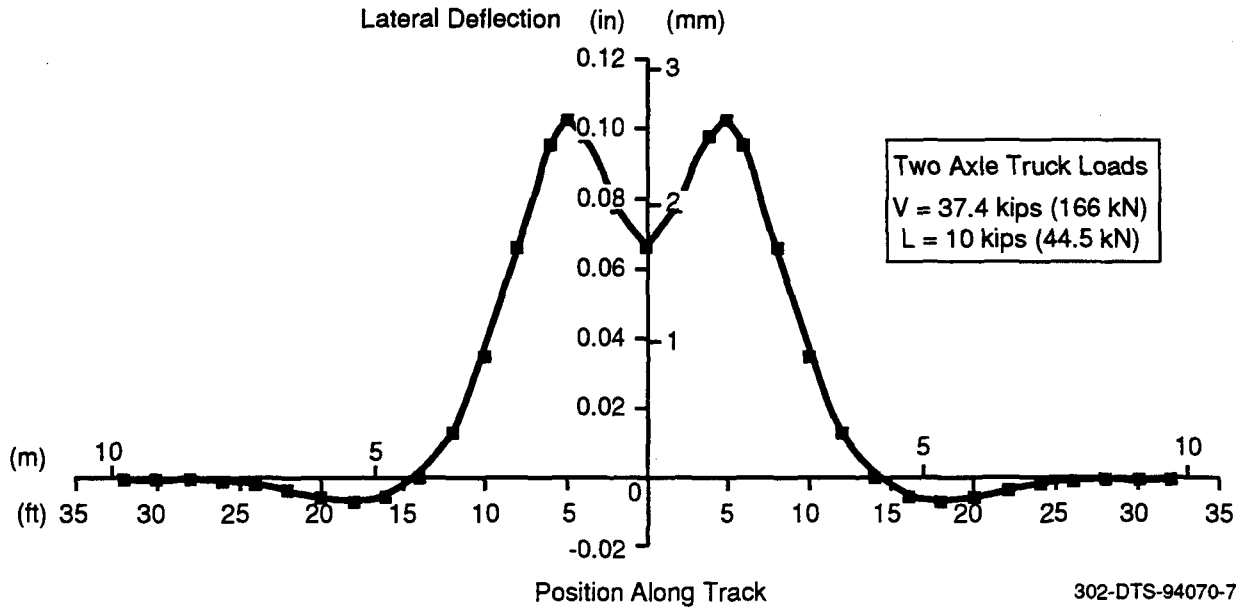

Figure B-6. Track lateral response for a truck load

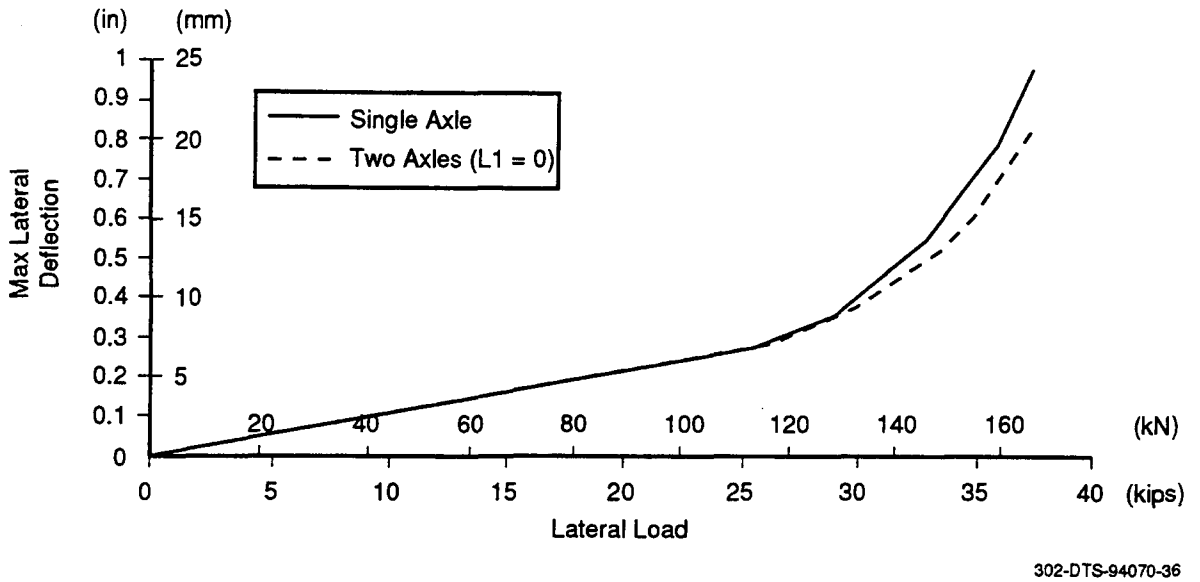

Figure B-7. Track lateral response for TGV-type loads

results for these two cases shows that the single axle case has a maximum loaded deflection about 20 percent greater than the two axle load in the extreme case of L/V = 1.

Figure B-8 shows the deflected profiles of the single and two axle cases. The wavelengths are also reasonably close. Thus the single axle idealization may be adequate in practical applications and is also conservative for the loads and axle spacing considered here. This has also been the conclusion of the SNCF researchers, as reported in (1).

B.5 INFLUENCE OF FREIGHT LOADS AND AXLE SPACING

In the foregoing numerical studies, the axle loads and spacing approximate those of a TGV-type vehicle. One would expect the influence of the adjacent axle to increase as the axle spacing is reduced and the vertical axle load is increased. Figure B-9 shows the track lateral deflection under a freight vehicle vertical load of 65 kips (289 kN) per axle and an axle spacing of 72 in. (1.8m). Note that in this case, the stabilizing effect of the adjacent axle is more pronounced in reducing the deflection, although the difference in deflection between the single axle and two axle cases shown here is still small, particularly for lateral loads within the "elastic limit" of the track (≈32 kips) (142 kN).

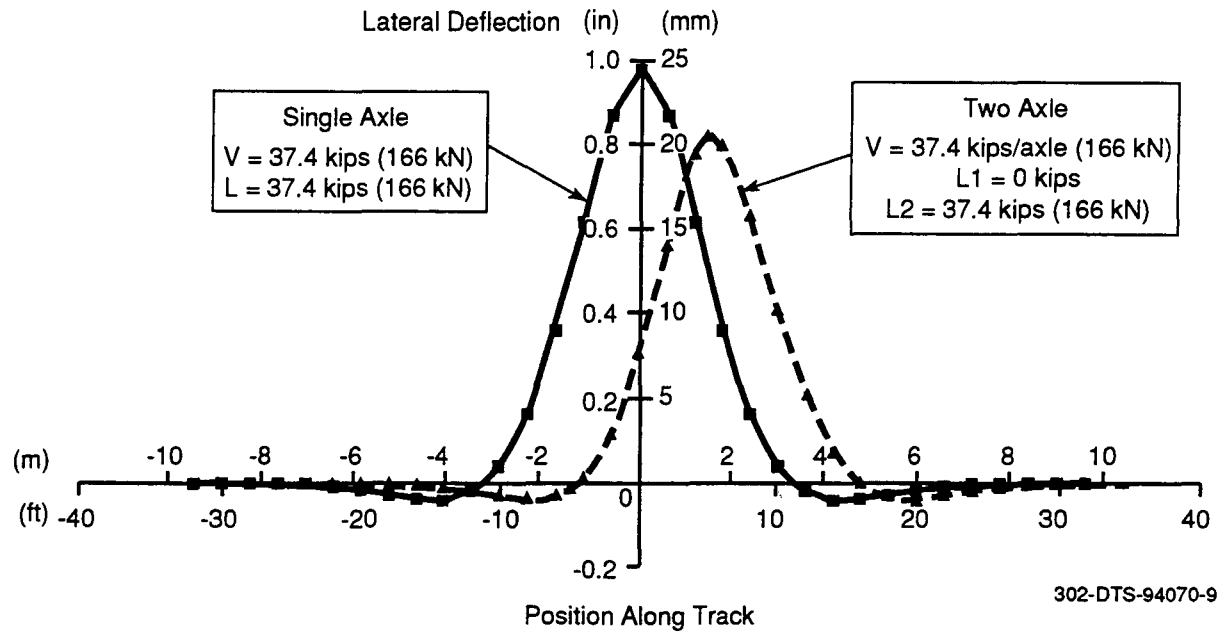

Figure B-8. Track lateral deflection profile (L/V = 1)

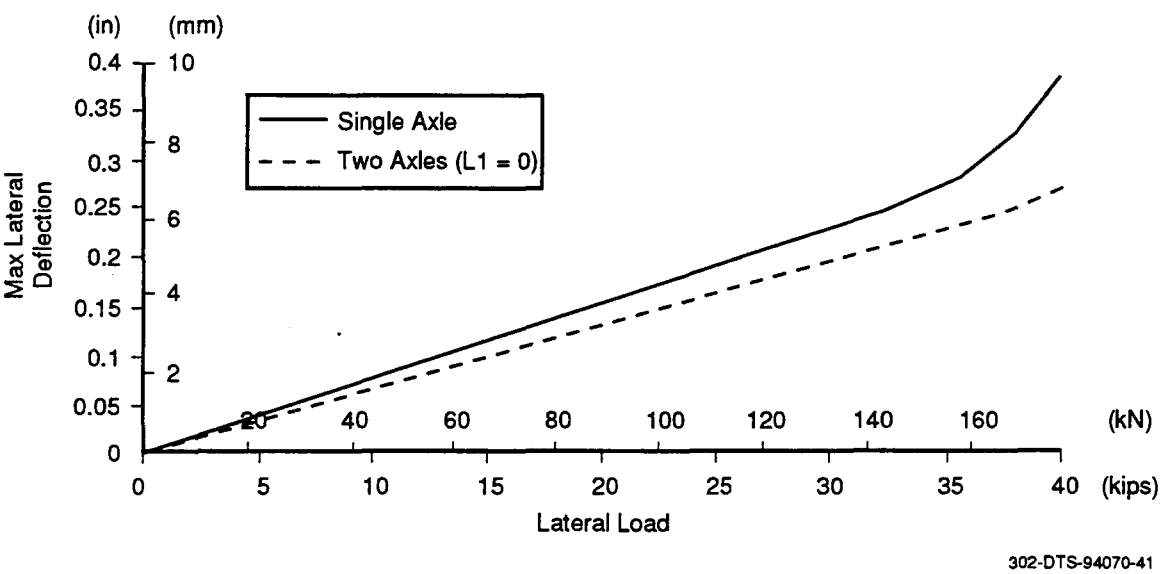

Figure B-9. Track lateral response for freight vehicle loads

B.6 SUMMARY

1. For the TGV-type loads and axle spacing considered here, the influence of the vertical load of an adjacent axle on the lateral response of a laterally loaded axle is negligible at low L/V (<0.6), and is small (within 20 percent at high L/V).

2. For these cases, the maximum lateral deflections due to single axle, truck and two adjacent truck loads are almost equal if the lateral and vertical loads on each axle are equal, particularly for low L/V (<0.6).

3. The lateral deflection under the truck loads is minimum in comparison to the single axle configuration when both axles carry equal lateral loads. If the net lateral loads is unequally proportioned on the two axles, the lateral deflection will increase compared to that of the case when the net load is equally shared.

4. For the TGV-type loads considered here, the single axle model for track shift appears to be adequate. Both axles of the truck would of course be required in the vehicle dynamic simulations, since the leading and trailing axles will have different L/Vs as they negotiate track imperfections. Both axles may also need to be considered for cases where gauge spreading or rail rollover loads are appreciable, for steady-state curving, and for vehicles using radially steered trucks. However in all cases, the influence of each axle on track shift can be separately studied and appropriately superimposed.

5. The stabilizing influence of the adjacent axle in reducing lateral deflections under load is more pronounced when heavy freight vehicle loads and axle spacing are considered. However, the effect is still small unless the "elastic limit" of the track is exceeded.

APPENDIX C

TRACK RESIDUAL DEFLECTION ANALYSIS

The equations governing the track lateral response are derived as follows neglecting the torsional stiffness in the fasteners, which is expected to be small due to small deflection involved. The lateral shear, Q(x) and bending moment, M(x), due to the applied loads and boundary conditions are given by

$$Q(x) = \sum_i -L_i\langle x - x_i\rangle^0 - \sum_n F_n\langle x - n\Delta\rangle^0 + C_1 \tag{C-1}$$

$$M(x) = \sum_i L_i\langle x - x_i\rangle + \sum_n F_n\langle x - n\Delta\rangle - C_1 x + C_2 \tag{C-2}$$

where

x_i = location of applied lateral load
n = tie number
Δ = tie spacing
$2m-1$ = total number of ties
F_n = lateral resistance force at tie "n" ($-m + 1 \le n \le m - 1$)
L_i = applied lateral load
C_1, C_2 = constants of integration
$\langle x-a\rangle^{\ell} = 0$ if $(x-a) < 0$
$(x-a)^{\ell}$ if $(x-a) > 0$

The lateral deflection is found by double integration of the bending moment equation, $M(x) = EIy''$.

$$y(x) = \iint \frac{M(x)}{EI}dx = \frac{1}{EI}\left[\frac{1}{6}\sum_i L_i\langle x - x_i\rangle^3 + \frac{1}{6}\sum_n F_n\langle x - n\Delta\rangle^3 - C_1\frac{x^3}{6} + C_2\frac{x^2}{2}\right]$$

$$+C_3x + C_4 \tag{C-3}$$

By applying the boundary conditions of zero deflection and zero slope at the beam ends ($x = \pm m\Delta$), it can be shown that the constants of integration C_1, C_2, C_3 and C_4 are given by

$$C_1 = \frac{3}{2(m\Delta)^2}\left[\sum_i \frac{L_i}{2}\langle m\Delta - x_i\rangle^2 + \sum_n \frac{F_n}{2}\langle m\Delta - n\Delta\rangle^2\right]$$

$$-\frac{3}{2(m\Delta)^3}\left[\sum_i \frac{L_i}{6}\langle m\Delta - x_i\rangle^3 + \sum_n \frac{F_n}{6}\langle m\Delta - n\Delta\rangle^3\right] \tag{C-4}$$

$$C_2 = \frac{-1}{2m\Delta}\left[\sum_i \frac{L_i}{2}\langle m\Delta - x_i\rangle^2 + \sum_n \frac{F_n}{2}\langle m\Delta - n\Delta\rangle^2\right] \tag{C-5}$$

$$C_3 = \frac{1}{EI}\left[C_1\frac{(m\Delta)^2}{2} - \frac{1}{2}\left[\sum_i \frac{L_i}{2}\langle m\Delta - x_i\rangle^2 + \sum_n \frac{F_n}{2}\langle m\Delta - n\Delta\rangle^2\right]\right] \tag{C-6}$$

$$C_4 = \frac{C_1}{EI}\left[\frac{(m\Delta)^3}{3}\right] + \frac{1}{EI}\left[\frac{-m\Delta}{4}\right]\left[\sum_1 \frac{L_i}{2}(m\Delta - x_i)^2 + \sum_n \frac{F_n}{2}(m\Delta - n\Delta)^2\right] \tag{C-7}$$

Substituting the above into equation (C-3) yields the following general expression for the track lateral displacement.

$$y(x) = \frac{1}{EI}\left\{\left[\sum_1 \frac{L_i}{6}(x - x_i)^3 + \sum_n \frac{F_n}{6}(x - n\Delta)^3\right]\right.$$

$$+\left[\sum_i \frac{L_i}{2}\langle m\Delta - x_i\rangle^2 + \sum_n \frac{F_n}{2}\langle m\Delta - n\Delta\rangle^2\right]\bullet\left[\frac{-x^3}{4(m\Delta)^2} - \frac{x^2}{4(m\Delta)} + \frac{x}{4} + \frac{m\Delta}{4}\right]$$

$$\left.+\left[\sum_i \frac{L_i}{2}\langle m\Delta - x_i\rangle^3 + \sum_n \frac{F_n}{2}\langle m\Delta - n\Delta\rangle^3\right]\bullet\left[\frac{x^3}{12(m\Delta)^3} - \frac{x}{4(m\Delta)} - \frac{1}{6}\right]\right\} \tag{C-8}$$

Due to the nonlinear lateral resistance, equation (8) above must be solved incrementally. The resulting equation for a load applied incrementally is as follows:

$$\delta_y(x_j) = \frac{1}{EI}\left\{\left[\frac{\delta L_i}{6} < x_j - \bar{x} >^3 + \sum_n \frac{\delta F_n}{6} < x_j - n\Delta >^3\right]\right.$$

$$+\left[\sum_i \frac{\delta L_i}{2} < m\Delta - \bar{x} >^2 + \sum_n \frac{\delta F_n}{2} < m\Delta - n\Delta >^2\right]\bullet\left[\frac{-x_j{}^3}{4(m\Delta)^2} - \frac{x_j{}^2}{4(m\Delta)} + \frac{x_j}{4} + \frac{m\Delta}{4}\right]$$

$$\left.+\left[\sum_i \frac{\delta L_i}{2} < m\Delta - \bar{x} >^3 + \sum_n \frac{\delta F_n}{2} < m\Delta - n\Delta >^3\right]\bullet\left[\frac{x_j{}^3}{12(m\Delta)^3} - \frac{x_j}{4(m\Delta)} - \frac{1}{6}\right]\right\} \tag{C-9}$$

Applying the equation above to each tie in the track section yields a matrix of N equations for the incremental displacements of each tie. These displacement increment equations are solved using Newton-Raphson iteration. As a result, the lateral displacements of each tie in the track section are determined for the loading/unloading process.

Moving Load Equations:

$$\delta_y(x_j) = \frac{1}{EI}\left\{\left[\frac{L}{6}\left(< x_j - (\bar{x} + \delta\bar{x}) >^3 - < x_j - \bar{x} >^3\right) + \sum_n \frac{\delta F_n}{6} < x_j - n\Delta >^3\right]\right.$$

$$+\left[\frac{L}{2}\left(< m\Delta - (\bar{x} + \delta\bar{x}) >^2 - < m\Delta - \bar{x} >^2\right) + \sum_n \frac{\delta F_n}{2} < m\Delta - n\Delta >^2\right]$$

$$\bullet\left[\frac{-x_j^3}{4(m\Delta)^2} - \frac{x_j^2}{4(m\Delta)} + \frac{x_j}{4} + \frac{m\Delta}{4}\right] \qquad \text{(C-10)}$$

$$+\left[\frac{L}{2}\left(< m\Delta - (\bar{x} + \delta\bar{x}) >^3 - < m\Delta - \bar{x} >^3\right) + \sum_n \frac{\delta F_n}{2} < m\Delta - n\Delta >^3\right]$$

$$\left.\bullet\left[\frac{x_j^3}{12(m\Delta^3)} - \frac{x_j}{4(m\Delta)} - \frac{1}{6}\right]\right\}$$

where $\delta\bar{x}$ is the incremental distance the load has moved.

Figure C-1 shows a flow diagram for the solution procedure used in the moving load model. At the initial load location, the model first determines the vertical reaction of the ties due to the axle load, and the resulting lateral resistance. A matrix of N equations can then be established to describe the displacement of N ties. The Jacobian, used in the Newton-Raphson iterative solution procedure, is determined. The model then solves for each of these equations using Gaussian elimination, with the Jacobian forming the RHS of the equations. The method is based on the algorithm originally developed by Snyder (6) for thermoelastic-plastic creep analysis.

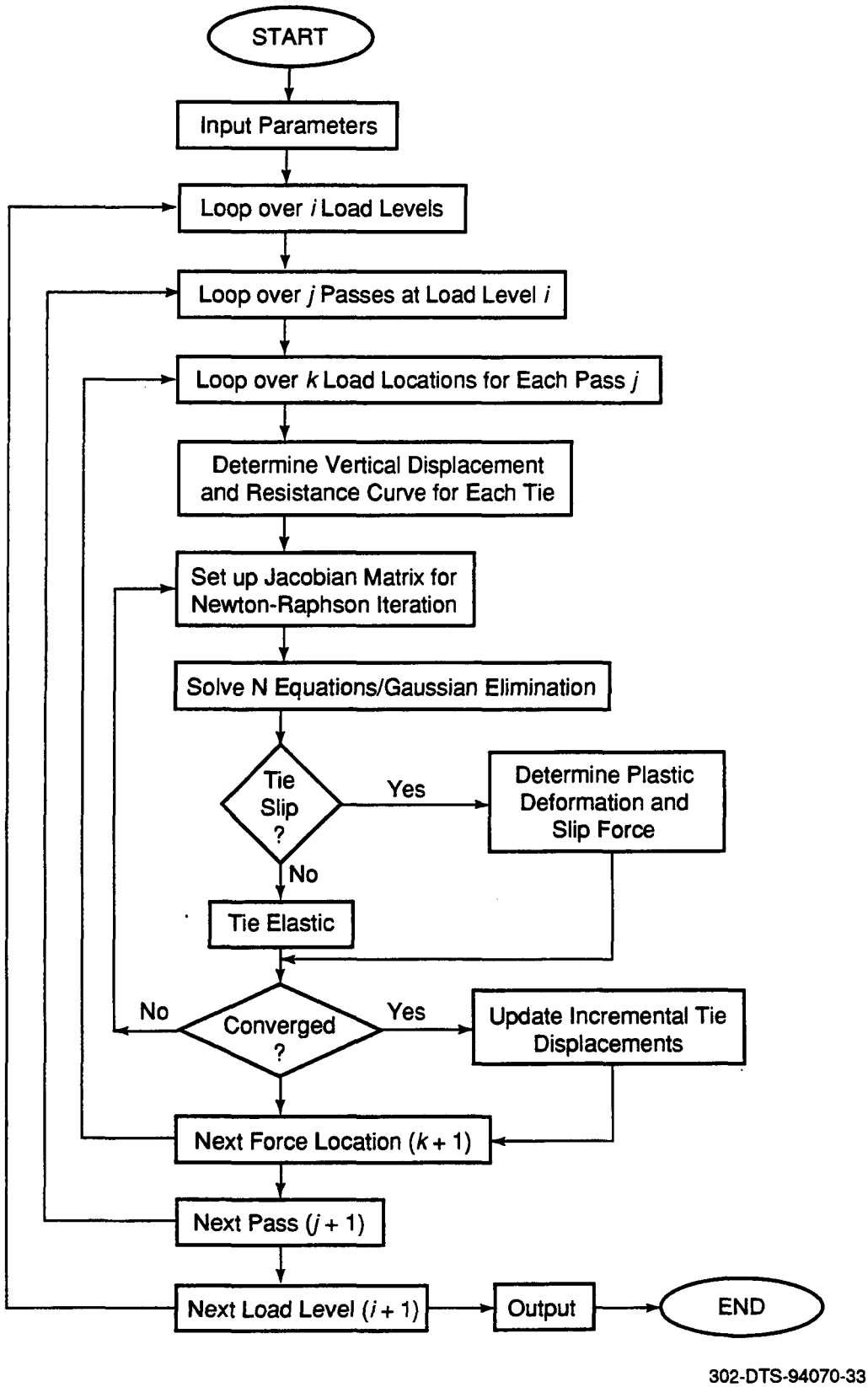

Figure C-1. Algorithm for moving load

Each tie is then checked for slipping. If the displacement exceeds the elastic slip conditions for the current load level, the displacement is re-evaluated according to the lateral resistance curve. The results are checked for convergence. If convergence is not met, the displacement equations are again solved with the recalculated Jacobian. Once converged, the vertical and lateral load locations are incremented an amount, δx, the vertical reactions are recalculated, and the process is repeated. When the load reaches the end point of the beam, the load is released, and the residual displacements are determined. The load then begins again at the first end for the next pass or load level.

APPENDIX D

VEHICLE DYNAMIC ANALYSIS ISSUES

D.1 INTRODUCTION

The objective of the study presented here is to evaluate the adequacy of a single truck model in the vehicle dynamic simulations. This evaluation will be done through comparison of responses of a single truck model to that of a full consist.

As has been stated in Section 1, simplicity and operating speed are important in the development of a user-friendly track shift model. Working as an integral part of the overall model, the dynamic simulation uses a lumped parameter vehicle model to determine the loads exerted on the track. The processing speed or "run time" of the simulation on a PC is directly related to the number of degrees of freedom used in the vehicle model. This implies that a multi-vehicle consist model will run much more slowly than a simple model consisting of only a single vehicle, or a single truck. For an approximate track shift analysis, a single truck simulation may be adequate, if it predicts the wheel lateral loads exerted on the rails with reasonable accuracy.

The single truck model constructed for this analysis is shown in Figure D-1. The model consists of a two axle TGV-type truck with primary and secondary suspensions. The secondary suspension supports a mass with the size and inertias of a typical TGV-type car body. The trailing end of the mass is supported by a position input which follows the path of the track, and simulates the effects of the trailing truck on the car body.

To validate the single truck model, a series of runs was conducted using sinusoidal track misalignments ranging from 4 to 20 mm in amplitude, with wavelengths ranging from 8 to 20m.

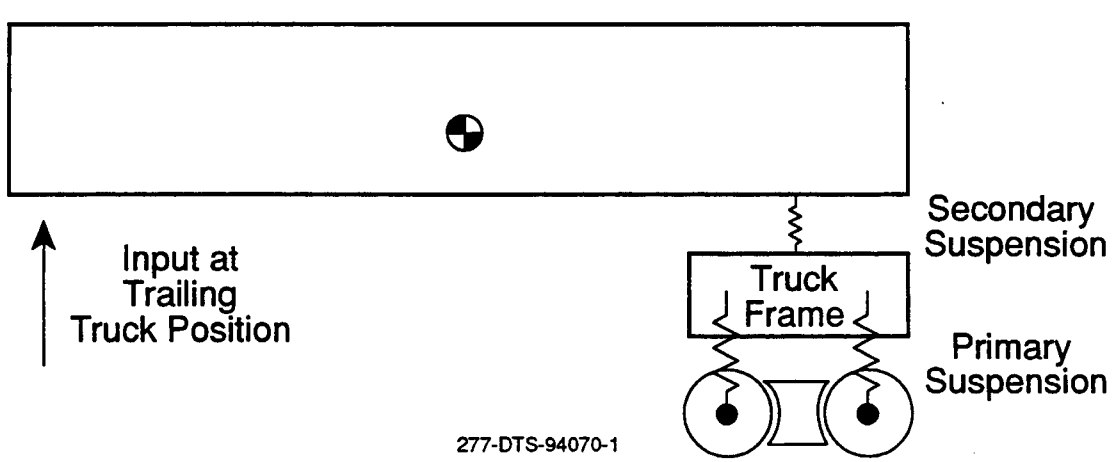

Figure D-1. Single truck model

The results of these tests were then compared to data presented in (1) for a multi-car TGV consist running over these same track misalignments. Two factors were of primary interest in this comparison study:

- The ability of the single truck model to correctly predict the instances of wheel climb derailment.

- The accuracy of the single truck net axle forces exerted on the track.

Results of these studies are presented below.

Wheel Climb Derailment

A summary of wheel climb derailment results is presented in Table D-1 for a vehicle speed of 300 km/hr (186 mph). Note that there is excellent agreement between the results of the single truck and full consist models. The single truck model successfully predicted the occurrence and location of each derailment. The single truck and full consist models also agree in cases where derailment does not occur, as shown by the last entry on the table.

Net Axle Lateral Loads

Figure D-2 presents a comparison of results for the net lateral axle loads exerted on the track during negotiation of a 12 mm misalignment. Note that there is excellent agreement between the results for the single truck and full consist models. The single truck model successfully

Table D-1. Comparison of wheel climb derailment results

Lateral Misalignment Size (amplitude/wavelength)	Results for Full Consist Model	Results for Single Truck Model
20 mm/8m	Derailment at track position x = 45.9m	Derailment at track position x = 45.7m
20 mm/10m	Derailment at track position x = 47.1m	Derailment at track position x = 47.1 m
20 mm/15m	Derailment at track position x = 49.8m	Derailment at track position x = 49.8m
20 mm/20m	No derailment	No derailment

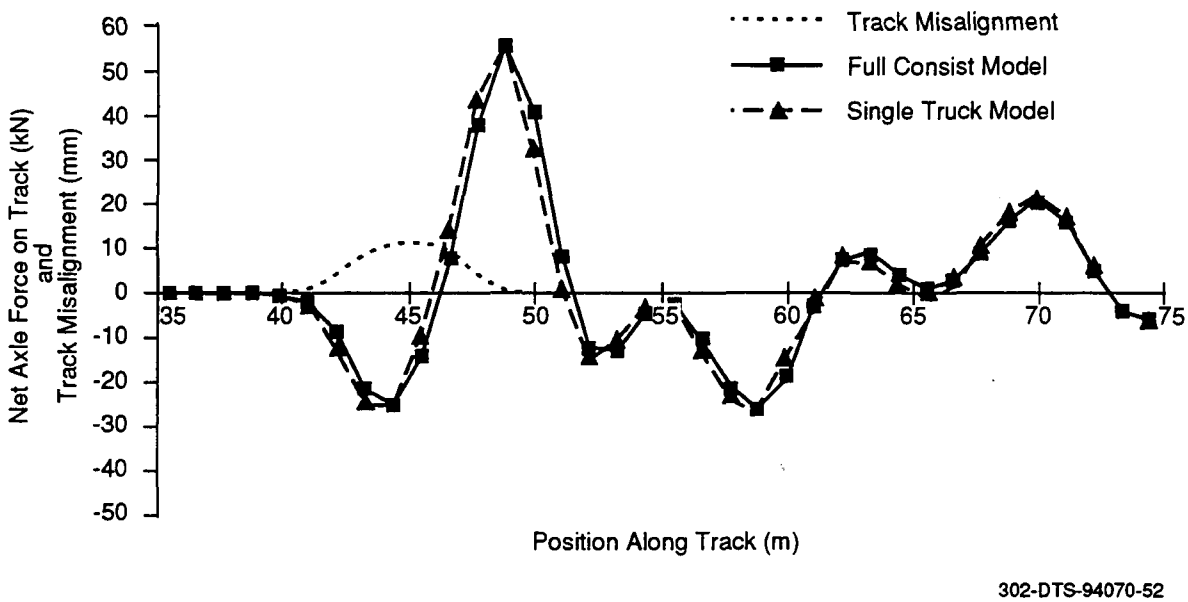

Figure D-2. Comparison of net axle forces for single truck and full consist models

predicted the direction, magnitude and duration of the net lateral loads, with a maximum discrepancy of approximately 8 kN (2 kips).

D.2 SUMMARY ON SINGLE TRUCK MODEL INVESTIGATION

1. The TGV-type single truck model provides an adequate assessment of the wheel climb derailment potential and net lateral forces exerted on the track by a full TGV-type consist model.

2. The single truck model provides a significant run time advantage over larger models. The model runs approximately three times faster than the full consist model.

3. Based on the results presented here, the single truck model should provide a reasonable tool for the assessment of track lateral loads and wheel climb derailment.

APPENDIX E

OMNISIM DESCRIPTION

THE PROGRAM OMNISIM

This report gives the background and theory of the program **OMNISIM**. It has been used extensively in the project reported. Whereas much of the work reported elsewhere on the behavior of rail vehicles during derailment has a very limited model of the track, this restriction has been eliminated in **OMNISIM** which permits a track model similar in accuracy to that of the vehicle. It has been used here to aid in the investigation of dangerous service conditions which may arise from lateral track shift. The program accounts for the track or guideway masses and flexibilities in both the lateral and vertical plane. Thus, the influence of the vertical wheel loads on the lateral forces are modeled with improved accuracy and has been used to provide the loads between the wheel and rail for input to the separate more detailed track shift model and program for finding the track residual deflections after vehicle passage. The resulting experience has allowed special connections to be introduced into **OMNISIM** to allow a more accurate model of both vehicle and track behavior.

The models in **NUCARS**[7] or **SYSSIM** are limited to the vehicle as a multibody system, terminating either in simple body supports or in a wheel-on-rail connection which determines the connection to ground through a simple nonlinear vertical connection and a linear lateral connection, both allowing for relative displacements of the shape of the rail, either as a digital measured or a constructed analytical shape. There are certain approximations within this model which allow, with care and an appropriate choice of parameters, an accurate representation of wheel climb derailment. However, it is a requirement of the model that the rail motion remain small and not be coupled to that at the adjacent wheel. This remains a very limiting factor in the simulation of the performance of vehicles under danger from derailment due to gage widening and/or track shift.

In addition, **OMNISIM** has been shown to provide an accurate assessment of vehicle hunting, including the effect of the supporting track or guideway structure. In other less complete simulations, such as those using **SYSSIM** or the current version of **NUCARS**, this can lead to nonconservative results. However the present model of **OMNISIM** does not allow for the accumulation of lateral track shifts with the passage of many wheels and axles. This requires that the coordinates of the guideway or track not move along with the vehicle and will be added at a later stage. Thus the track shift model is used in this part of the work where the accumulation of lateral movement is important. The objective is to provide a comprehensive, user-friendly tool in the public domain for use by Government, industry and the research community.

A General Description of OMNISIM

OMNISIM is a multi-body system simulation modeling both vehicle and supporting structures in a generalized manner. The program can predict their behavior in transient and steady-state response in the time domain. It can work with English or metric units and with measured or analytically constructed inputs or a combination of both. It represents a single means to predict any system response, such as that of a rail vehicle, to a variety of inputs, such as those from the guideway, an actuator or wind forces. Thus, in rail vehicles, **OMNISIM** allows a fundamental observation of the response to rail shift or gauge spreading or wheel climb derailments. Vehicle ride quality may also be assessed. The flexible structure of the input allows the user to model any new or existing system including experimental guideway and vehicle structures and designs.

In addition to the main run processor, pre- and post- processing programs have also been created. For post-processing, **PLOTS** produces graphs of the output for a monitor or for hardcopy output. **TEXTS** produces numerical information for viewing or passing to other post-processors, such as spreadsheets' for further manipulation. The program requires the user to define a system model with inertial and geometric properties for both vehicle and guideway, connection characteristics, wheel/rail geometry data if required, and displacement or force inputs for making a simulation run. **OMNISIM** models the interaction of rigid or flexible bodies joined through connections, i.e., suspension elements.

Means are provided to vary the number and identity of the degrees of freedom for each body. The potential choices include all translational and rotational rigid body motions and the first free-free flexible modes in twist and in vertical and lateral bending. The system is defined in a text file called the definition file, using an appropriate word processor, which is then preprocessed to the required format and units by the preprocessing program **DEFINE**. This program not only rearranges the data and the unit system chosen, but also permits the user to see the system in diagrammatic form, displaying its geometry and characteristics. The program will also display previously pre-processed system files.

Guideway and vehicle interbody connections are represented in a number of types. Their characteristics range from simple spring and damper pairs in parallel or in series to more complex friction elements. The characteristic of each spring or damper is defined using a piecewise linear function of displacement or velocity respectively. The representation of hysteresis requires two piecewise linear functions which represent the assymptotic loading and unloading curves. Additional information, such as the speed of closure to the assymptote in hysteresis, may be required. Other characteristics are used to represent friction surfaces, especially useful for modeling ballasted track with ties. Several subcategories of this connection type are available, in which the value at which the friction force becomes saturated is chosen for the direction of motion, or others types which are dependant on the normal load. The rate at which the friction force builds may also be chosen to be constant or dependant on the normal load. The shape of the friction curve is again in generalized piecewise linear form. Although other moving support connections, such as magnetic, may be inserted, a special characteristic is included which may be used to connect a steel wheel to its rail.
The present wheel/rail connection assumes no roll rotation of the rail and the vehicle and track system are in the same moving coordinates. This is equivalent to a track model which generates a constant moving wave at each wheel as the vehicle moves down the track. Although useful in identifying rail motions, further improvements are contemplated which will allow the rails to be modeled as a stationary continuum, reducing the number of degrees of freedom and release the rail support model from moving with the vehicle. Each individual wheel/rail connection uses a look up table for its profile geometric variables and the rolling contact forces for the steel wheels on steel rails of railway vehicles. The profile data tables are precomputed using a more flexible version of Law and Cooperrider's program **WHRAILA**[8], which is called **PROFIT**. A four dimensional look up of creep force coefficients, according to Kalker[9] and as adapted by British Rail, is used in determining the forces and moments on each wheel. The rotational speed of the rotating body, which may be a solid axle or an independent wheel, is regarded as a special variable and is held locally and used to obtain the wheel/rail forces. The method assumes that the dominant changes in the wheel/rail contact

geometry are those due to relative displacement between each wheel and the rail to which it is connected.

Any input may be measured or analytically constructed in segments using several optional functions. For inputs representative of laboratory simulation, generally as a function of time, these can be defined in a general input text file which is read by the run program **OMNISIM** at commencement. However, at the option of the user, this file may call on preprocessed measured or analytic data, formatted as digital information in steps of the distance along a chosen path or track. This preprocessor, called **INPUTS**, may itself call in data from track geometry in a file called HISFIL. **INPUTS** requires a text setup file to identify the source and preprocess the path and input data which may be of mixed origins.

Inputs defining the path or track for the system are classed as being of long or short wavelength. The short wavelength effects are regarded as local guideway or rail perturbations and are introduced as variations in lateral or vertical position of the guideway. For the analytically defined inputs, a repeated shape and amplitude for a segment of the guide or rail may be chosen from a combination of cusps, bends, or sine waves, including a swept frequency sine wave, allowing vibration testing of a stationary vehicle. The long wavelength variations define the overall path and are linearly interpolated from positions along the track at which curvature and superelevation are either chosen analytically or taken from the measured data set. These are transformed into components of the connection strokes, so that the degrees of freedom for each body remain those relative to its local inertial coordinate system. Provision is made to allow both external displacement and forcing inputs to the model. Guideway or rail irregularity is an example of a displacement input, a coupler load due to train action is an example of a forcing input.

THE THEORY OF OMNISIM

In this section, it is shown that **OMNISIM** presently represents a significant advance in the simulation of rail vehicles and track up to and including all types of derailment behavior. Further improvements are define in a later section.

The Form of the Equations in OMNISIM

OMNISIM is designed to handle an arbitrary number of bodies, joined through connections, all of which must have characteristics defined. "Rigid" connections are given large stiffness. Means are provided for varying the number and identity of the degrees of freedom chosen for each body. These are chosen from a list which includes all translational and rotational rigid body degrees of freedom and the first flexible modes for the long bodies in twist, vertical and lateral bending. At present, all bodies are assumed to travel at the same speed along the direction of travel. This will be modified in later versions to add both stationary and moving body coordinates. As an example of the method used to manipulate the equations of motion, consider Fig. 1 with variables in pitch and vertical translation,

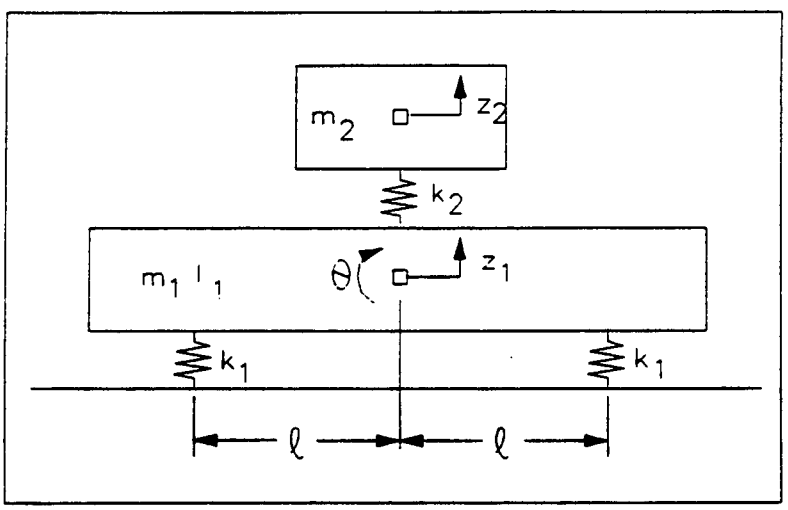

Figure 1 A Simple 2-Mass System

The equations of motion for the system may be written by inspection as,

$$m_1\ddot{z}_1 + k_1(z_1 + l\theta) + k_1(z_1 - l\theta) - k_2(z_2 - z_1) = 0$$

$$I_1\ddot{\theta} + lk_1(z_1 + l\theta) - lk_1(z_1 - l\theta) = 0$$

$$m_2\ddot{z}_2 + k_2(z_2 - z_1) = F \qquad (1)$$

These are often reduced for the symmetric case to,

$$m_1\ddot{z}_1 + 2k_1z_1 - k_2(z_2 - z_1) = 0$$

$$I_1\ddot{\theta} + 2l^2k_1\theta = 0$$

$$m_2\ddot{z}_2 + k_2(z_2 - z_1) = F \qquad (2)$$

However an alternative representation is possible in Eq. (1), by retaining the strokes across the springs. Hence, if $s_1 = z_1 + l\theta$, $s_2 = z_1 - l\theta$ and $s_3 = z_2 - z_1$, the equation may be written,

$$m_1\ddot{z}_1 + k_1 s_1 + k_1 s_2 - k_2 s_3 = 0$$

$$I_1\ddot{\theta} + lk_1 s_1 - lk_1 s_2 = 0$$

$$m_2\ddot{z}_2 + k_2 s_3 = F \tag{3}$$

In matrix form the equations may be written as,

$$\begin{Bmatrix} s_1 \\ s_2 \\ s_3 \end{Bmatrix} = \begin{bmatrix} 1 & l & 0 \\ 1 & -l & 0 \\ -1 & 0 & 1 \end{bmatrix} \begin{Bmatrix} z_1 \\ \theta \\ z_2 \end{Bmatrix} \tag{4}$$

and,

$$\begin{bmatrix} m_1 & 0 & 0 \\ 0 & I_1 & 0 \\ 0 & 0 & m_2 \end{bmatrix} \begin{Bmatrix} \ddot{z}_1 \\ \ddot{\theta} \\ \ddot{z}_2 \end{Bmatrix} = \begin{Bmatrix} F \\ 0 \\ 0 \end{Bmatrix} - \begin{bmatrix} 1 & 1 & -1 \\ l & -l & 0 \\ 0 & 0 & 1 \end{bmatrix} \begin{Bmatrix} k_1 s_2 \\ k_1 s_1 \\ k_2 s_3 \end{Bmatrix} \tag{5}$$

For any system of masses, including the equations for the fundamental modes in twist, vertical and lateral bending, if the masses are all in the same coordinates, the general equation takes the form,

$$\mathrm{M}\ddot{q} = -\mathrm{T}^T \mathrm{f}(s, \dot{s}) - \mathrm{D}\dot{q} - \mathrm{K}q + \mathrm{F} \tag{6}$$

where, $s = \mathrm{T}q$, $\dot{s} = \mathrm{T}\dot{q}$, M is the mass matrix, D and K are the structural damping and stiffness matrices, T is the geometric transformation matrix, q, $\dot{q}$ and $\ddot{q}$ are the vector of degrees of freedom and input degrees and their first and second derivatives, f is a vector of nonlinear characteristic functions of the connection strokes or stroke velocities, s and $\dot{s}$, and F is a vector of forcing inputs.

In the simple example above, the geometric transformation matrix is given by,

$$\mathrm{T} = \begin{bmatrix} 1 & l & 0 \\ 1 & -l & 0 \\ -1 & 0 & 1 \end{bmatrix} \text{and} \mathrm{T}^T = \begin{bmatrix} 1 & 1 & -1 \\ l & -l & 0 \\ 0 & 0 & 1 \end{bmatrix} \tag{7}$$

For simplicity, the springs were given a linear characteristic. However Eq. (5) could have contained nonlinear springs. For example, the expression $k_1 s_2$ could have been written $f_1(s_2)$ where f_1 represents any known nonlinear function of its stroke s_2. Similarly the spring elements may have been chosen with damping such that the function becomes $f_1(s_2, \dot{s}_2)$.

The Procedure used to Establish the Equation of Motion

The procedure adopted by the computer in setting up the equations of motion is given here in a second example having the same form given in Eq. (6). The example in this case is that of an incomplete simple car with a flexible frame and wheels on suspended rails, shown in Fig. 2.

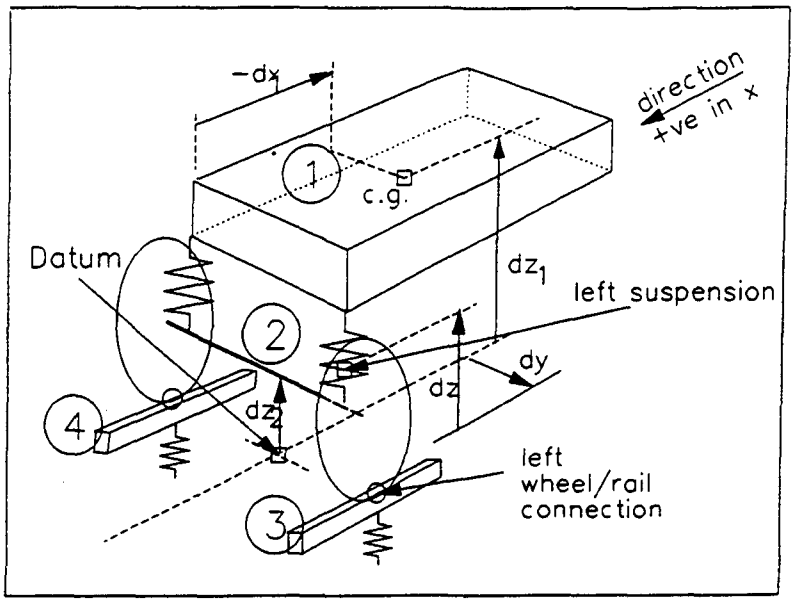

Figure 2 A Simple Car and Axle on Suspended Rails

Since the car body and axle are assumed to have the same velocity and are centered on the track, no longitudinal degree of freedom is include for them. The car body may move laterally and vertically and may roll, pitch, yaw and twist. The axle may move laterally and vertically, yaw relative to the track or roll. In general, the axle may also be allowed to move longitudinally. The rails may move laterally and vertically and may pitch and yaw. The vector of degrees of freedom will include the following,

$$\{q\} = \{y_1, z_1, \phi_1, \theta_1, \psi_1, \xi_1, y_2, z_2, \phi_2, \psi_2, y_3, z_3, \theta_3, \psi_3, y_4, z_4, \theta_4, \psi_4\}^T \qquad (8)$$

The Form of the Mass, and Structural Damping and Stiffness Matrices

The mass matrix M is diagonal and is stored as a vector. The inverse M^{-1} is also diagonal and is stored as a vector of the reciprocals of the masses and inertias. The flexible modal stiffness and damping matrices, K and D are also diagonal and stored as vectors. The terms in K are of the form $\omega^2 I$ and those in D are of the form $2\zeta\omega I$, where ω is the first modal frequency, I is the appropriate inertia or mass, and ζ is the modal damping ratio.

In this example, the mass and roll, pitch, yaw inertias for the carbody, mass roll and yaw inertias for the axle and the mass, pitch and yaw inertias for the rails are included in a vector of their inverses as follows,

$$M^{-1} = DIAG\{\frac{1}{m_1}, \frac{1}{m_1}, \frac{1}{I_{x1}}, \frac{1}{I_{y1}}, \frac{1}{I_{z1}}, \frac{1}{I_{x1}}, \frac{1}{m_2}, \frac{1}{m_2}, \frac{1}{I_{x2}}, \frac{1}{I_{z2}},$$

$$\frac{1}{m_3}, \frac{1}{m_3}, \frac{1}{I_{y3}}, \frac{1}{I_{z3}}, \frac{1}{m_4}, \frac{1}{m_4}, \frac{1}{I_{y4}}, \frac{1}{I_{z4}}\} \qquad (9)$$

This example only contains one flexible mode, that in twist for the carbody. However, it requires that a frequency and modal damping ratio be provided in the data so that the terms in K and D can be computed.

Transformation from Degrees of Freedom to Strokes and Stroke Velocities

The program stores the transformation matrix T as a compressed vector, to carry out the transformation from the body inputs and degrees of freedom to the strokes or stroke velocities at all the connections. This is made possible by the fact that each connection has only two ends and each stroke across it can only be a linear combination of the degrees of freedom associated with two bodies and not all of these. Only the degrees of freedom used at the end of each connection are stored in the vector and a vector multiplier is used to carry out the required multiplication.

The lead left vertical suspension member is used to illustrate the procedure for the connections between bodies. This suspension has only the vertical direction of motion and this must is identified in the data so that the transformation matrix elements have the appropriate values. Other more complex connections such as that for the wheel on rail require several directions to be identified. The suspension in this example connects masses numbered 1 for the main body and 2 for the axle. Its location relative to the datum is given. The position of the lead axle center at track height is chosen as the datum. All bodies are behind the datum along the track and the heights are given relative to the track surface, a common convention. Thus, the position of the lead left suspension relative to the datum is $\{0, dy, dz\}$. It is necessary to locate the suspension within each of the bodies it connects. This is carried out in a general manner, using the information provided in the data for each of the bodies, relating the locations of their mass centers to the same datum. If the location of the main body is $\{-dx_1, 0, dz_1\}$ and that of the lead axle $\{0, 0, dz_2\}$, then by the appropriate subtractions, the computer assigns the location of the lead left suspension in the main body coordinates to $\{dx_1, dy, (dz - dz_1)\}$ and in the axle body coordinates to $\{0, dy, (dz - dz_2)\}$.

The transformation matrix in the expressions, $s = Tq$ or $\dot{s} = T\dot{q}$, is potentially large, especially for systems which include a detailed definition of the track or guideway. The lead left suspension used in this example is vertical. The stroke across it may be expressed as, $s = r_1 + (-r_2)$. A convention is used so that if the second body is grounded, then $r_2 \to 0$. In the above expressions, the vectors, r_1 and r_2 are the displacements of the ends of the suspension in the bodies numbered 1 and 2. They are linear combinations of the degrees of freedom of the bodies.

Thus, $r_1 = C_{11}y_1 + C_{12}z_1 + C_{13}\phi_1 + C_{14}\theta_1 + C_{15}\psi_1 + C_{16}\xi_1$ (10)

where, $C_{11} = 0; C_{12} = 1; C_{13} = dy; C_{14} = -dx_1; C_{15} = 0; C_{16} = \sqrt{2}\{dy\}\cos\left(\frac{n dx_1}{L}\right)$

and, $-r_2 = C_{21}y_2 + C_{22}z_2 + C_{23}\phi_2 + C_{24}\psi_2$ (11)

where, $C_{21} = 0; C_{22} = -1; C_{23} = -dy; C_{24} = 0$

The complete transformation matrix for the system is large. The following equation identifies only the elements for the two vertical car suspensions,

$$
\begin{Bmatrix} s_{1l} \\ s_{1r} \\ \cdot \\ \cdot \\ \cdot \\ \cdot \\ \cdot \\ \cdot \\ \cdot \\ \cdot \\ \cdot \\ \cdot \end{Bmatrix} =
\begin{bmatrix}
0 & 1 & dy & -dx_1 & 0 & \sigma & 0 & -1 & -dy & 0 & 0 & 0 & 0 & 0 & 0 & 0 & 0 & 0 \\
0 & 1 & -dy & -dx_1 & 0 & -\sigma & 0 & -1 & dy & 0 & 0 & 0 & 0 & 0 & 0 & 0 & 0 & 0 \\
\cdot & \cdot & \cdot & \cdot & \cdot & \cdot & \cdot & \cdot & \cdot & \cdot & \cdot & \cdot & \cdot & \cdot & \cdot & \cdot & \cdot & \cdot \\
\vdots & & & & & & & & & & & & & & & & & \vdots \\
\cdot & \cdot & \cdot & \cdot & \cdot & \cdot & \cdot & \cdot & \cdot & \cdot & \cdot & \cdot & \cdot & \cdot & \cdot & \cdot & \cdot & \cdot
\end{bmatrix}
\begin{Bmatrix} y_1 \\ z_1 \\ \phi_1 \\ \theta_1 \\ \psi_1 \\ \xi_1 \\ y_2 \\ z_2 \\ \phi_2 \\ \psi_2 \\ y_3 \\ z_3 \\ \theta_3 \\ \psi_3 \\ y_4 \\ z_4 \\ \theta_4 \\ \psi_4 \end{Bmatrix}
\tag{12}
$$

where the modal element for the body twist is, $\sigma = \sqrt{2}\{dy\}\cos\left(\frac{\pi dx_1}{L}\right)$. L is the body length.

The same matrix governs the relationship between the degree of freedom time derivatives and the stroke velocities. The form of the matrix shows clearly the existence of unused zeros where the connection between the suspension and body does not exist. Generally, the larger the model, the more zeros are created in the matrix. The solution in has been to identify and use only nonzero elements connecting degrees of freedom to the strokes between the bodies at its ends. The result is stored as a vector and has the following appearance.

$$
T_{vector} = \left\{\left(\frac{\{r_{11}\}+\{-r_{12}\}}{for\, s_1}\right)\left(\frac{\{r_{21}\}+\{-r_{22}\}}{for\, s_2}\right)....etc.\right\}^T \tag{13}
$$

For the lead left vertical suspension discussed, the elements in the compressed vector with the zeros omitted are, $(1), (dy), (-dx_1), (\sigma), (-1), (-dy)$. The multiplication scheme for the process includes the indexing of the elements in the vector for T so that they are called upon to multiply the appropriate degree of freedom.

The program speed is also increased by selecting a minimal representation of the connections, which is under the control of the user. Thus pairs of spring/damper combinations may sometimes be combined into rotational elements with advantage, especially since all longitudinal masses centered on the track centerline are often assumed to have the same speed and therefore do not need a connection between them.

Insertion of the Connection Forces into the Equation

The forces from the connections described more fully below are added to the equations for each degree of freedom following their individual computation to form the vector of connection forces, $f(s, \dot{s})$, if Eq. (6). This is carried out through the multiplication $T^T f(s, \dot{s})$. However, in order to justify the equation, the term in the multiplying transformation will be established from first principles.

Designating the vertical forces in the suspensions, F_{1l}, F_{1r} as the forces in the left and right suspensions for the axle, it may be determined from the summation of the forces and moments that the sample equations of motion which follow, include the terms given.

$$M_1\ddot{z}_1 = -\{F_{1l} + F_{1r} + \ldots\}$$

$$I_{xl}\ddot{\phi}_1 = -\{(dy)F_{1l} - (dy)F_{1r} + \ldots\}$$

$$I_{yl}\ddot{\theta}_1 = -\{-(dx_1)F_{1l} - (dx_1)F_{1r} + \ldots\}$$

$$I_{xl}\ddot{\xi} = -\{\sigma F_{1l} - \sigma F_{1r} + \ldots\}$$

$$M_2\ddot{z}_2 = -\{-F_{1l} - F_{1r} + \ldots\}$$

$$I_{x2}\ddot{\phi}_2 = -\{-(dy)F_{1l} + (dy)F_{1r} + \ldots\}$$

It can be seen that the matrix in the expression below is T^T where T is the transformation matrix derived in Eq. (12). As with the determination of the strokes from the degrees of freedom, the full matrix contains many zeros. However, the vector used in **OMNISIM** to store the matrix information is used in a similar manner to that used in obtaining the strokes but in this case the multiplication is by the transposed elements and the vector multiplied has the dimension of the number of connections.

These expressions form part of a general matrix as follows.

$$\begin{Bmatrix} F_{y1} \\ F_{z1} \\ F_{\phi 1} \\ F_{\theta 1} \\ F_{\psi 1} \\ F_{\xi 1} \\ F_{y2} \\ F_{z2} \\ F_{\phi 2} \\ F_{\psi 2} \\ F_{y3} \\ F_{z3} \\ F_{\theta 3} \\ F_{\psi 3} \\ F_{y4} \\ F_{z4} \\ F_{\theta 4} \\ F_{\psi 4} \end{Bmatrix} = - \begin{bmatrix} 0 & 0 & \cdots \\ 1 & 1 & \cdots \\ dy & -dy & \cdots \\ -dx_1 & -dx_1 & \cdots \\ 0 & 0 & \cdots \\ \sigma & -\sigma & \cdots \\ 0 & 0 & \cdots \\ -1 & -1 & \cdots \\ -dy & dy & \cdots \\ 0 & 0 & \cdots \\ 0 & 0 & \cdots \\ 0 & 0 & \cdots \\ 0 & 0 & \cdots \\ 0 & 0 & \cdots \\ 0 & 0 & \cdots \\ 0 & 0 & \cdots \end{bmatrix} \begin{Bmatrix} F_{1l} \\ F_{1r} \\ \cdot \\ \cdot \\ \cdot \\ \cdot \\ \cdot \\ \cdot \\ \cdot \\ \cdot \\ \cdot \\ \cdot \\ \cdot \\ \cdot \end{Bmatrix} \tag{17}$$

The Characteristic Equations for Flexible Modes

The theory of elastic rods and beams is found in many texts and will not be repeated in full here. However a summary is required for the understanding of the dynamics of such elements as they appear in **OMNISIM**. In shear, and in tension or compression, structural materials are generally described by a constant representing the ratio of the applied stress to the resulting strain. In shear, this constant is G and in tension E, commonly known as Young's modulus, is used. For the cases of the torsion of a rod or bending of a beam, the relationship of the applied effort to the resulting deformation is generally established by integration over a cross section of the element to establish the total moment about a suitable axis. This results in the use of properties of the area and its shape. The shape properties are the second moment of area about the appropriate axis, J about the central axis in torsion and I about the transverse axis in bending.

The resulting equation for the torsion of a rod is,

$$GJ\frac{\partial \phi}{\partial x} = T \tag{18}$$

and for the bending beam,

$$EI\frac{\partial^2 z}{\partial x^2} = M \tag{19}$$

Thus the constitutive relationships take the general form,

$$\mathrm{K}\frac{\partial^n u}{\partial x^n} = M \tag{20}$$

where, K is the flexural rigidity GJ or EI, M is the applied torque or moment, u is the angle in torsion, deflection in bending, and n derivative order, 1 for torsion, 2 for bending.

The Equilibrium of the Unforced Body

For an unforced vibration in the body mode of interest, the distributed inertial loads are added to the equations of equilibrium of an elemental length of the rod or beam. Thus,

$$\frac{\partial^m M}{\partial x^m} - \rho\frac{\partial^2 u}{\partial t^2} = 0 \tag{21}$$

where, ρ is inertial quantity per unit length, and m is the order of the derivative. The order m is equal to the order n, in the cases discussed here. The equation for the normal modes in an unforced body may be stated as,

$$\frac{\partial^2 u}{\partial t^2} = a^2\frac{\partial^{2n} u}{\partial x^{2n}} \tag{22}$$

where, $a^2 = \frac{\mathrm{K}}{\rho}$

This may be recognized as the wave equation, with wave velocity a. The solution has the general form,

$$u = T(t)X(x) \tag{23}$$

where, $T(t)$ is the periodic amplitude in time t, and $X(x)$ is the required normal mode, x along the body. Substituting and separating the partial differential equations,

$$\frac{d^2 T}{dt^2} + \omega_f^2 T = 0 \tag{24}$$

where, ω_f is the flexible mode frequency, rad/sec. The general modal equation may be expressed as,

$$\frac{d^{2n}X}{dx^{2n}} + \frac{\omega_f^2}{a^2}X = 0 \qquad (25)$$

Equilibrium Equations for a Forced Body

The forced equations may be developed using D'Alembert and the principle of virtual work. Only a single modal shape, X(x), is considered from the solution of the equation above. The virtual displacement is,

$$\delta u = \{\delta T(t)\}X(x) \qquad (26)$$

The virtual work done by the inertial efforts, WI, is,

$$WI = -\int_0^L \{\rho\, dx\}\left\{\frac{\partial^2 u}{\partial t^2}\delta u\right\} \qquad (27)$$

or rewriting noting that the body cross-section and material are constant along its length, and substituting for the virtual displacement,

$$WI = -\rho\frac{d^2T}{dt^2}\delta T\,\Phi_1 \qquad (28)$$

where, $\Phi_1 = \int_0^L X^2 dx$, and L is the length of the body.

The strain energy on an elemental section of the body is,

$$V = \frac{1}{2}\left\{K\frac{\partial^n u}{\partial x^n}\right\}\left\{\frac{\partial^n u}{\partial x^n}dx\right\} \qquad (29)$$

and for the whole body,

$$V = \frac{1}{2}KT^2\Phi_2 \qquad (30)$$

where, $\Phi_2 = \int_0^L \left\{\frac{d^n X}{dx^n}\right\}^2 dx$, and L is again the length of the body.

The virtual work from strain energy, WS, may be stated as,

$$WS = -\frac{\partial V}{\partial u}\delta u \qquad (31)$$

and since $\frac{\partial u}{\partial T} = X$ and $\delta u = \delta T\, X$,

$$WS = -\frac{\partial V}{\partial T}\delta T \qquad (32)$$

Hence,

$$WS = -KT\delta T\Phi_2 \qquad (33)$$

The virtual work, WF, due to the applied external force or moment at a position along the body, x = c, is,

$$WF = P(t)\delta u_{x=c}$$

$$= P(t)\delta T X_{x=c} \qquad (34)$$

The Equation of Motion

The resulting equation of motion is,

$$\rho \frac{d^2T}{dt^2}\Phi_1 + KT\Phi_2 = P(t)X_{x=c} \qquad (35)$$

The equation of motion above may be rewritten,

$$\frac{d^2T}{dt^2} + a^2\frac{\Phi_2}{\Phi_1}T = \frac{1}{\rho\Phi_1}P(t)X_{x=c} \qquad (36)$$

It can be shown, for the mode assumed in the program, that,

$$\frac{\Phi_2}{\Phi_1} = \frac{\omega_f^2}{a^2} \qquad (37)$$

giving,

$$\frac{d^2T}{dt^2} + \omega_f^2 T = \frac{1}{\rho\Phi_1}P(t)X_{x=c} \qquad (38)$$

A further simplification may be made, allowing the use of the full rigid body inertias in the equation. The integral is chosen such that $\Phi_1 = L$ giving,

$$\frac{d^2T}{dt^2} + \omega_f^2 T = \frac{1}{Z}P(t)X_{x=c} \qquad (39)$$

where, Z is the total body inertial parameter, polar mass moment of inertia for the torsion equations or mass for the bending equations.

The integral relationship above is satisfied by selecting appropriate magnitudes for the normal modes. The normal mode for torsion with free ends is,

$$X(x) = \sqrt{2}\cos(kx) \qquad (40)$$

and for the bending, again with free ends, the normal mode is,

$$X(x) = \{\cos(kx) + \cosh(kx)\} - 0.9825\{\sin(kx) + \sinh(kx)\} \qquad (41)$$

where, $k^{2n} = \frac{\omega_f^2}{a^2}$

These are the normal modes used in **OMNISIM.**

Curves in the Track and "Inverted Pendulum" Forces

The inputs at the wheels are divided between excursions from straight track of either long or short wavelength. The short wavelength effects are regarded as local rail perturbations. They are defined in the input data as variations in lateral or vertical rail position. A repeatable shape function and amplitude for each section of rail may be chosen from a combination of rail cusps, bends and/or

sin waves. The program treats these as special identified inputs to the rail/wheel connections. Selecting time as the stepping variable instead of distance along the track permits the selection of a frequency scan for the sinusoidal input.

The method used in **OMNISIM** to incorporate the effect of linearly changing curvature and superelevation is to position each body in its local track coordinates so that so long as the angles between connected bodies are small the total angle of a long articulated car does not limit the accuracy of the solution. The relative angles and offsets and their time rates of change between the bodies connected are computed and added to the strokes and stroke velocities when they are computed. This requires that each pair of bodies be identified so that only the relative movements between the connected bodies are computed.

The accelerations due to the curved path of the track coordinates for each mass are added to the vector F in Eq. (6), along with the gravitational acceleration. Thus, the equations for each mass are modified to include in the force vector,

For the lateral degree of freedom,

$-M(gE + CV^2)$

For the vertical degree of freedom,

$-M(g - CEV^2)$

For the roll degree of freedom,

$-T_x\phi$

For the pitch degree of freedom,

$-T_y\theta$

For the yaw degree of freedom,

$$-I_z\frac{\partial C}{\partial s}V - T_z\psi \qquad (42)$$

where, M is the mass and I_z the roll inertia, g is the gravitational constant, E and C are the instantaneous superelevation and curvature at distance s along the track, T_x, T_y, T_z are the sums of the products of the suspension forces in direction x, y, z times the distance along each's direction to the body center of gravity, ϕ, θ, ψ are the instantaneous roll, pitch and yaw angles of the body, and V is the along track velocity.

The inclusion of the terms in roll, pitch and yaw here is one of convenience, since the sum of the moments must be computed when the connection forces are known. It is important where large almost static forces exist and act at a significant distance from the center of rotation. In roll, it may be recognized as the term which causes an inverted pendulum to fall over. In this formulation the terms are of second order, since the resulting moments are a function of the connection's deflection and the rotational angle. They may however be large and a very significant part of the dynamic behavior of the body. Such a term exists in the wheel/rail connection and its effect on the axle yaw rotation.

The long wavelength variations are linearly interpolated from positions along the track at which the curvature and super-elevation are provided in the input data. They are included in the transformation into connection strokes, so that the degrees of freedom for each body remain those relative to its local track based inertial coordinate system. Since the curvature along the track is assumed to be linear between the values given in the data, the value of the yaw angle and lateral offset of any point on the track from any other point may be established using the following analysis.

The curvature, C, at any point in a track section with linear curvature is given by, $C = C_1 + ms$, where, s is any distance from point 1 at the section beginning, C_1 is the curvature at point 1 and m is the slope of the curvature change with distance along the track in the section. The change in yaw angle, $\delta\psi$, of the track is given by,

$$\delta\psi = \int_0^l C\,ds = \int_0^l (C_1 + ms)\,ds \tag{43}$$

and since $m = \frac{C_2 - C_1}{l}$ where C_2 is the curvature at the end of the section,

$$\delta\psi = \frac{1}{2}(C_1 + C_2)\,l \tag{44}$$

A similar analysis to that above for the yaw angle is carried out for the change in superelevation between points along the track. The change can be seen to be the mean value times the distance between the section ends.

The change in lateral offset, δy, at the end of the section from that at the beginning is given by,

$$\delta y = \int_0^l d(\delta y) = \int_0^l \left(C_1 s + \frac{m}{2} s^2 \right) ds \tag{45}$$

and substituting for the rate of change of curvature,

$$\delta y = \frac{1}{3} C_1 l^2 + \frac{1}{6} C_2 l^2 \tag{46}$$

The superelevation, yaw angle and lateral offset differences are precomputed at data entry for each of the linear sections of track identified in the data. This reduces the run time which only requires that the superelevation, yaw angle and lateral offsets be calculated for the part of the section in which each body center is positioned at the time of the step. The total differences between bodies is summed for each pair to include the complete sections which lie between them.

The Stepping Algorithm

A simple constant time stepping algorithm is used, sometimes referred as the modified Euler algorithm. Given $\ddot{q}_i$, compute $\dot{q}_{i+1} = \dot{q}_i + \ddot{q}_i \Delta t$, and then $q_{i+1} = q_i + \dot{q}_{i+1} \Delta t$, where i is the present value, $i + 1$ is the next extrapolated value. Δt is the time step.

Forces and Moments in the Connection Elements

The simplest connection element is that in which the force or moment generated in the element is a direct function of time or distance moved along the track, identified through an input. The most common connection element is that in which the connection has stiffness and some damping in parallel. This may be through the inclusion of springs and dampers in the suspension design or through an energy dissipating rigid link. However several other types of connection are presently available.

These include the series element in which a stiffness is in series with a damper, a situation often used in the yaw connection between the truck and carbody to allow the car to follow the curves while preventing hunting, a special characteristic describing hysteresis effects between two arbitrary stiffness characteristics and a special series element in which friction is in series with a spring and damper in parallel. The special friction element included has a choice of frictional limiting values. In the series pairs, the intermediate state is carried locally in the computing subroutine.

At present, for simplicity, the connections are defined as along purely longitudinal, lateral or vertical directions. Each may require the definition of up to two characteristics through the provision of the break point coordinates of piecewise linear functions of either displacement or velocity. The general method used in to define the various required characteristics is as piecewise linear functions. An example is shown in Fig. 3. The abscissa may be a stroke or stroke velocity and the characteristic is defined at the corners and at a point on the extreme slopes. Extremes are linearly extrapolated beyond the last point. The only characteristic presently not treated in this manner is the wheel/rail connection.

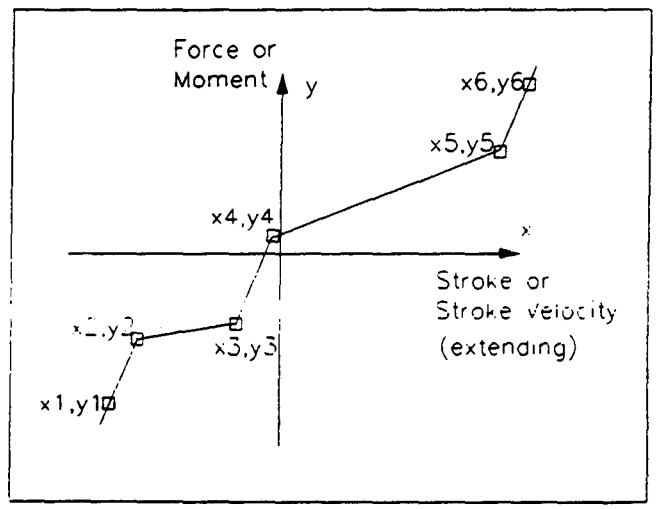

Figure 3 A General Piecewise-Linear Characteristic

TYPE 1 - Time or Distance Dependent Inputs

The inputs which are a function of time or distance travelled may generally be analytically described or for distance may be preprocessed from measured data, such as track or guideway geometry. In the preprocessor, short wave phenomena which are distance dependent are converted using a cubic spline representation and coefficients for subsequent computing of their value at any distance travelled. The preprocessor also permits their values to be prefiltered before spline fitting and passing into the equations of motion of the bodies. Presently only analytically described time dependent inputs are available. These are computed directly as required. The general long wave data is used to determine the path followed by the system in which the degree of freedom coordinates are measured. They are interpolated linearly at the required distance down the path and are described later.

An example of an analytic input is given in Fig. 4. Where they are forces or moments in a connection element, such as that produced by a hydraulic actuator, the appropriate force is computed and inserted at the connection masses. In this case the input number is indicated in the system data as that to be used for computing the force. A direct displacement input may be achieved by inserting a degree of freedom in a special body in the vector q of Eq. (6). Such a body, called here an input body, does not have mass and requires only position data.

Variations in rail position as a function of distance along the track are added to the wheel/rail connection element which requires their input number in the characteristic list. Similarly, the rotating body which may be an independent wheel or complete axle may be subject to an input torque through an input number in the same list.

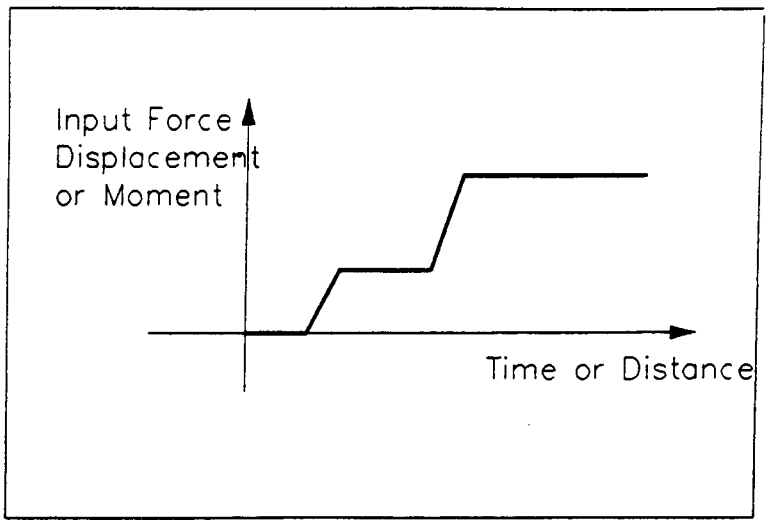

Figure 4 Analytic Form for an Input

TYPE 2 - The Parallel Connection

Forces through parallel elements add, so that this type of connection requires the computation of the values of the force through a damper and a spring from the stroke velocity and stroke respectively, and adding the result to give the total force through the pair. The process is shown symbolically in Fig. 5.

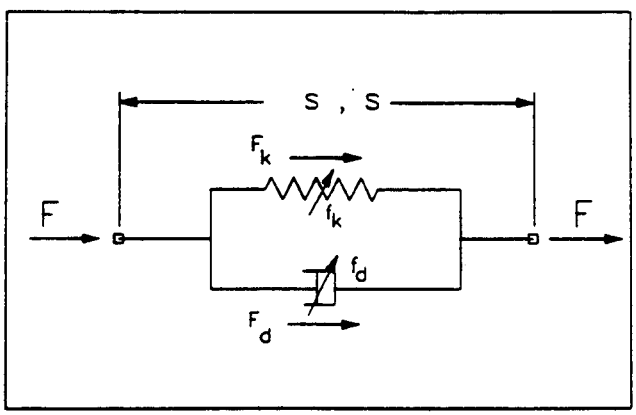

Figure 5 The Parallel Connection

TYPE 3 - The Series Connection

This connection is made more complex than the parallel pair by the existence of an unknown intermediate state at the junction of the spring and damper, as shown in Fig. 6.

The algorithm used to solve for the force through both elements uses the relationship for stepping the stroke in the form $s_k(new) = s_k(old) + \dot{s}_k \Delta t$. It should also be noted that $s = s_d + s_k$, $\dot{s} = \dot{s}_d + \dot{s}_k$ and $F = F_d = F_k$.

In the following equations, $t - \Delta t$ represents a value from the last step, t is the present value and $t + \Delta t$ is for the next time step. The prime, e.g. in s' , defines the use of a stored value.

The computer procedure is as follows.

Calculate and store, $s_k(t) = s'_k(t - \Delta t) + (\dot{s}(t) - \dot{s}'_d(t))\Delta t$

calculate, $F(t) = f_k(s_k(t))$

calculate, $\dot{s}_d = f_d^{-1}\{F(t)\}$

predict, $s_k(t + \Delta t) = s_k(t) + (\dot{s}(t) - \dot{s}_d(t))\Delta t$

and $F(t + \Delta t) = f_k(s_k(t + \Delta t))$.

Finally store, $\dot{s}_d(t + \Delta t) = f_d^{-1}\{F(t + \Delta t)\}$

(47)

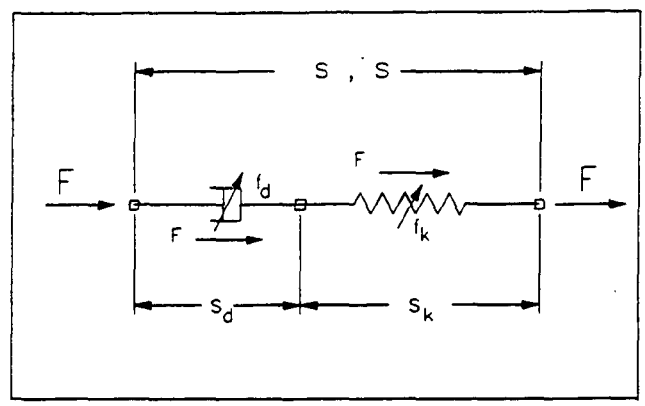

Figure 6 The Series Connection

TYPE 4 - The Connection with Hysteresis

The hysteresis connection option in **OMNISIM** has the characteristic form shown in Fig. 7. The envelope is defined by choosing in the data an upper, increasing, and lower, decreasing, piecewise linear characteristic from the general list of such characteristics provided by the user.

The algorithm used is to find the sum and difference of the values at the two characteristics for the stroke value at the time. If the stroke velocity is less than a calculated *limit* , the force due to the difference is treated as if it is a viscous force proportional to the velocity. This force "saturates" when the limit is reached. The *limit* is calculated from a leading edge damping constant given in the system data and the difference of the forces at the asymptotes for the stroke at the time of the calculation.

Thus,

$$limit = \frac{1}{2D}(F_1 - F_2)$$

where D is the leading edge damping coefficient.

If $\dot{s} > limit$ then R = 1

or if $\dot{s} < -limit$ then R = -1

otherwise $R = \frac{\dot{s}}{limit}$

The total force in the element is given by,

$$F = \frac{1}{2}\{(F_1 + F_2) + R(F_1 - F_2)\} \qquad (48)$$

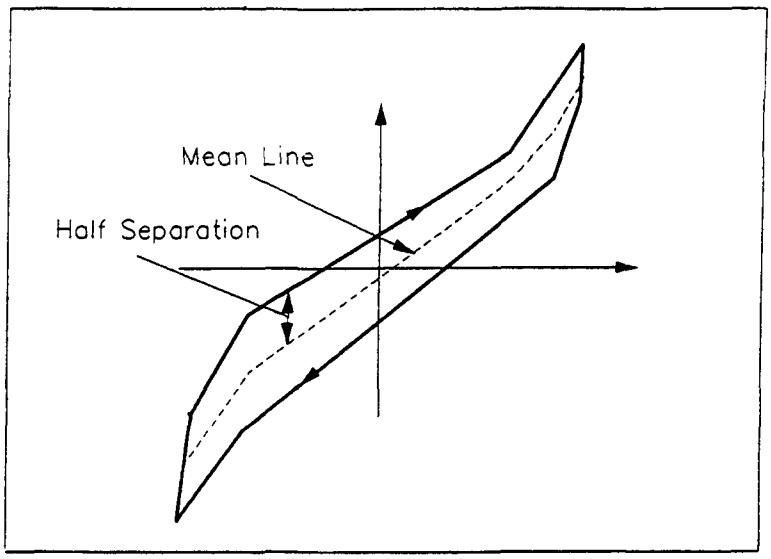

Figure 7 The Connection with Hysteresis

TYPE 5 - Special Series Friction Element

This characteristic has been added to represent various types of friction surface under a variety of normal loads. It is particularly useful in modeling a track at the interface between ties and ballast. Like the series connection, this element requires that an additional state be created and this is carried and stepped locally. The element is shown in Fig. 8.

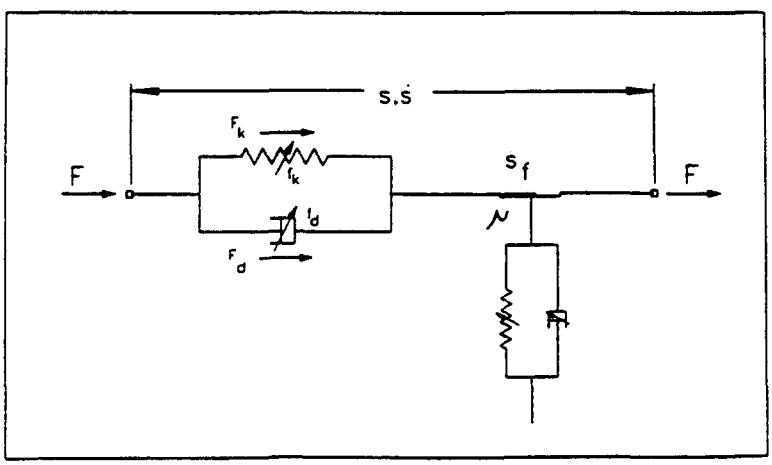

Figure 8 The Special Series Friction Connection

The algorithm used follows the analysis below.

For equilibrium across the elements, $F = F_d + F_k$. Since the velocity across the damper may be written as $\dot{s} - \dot{s}_f$, the damper force is $F_d = f_d(\dot{s} - \dot{s}_f)$. This permits the equilibrium equation to be rewritten,

$$f_d^{-1} F_{e,c} = f_d^{-1} F_k + \dot{s} - \dot{s}_f \quad .$$

where $F_{e,c}$ are the limiting values of F in extension or compression.

Using $\dot{s}_r = f_d^{-1} F_k + \dot{s} = \dot{s}_{dk} + \dot{s}$, and $\dot{s}_{e,c} = f_d^{-1} F_{e,c}$ this expression becomes,

$$\dot{s}_f = \dot{s}_r - \dot{s}_{e,c}$$

Thus,

if $\dot{s}_f > 0$	$F = F_e; \dot{s}_f = \dot{s}_r - \dot{s}_e$
if $\dot{s}_f < 0$	$F = F_c; \dot{s}_f = \dot{s}_r - \dot{s}_c$
otherwise	$F = F_k + F_d; \dot{s}_f = 0$

(49)

In OMNISIM, the values of F_e and F_c may be chosen in several ways. They may be submitted as data, or be chosen to be calculated as the product of the friction and normal load which is taken from the preceding connection in the list. In the latter case there is a further option which permits the force from the piecewise linear characteristic of the series spring also to be made proportional to the normal load. This method allows a full range of nonlinear descriptions for both the normal and tangential forces with the restriction that the tangential damper characteristic must be invertible, i.e. it must always have a small positive slope.

TYPE 10 - The Special Wheel/Rail Connection Element

Special characteristics are provided for each wheel-to-rail connection, which uses look up tables for the wheel/rail profile geometric properties and the rolling contact forces. The tables of profile data are precomputed using **PROFIT**, a modified version of the program of WHRAILA[8]. A four-dimensional look up of the table of creep force coefficients of Kalker[9] is used to obtain equilibrium of the axles, which are assumed rigid. The rotational speed of the axle is regarded as a special variable and is computed locally to determine the correct forces acting on the wheels from the rails.

The theory of the determination of wheel/rail forces and moments is presented below.

The Computation of Creepages

Creepage is expressed in terms of the steady-state velocity difference between the surfaces on the wheel and rail profiles. Since these bodies are distorted in the contact region, the velocities referred to in the creepage expressions are the so-called rigid-body velocities, i.e., the velocities the bodies would have in the contact region if they were not locally distorted. Fig. 9 and the equations below give formal definition to the creepages.

The longitudinal creepage is defined as the difference between the components in the longitudinal direction of these rigid body velocities divided by the mean rolling velocity. The lateral creepage is similarly defined as the lateral difference divided by the mean rolling velocity. Finally, spin is defined as the difference in rigid body angular velocities about an axis normal to the contact area divided by the mean rolling velocity. Thus,

V_1, V_2, etc. are rigid-body velocities relative to an origin moving with the contact point. The creepages of the wheel relative to the rail are defined as:

$$\text{Longitudinal: } \gamma_1 = \frac{V_1^- - V_1^+}{V}, \quad \text{Lateral: } \gamma_2 = \frac{V_2^- - V_2^+}{V}, \quad \text{Spin: } \omega_3 = \frac{\Omega_3^- - \Omega_3^+}{V} \tag{50}$$

where, $V = -\frac{1}{2}(V_1^- + V_1^+)$

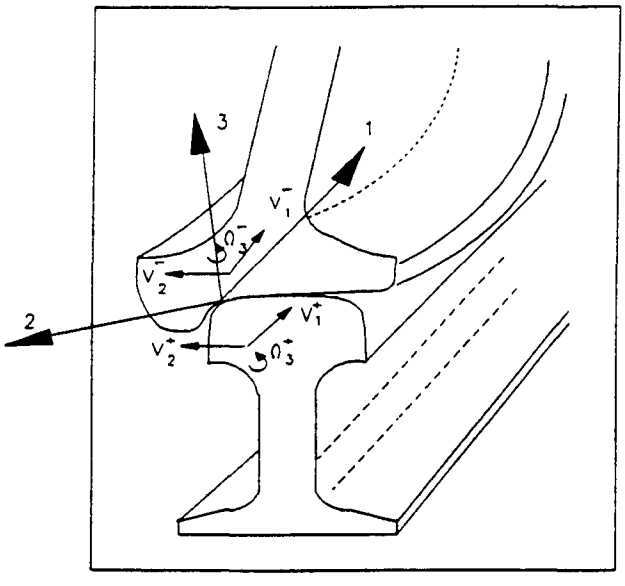

Figure 9 Creepages in the Contact Plane

Using the coordinate θ for rotation of the wheel body about its axis, which is computed and held locally in the program, and the strokes s_1, s_2, and s_6 for the longitudinal, lateral and yaw relative motions, which are computed in the usual manner, the following expressions are obtained for the creepages at the interface between the rotating wheel and rail bodies. The geometric variables are δ for the flange angle, r for the rolling radius, l_0 for half the distance between rail centers and R_0 for the curve radius. Subscripts l and r are used to denote contact with the left and right rails respectively. Hence for the left wheel/rail connection,

$$\gamma_{1l} = 1 + \frac{\{\dot{s}_1 - \dot{\theta} r_l\}}{V} - \frac{l_0}{R_0}$$

$$\gamma_{2l} = \left(\frac{\{\dot{s}_2 - \dot{\theta} r_l s_6\}}{V}\right) \sec\delta_l$$

$$\omega_{3l} = \left(\frac{\dot{s}_6}{V} + \frac{1}{R_0}\right)\cos\delta_l - \left(\frac{\dot{\theta}}{V}\right)\sin\delta_l \tag{51}$$

and for the right, $l_0 \rightarrow -l_0$ and $\delta_r = -\delta_l$ giving,

$$\gamma_{1r} = 1 + \frac{\{\dot{s}_1 - \dot{\theta} r_r\}}{V} + \frac{l_0}{R_0}$$

$$\gamma_{2r} = \left(\frac{\{\dot{s}_2 - \dot{\theta} r_r s_6\}}{V}\right) \sec\delta_r$$

$$\omega_{3r} = \left(\frac{\dot{s}_6}{V} + \frac{1}{R_0}\right)\cos\delta_r + \left(\frac{\dot{\theta}}{V}\right)\sin\delta_r \qquad (52)$$

where, $r_l = r_o\left(1 + \frac{\Delta r}{2r_o}\right); r_r = r_o\left(1 - \frac{\Delta r}{2r_o}\right)$

The Computation of Creep Forces

The creepages are produced by a tangential force and a moment about the normal axis, the tangential force normally also being resolved into its longitudinal and lateral components. The creep forces occurring at the interface between wheel and rail are functions of the previously derived creepages, a/b the ellipticity of the contact patch, T_3 the normal force on the contact patch, and μ the coefficient of friction. Kalker[9] has shown that by choosing the following nondimensional creepage parameters, the nondimensional functions for the forces obtained from the table, $\tau_1(\xi, \eta, \chi)$ and $\tau_2(\xi, \eta, \chi)$ are themselves dependent only on a/b. A fast four-dimensional linear interpolation of the Kalker table is used in **OMNISIM**. The non-dimensional creepage parameters are,

$$\xi = \frac{\rho\gamma_1}{\mu c}, \qquad \eta = \frac{\rho\gamma_2}{\mu c}, \qquad \chi = \frac{\rho\omega_3}{\mu} \qquad (53)$$

where $c = \sqrt{ab}$ the geometric mean of the contact patch semi-axes. As used in **OMNISIM**, this is calculated as $c = \sqrt{\frac{area}{\pi}}$, and $area$ is the contact patch area taken from a precomputed table.

PROFIT provides a table of the required geometric parameters for the wheel as a function of its lateral position on the rail. The lateral position of the wheel on the rail is established using the lateral stroke between the wheel and rail. A linear interpolation is used to obtain any required intermediate values, except when there exist two separate points of contact. This is identified at the outset through a computation of the rapidity of the change in the contact angle. In this case, the two adjacent values for each variable in the list are used separately and only the vertical load is interpolated linearly between the points.

The geometry table from **PROFIT** includes, for each lateral displacement of the wheel relative to the rail,

The difference of the rolling radius from nominal.
The angle of inclination of the plane of contact to the horizontal.
The area of the contact assuming Hertzian theory.
The ellipticity or ratio of the major to minor axes of the ellipse.
The radius of curvature, ρ in the contact patch computed from,

$$\frac{1}{\rho} = \frac{1}{4}\left(\frac{1}{R_1^+} + \frac{1}{R_1^-} + \frac{1}{R_2^+} + \frac{1}{R_2^-}\right),$$

$R_1^+, R_1^-, R_2^+, R_2^-$ being the principal radii of curvature of the wheel and rail.

The creep forces are related to the nondimensional forces by the following expressions:

$$T_1 = \mu T_3 \tau_1, \qquad T_2 = \mu T_3 \tau_2 \tag{54}$$

Kalker has published a table of results[9] for τ_1, τ_2 for a range of values of ξ, η, χ and a/b. His original results were obtained using his "numerical theory", up to $a/b = 2$. He later developed an improved prediction method, known as "Duvorol", which is able to predict for larger values of a/b. This method has been used in order to extend the table of nondimensional creep force/creepage data up to a/b of 10.

The creep forces in contact plane axes are transformed into forces in the track axis system using the relationships apparent in Fig. 10.

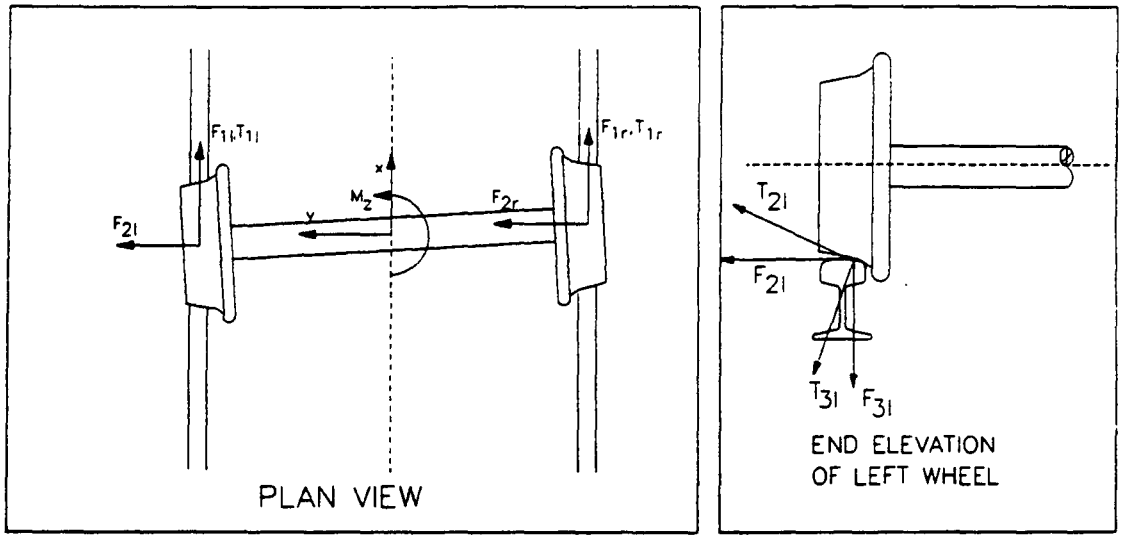

Figure 10 Forces and Moments on the Axle

Using the symbols given in the figure and considering the analysis for the wheels separately, the equivalence may be established between the forces in track coordinates and those of the contact patch.

Thus for the left wheel/rail connection,

$$F_{1l} = T_{1l}$$

$$F_{2l} = T_{2l}\cos\delta_l - T_{3l}\sin\delta_l$$

$$F_{3l} = T_{3l}\cos\delta_l + T_{2l}\sin\delta_l$$

and for the right, changing only the sign of the terms in $\sin\delta$

$$F_{1r} = T_{1r}$$

$$F_{2r} = T_{2r}\cos\delta_r + T_{3r}\sin\delta_r$$

$$F_{3r} = T_{3r}\cos\delta_r - T_{2r}\sin\delta_r \tag{55}$$

The moment expressions for the forces above are inserted into the equations of motion in the manner already described, including the terms previously called the "inverted pendulum". There are certain additional terms which require an understanding of the three dimensional geometry at the contact point after yaw rotation of the wheel. The shift in the position of the contact point is shown in Fig. 11 for the left wheel for an arbitrary yaw angle ψ. On the left wheel, contributions to the moments come from F_{2l} and F_{3l}. The components of these forces are modified due to the movement of the contact points from vertically below the wheelset axis of rotation at the rail when the wheelset is yawed. Thus corrective moments are applied to the moment calculations discussed previously as part of the transformation and insertion into the equilibrium expressions. The moment about the axis of the wheel is also given as required for dynamic equilibrium. This rotational degree of freedom is carried locally as a speed and determined as shown below. At each contact point, the moments on the axle in rotation about y and yaw about z, using s_6 for the yaw stroke, are given for the left wheel by,

$$M_{yl} = r_l(F_{1l} + F_{2l}s_6 + F_{3l}\tan\delta_l s_6)$$

$$M_{zl} = -s_6 F_{2l} r_l \tan\delta_l$$

and for the right wheel/rail contact by,

$$M_{yr} = r_r(F_{1r} + F_{2r}s_6 - F_{3r}\tan\delta_r s_6)$$

$$M_{zr} = s_6 F_{2r} r_r \tan\delta_r \qquad (56)$$

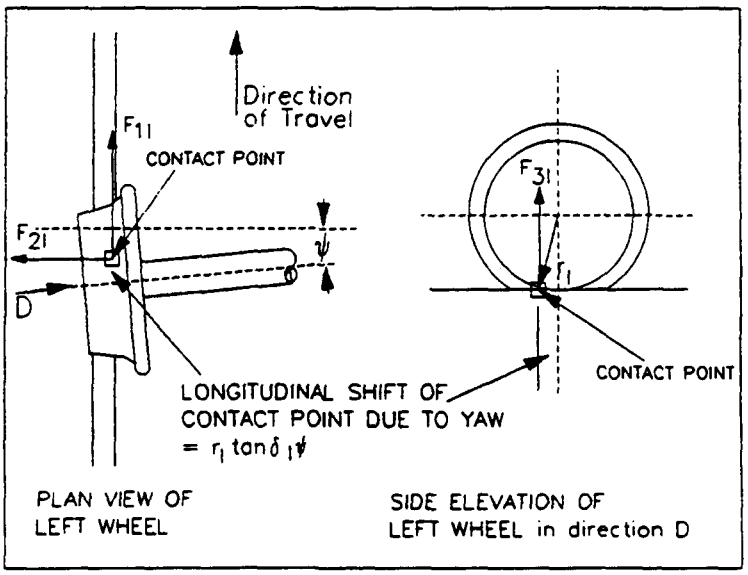

Figure 11 Longitudinal Shift in the Point of Contact

These equations are used in **OMNISIM** to establish the forces and moments due to creepage between each wheel and rail. Although the analysis above suggests that only one point of contact occurs between each wheel and rail, this limitation is not necessary and multiple two points are possible. This is carried out by determining a separate vertical load on the wheel at each point of contact using the proportion of the lateral displacement in going from the first contact to the second in the wheel/rail geometry table. The existence of the two point

situation in the table is predetermined from the rate of change of the profile slope. The vertical load is establish for each contact point either side of the determined two point contact in the table. The procedure adopted for solving the equations at the contact is as follows. First, equations (54) and (55) are used to give,

$$T_{3l} = \frac{T_{zl}}{\cos\delta_l + \mu\tau_{2l}\sin\delta_l}$$

or for the right wheel,

$$T_{3r} = \frac{T_{zr}}{\cos\delta_r - \mu\tau_{2r}\sin\delta_r} \qquad (57)$$

then, $T_1 = \mu T_3 \tau_1$ and $T_2 = \mu T_3 \tau_2$.

The remaining forces are computed using Eqs. (55).

The rotational velocity of the wheelset about its bearing axis $\dot{\theta}$ has to be determined before the creepages can be evaluated. In order to calculate $\dot{\theta}$, **OMNISIM** steps the first order moment equation in $\dot{\theta}$ either for the wheelset as a rigid body or for each wheel independently, as required by the user. The moment due to creep forces is given in Eqn. (58) for each contact point and the stepping process is as follows.

$$\dot{\theta}(t) = \dot{\theta}(t-\Delta t) + \frac{\Delta t}{I_y}\left\{\frac{M_y(t) + M_y(t-\Delta t)}{2}\right\} \qquad (58)$$

where, $\dot{\theta}$ is the wheel (or axle) rotational velocity, and I_y is the wheel (or axle) polar inertia. The terms in $t - \Delta t$ and t are the values for the previous and present time respectively.